Thin Films of Polythiophene:
Linear and Nonlinear Optical Characterization

Dissertation zur Erlangung des Grades
"Doktor der Naturwissenschaften"

am Fachbereich Physik
der Johannes Gutenberg-Universität
in Mainz

vorgelegt von
Mohamad Jahja
geboren in Gorontalo, Indonesien

Mainz, 2010

Content

1 Introduction

1.1 Scientific and Technological Background

Organic molecules can have large third-order optical nonlinearity [Chance'80, Logsdon'88, McBranch'89, Nalwa'93, Bredas'94]. This means the optical constants of thin films are dependent on the intensity I of the laser. The intensity dependence of optical constants of the materials is described by

$$n(I) = n_0 + n_2 I \tag{1.1}$$

$$\alpha(I) = \alpha_0 + \alpha_2 I\,, \tag{1.2}$$

where n_0 and α_0 are linear refractive index and absorption coefficient respectively. The nonlinear refractive index n_2 and nonlinear absorption coefficient α_2 are proportional to the real and imaginary part of the complex nonlinear optical susceptibility $\chi^{(3)}(-\omega;\omega,-\omega,\omega)$, respectively [Butcher'90, Boyd'08]. Relatively large, ultrafast and reversibly changes of refractive index at $I <$ damage threshold intensity I_{th} requires materials with large n_2 and small α_2. The threshold intensity I_{th} is the maximum intensity of the laser which cannot cause any damage to the optical properties of the material. The combination of relatively large n_2, small α_2 and low propagation losses has been formulated in terms of figures of merit (FOMs) [Stegeman'93]

$$W(\lambda) = \frac{n_2 I}{\alpha_0 \lambda} \geq 1, \tag{1.3}$$

$$T(\lambda) = \frac{2\alpha_2 \lambda}{n_2} \leq 1 \tag{1.4}$$

at the working wavelength λ of the device. Due to many experimental difficulties in measuring all required optical constants which are needed according to Eq. 1.3 and 1.4, quantitative spectra of W and T are still rare to find.

The materials must be suitable for thin film processing and waveguide fabrication. Optical waveguides have many advantages for nonlinear optical application because they can be easily formed, integrated and offer large electric field intensity due to light confinement in the waveguides [Stegemann'89, Kajzar'96]. Realization of devices with

high throughput requires waveguides with low attenuation, i.e., propagation losses α_{gw} < 1 dB/cm [Stegeman'89, Bubeck'00]. Materials with high photostability at UV-Vis wavelengths and additionally at high intensity laser pulses are required for nonlinear optical waveguide applications.

Photo-oxidation could take place on waveguide surfaces upon irradiation of UV-Vis light and sample handling at ambient air, which leads to a decrease of optical constants of materials [Rothberg'96, Bader'02]. High intensity laser at NIR wavelengths, which are needed to change the refractive index of the materials, on the other hand, could cause photo-ablation of the material surface. To avoid these problems, one needs to apply an intensity lower than the damage threshold intensity I_{th} of the materials. Large damage threshold intensity I_{th} > 10 GW/cm^2 is required for nonlinear waveguide application.

Among materials which have potential for all-optical switching, organic materials have many advantages i.e. relatively low cost production and tailorability that allows to tune the chemical structures and materials properties for the desired applications [Brédas'94]. A delocalized π-electron system in conjugated polymers gives possibility for all-optical switching because of their large cubic nonlinear susceptibility and fast response time in the order of picoseconds (10^{-12} s) or less [Yoshizawa'91, Kuebler'00]. In particular, polythiophene or PT (see its chemical structure in Fig. 1.1) and its derivatives were identified as promising materials for applications in nonlinear optics because of large cubic nonlinearities with fast response times [Neher'90, Bubeck'91, Yang'92, Kishida'05, Faccinetto'08].

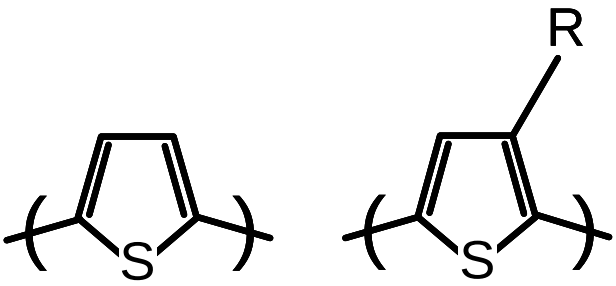

Fig. 1.1: Chemical structure of polythiophene (PT, left) and poly(3-alkylthiophene), where R denotes an alkyl chain.

Therefore, it is necessary to study the linear and nonlinear optical properties of polythiophene derivatives, their thin film formation and their waveguide performances. We focus our study on poly(3-alkylthiophene) with different alkyl chains and different regioregularity.

1.2 Task of the Work

We have to find a suitable material for all-optical switching applications among polythiophene derivatives. This needs to understand the relationships between the molecular structure and the optical properties of conjugated polymers that are useful for future materials development. The following tasks exist to achieve these goals.

Spin coating technique has been used to prepare thin polymer films and waveguides of polythiophene derivatives. Preparation conditions (solvents and casting temperatures) and parameters (concentration of solution, spinning speed and time) have been adjusted to achieve the high optical quality films and low-loss waveguides [Fitrilawati'99, Fitrilawati'00].

Linear optical spectra of thin polymer films were measured using reflectometry [Schwarz'92a, Schwarz'92b, Scholdei'07]. Linear refractive indexes of waveguides were determined using prism coupling technique [Tien'77]. These data are needed for designing optical devices, or at least to determine the waveguide thicknesses which are required prior to experiments where a specific waveguide mode is excited (for example non linear prism coupling and waveguide loss experiment).

Stability of polymers under UV-Vis and high intensity laser irradiation is an important criterion for all-optical switching application. Photooxidation could take place at the polymer surface if the sample is exposed to UV-Vis irradiation and/or high-intensity laser irradiation. The photostability of polymers is studied by irradiating thin films with UV light and measuring the absorption changes after certain exposure using cut-off filters. The damage threshold intensity is determined by varying exposure intensities and measuring diameters of ablated holes.

Materials with good combination of third-order optical nonlinearity, low waveguide propagation losses, relatively high photostability at UV irradiation and large damage threshold intensity are suitable for all-optical switching. In chapter 5, we will compare thermal and linear optical properties of poly(3-alkylthiophene) with different alkyl side chains and select the most suitable materials for all-optical switching applications.

Dispersion of nonlinear refractive index n_2 and nonlinear absorption coefficient α_2 of polymer in the near infrared (NIR) range are needed to be known, because most of materials show minima of their waveguide propagation loss and all of telecom windows are in the NIR range. Using nonlinear prism coupling [Ueberhofen'99, Koynov'02],

measurements of n_2 and α_2 can be performed with waveguides with high accuracy and sensitivity. From data of n_2, α_2 and waveguide loss α_{gw}, dispersion of figures of merit $W(\lambda)$ and $T(\lambda)$ has to be evaluated and the spectral range which fulfils the figure of merit requirements will be identified.

2 Theoretical Background

In this section we summarize the theoretical background. First, we introduce to optical constants and nonlinear optics and subsequently to planar waveguide and related topics. The following major references for nonlinear optics are the books of Butcher and Cotter [Butcher'90], Boyd [Boyd'08], and for planar waveguides: Kogelnik [Kogelnik'74], Adams [Adams'81] and Lee [Lee'86].

2.1 Optical Constants and Nonlinear Optics

The electrical polarization $\vec{P}$ is defined as number of dipole moments per unit volume of matter which is in general described as [Butcher'90, Boyd'08]

$$\vec{P} = \varepsilon_0 \left(\chi^{(1)} \vec{E} + K^{(2)} \chi^{(2)} \vec{E}\vec{E} + K^{(3)} \chi^{(3)} \vec{E}\vec{E}\vec{E} + ... \right), \tag{2.1}$$

where $\vec{E}$ is electric field, ε_0 is known as vacuum permittivity and has value of $8.86 \cdot 10^{-12}$ As/Vm and $\chi^{(\nu)}$ are ν-th order susceptibilities. $K^{(\nu)}$ are numerical factors which are related to the kind of the nonlinear optical process and to the number of distinguishable permutations of frequencies [Butcher'92]. First order processes are described by the linear susceptibility $\chi^{(1)}$ and the others are related to nonlinear susceptibilities of order-ν. Nonlinear terms cause that $\vec{\mathrm{P}}$ is no more linearly dependent on $\vec{\mathrm{E}}$. Since the nonlinear effects are small, they are observed after the discovery of the laser.

The light intensity *I* is related to $\vec{E}$ by

$$I = \frac{1}{2} \varepsilon_0 c n_0 \left| \vec{E} \right|^2, \tag{2.2}$$

where *c* is speed of light in vacuum and n_0 is linear refractive index of matter which is related with

$$n_0^2 = 1 + \chi^{(1)}. \tag{2.3}$$

We insert the electrical field for a plane wave which propagates in the z-direction and has frequency ω and wave vector $k = 2\pi/\lambda$ (λ is the wavelength)

$$E = E_0 \cos(\omega t - kz) \tag{2.4}$$

into Eq. (2.1). By using appropriate trigonometric identities, one can obtain

$$P = \varepsilon_0 \left\{ \chi^{(1)} E_0 \cos(\omega t - kz) + K^{(2)} \chi^{(2)} E_0^2 \frac{1}{2} \left[1 + \cos(2\omega t - 2kz) \right] \right.$$
$$\left. + K^{(3)} \chi^{(3)} E_0^3 \left[\frac{3}{4} \cos(\omega t - kz) + \frac{1}{4} \cos(3\omega t - 3kz) \right] \right\} \tag{2.5}$$

As can be seen in Eq. (2.5), the polarization contains not only the component that oscillates at the fundamental frequency ω, but also new frequencies 2ω and 3ω. The polarization in Eq. (2.5) can be arranged into three components regarding to the frequencies ω, 2ω, and 3ω, respectively

$$P(\omega) = \varepsilon_0 \left[\chi^{(1)} + K^{(3)} \frac{3}{4} \chi^{(3)} E_0^2 \right] E_0 \cos(\omega t - kz) \tag{2.6a}$$

$$P(2\omega) = \varepsilon_0 \frac{1}{2} K^{(2)} \chi^{(2)} E_0^2 \cos(2\omega t - 2kz) \tag{2.6b}$$

$$P(3\omega) = \varepsilon_0 \frac{1}{4} K^{(3)} \chi^{(3)} E_0^3 \cos(3\omega t - 3kz) \tag{2.6c}$$

The first term in $P(\omega)$ is related to the linear refractive index and the second term leads to an intensity-dependent refractive index n(I). The $P(2\omega)$ term gives rise to many important effects such as frequency doubling or second-harmonic generation (SHG), and sum- and difference-frequency generation. There is also a frequency-independent contribution in Eq. (2.5), which is referred to as optical rectification. Because of symmetry reasons, centrosymmetric materials will not have second-order polarization and all subsequent even-orders. The $P(3\omega)$ term corresponds to third-harmonic generation (THG).

Here, we focus only on third-order nonlinear effects. The terms in brackets of Eq. (2.6a) are treated as an effective susceptibility χ_{eff}, which is related to the refractive index n through

$$n^2 = 1 + \chi_{eff} = 1 + \chi^{(1)}(-\omega;\omega) + \frac{3}{4} K^{(3)} \chi^{(3)}(-\omega;\omega,-\omega,\omega) E_0^2 . \tag{2.7}$$

If the intensity I is used instead of E_0^2, we obtain

$$n^2 = 1 + \chi_{eff} = 1 + \chi^{(1)}(-\omega;\omega) + \frac{3}{4} K^{(3)} \chi^{(3)}(-\omega;\omega,-\omega,\omega) I \,. \tag{2.8}$$

By introducing the linear refractive index n_0 into Eq.(2.8) via $\chi^{(1)}(-\omega;\omega) = n_0^2 - 1$ and with the approximation $n^2 - n_0^2 \cong 2n_0(n - n_0)$, we obtain the intensity-dependent refractive index

$$n = n_0 + n_2 I \,. \tag{2.9}$$

To determine the relation between the real and imaginary part of $\chi^{(3)}$ and the nonlinear refractive index n_2 and nonlinear absorption coefficient α_2, the expression of the complex of the refractive index of Eq. (2.9) has to be squared, and yields

$$\tilde{n}^2 = (\tilde{n}_0 + \tilde{n}_2 I)^2 \tag{2.10}$$

where

$$\tilde{n}_0 = n_0 + i\kappa_0 \tag{2.11}$$

$$\tilde{n}_2 = n_2 + i\kappa_2 \tag{2.12}$$

$$\alpha_{0,2} = \frac{4\pi}{\lambda} \kappa_{0,2} \,. \tag{2.13}$$

where κ is the imaginary part of refractive index n. By using the combinations (2.8) and (2.31) and the comparison with (2.37), the following relations are obtained

$$n_0^2 - \kappa_0^2 = 1 + \mathrm{Re}[\chi^{(1)}(-\omega;\omega)] \tag{2.14}$$

$$\kappa_0 = \frac{\mathrm{Im}[\chi^{(1)}(-\omega;\omega)]}{2n_0} \tag{2.15}$$

$$n_0 n_2 - \kappa_0 \kappa_2 = \frac{3}{4n_0 \varepsilon_0 c} K^{(3)} \,\mathrm{Re}[\chi^{(3)}(-\omega;\omega,-\omega,\omega)] \tag{2.16}$$

$$n_0 \kappa_2 + \kappa_0 n_2 = \frac{3}{4n_0 \varepsilon_0 c} K^{(3)} \,\mathrm{Im}[\chi^{(3)}(-\omega;\omega,-\omega,\omega)] \tag{2.17}$$

The first two equations describe the linear refractive index and linear absorption. The last two equations describe the nonlinear refractive index and the two-photon absorption. As the two-photon effects denoted by n_2 and α_2 are only interesting outside a one-photon

resonance, the linear loss term can be assumed to be zero ($\kappa_0 \approx 0$). Consequently, the nonlinear refractive index n_2 and the two-photon absorption coefficient α_2 are directly proportional to the real and imaginary part of the third-order susceptibility $\chi^{(3)}$ through [Butcher'91]

$$n_2 = \frac{3}{4n_0^2\varepsilon_0 c} K^{(3)} \operatorname{Re}[\chi^{(3)}(-\omega;\omega,-\omega,\omega)] \tag{2.18}$$

$$\alpha_2 = \frac{3\pi}{n_0^2\varepsilon_0 \lambda c} K^{(3)} \operatorname{Im}[\chi^{(3)}(-\omega;\omega,-\omega,\omega)] \tag{2.19}$$

Here the appropriate $K^{(3)} = 3/4$ should be inserted, if $\chi^{(3)}$ is defined as in Eq. (2.1).

Relation (2.18) and (2.19) can be expressed numerically in SI units as

$$n_2\left(\frac{m^2}{W}\right) = \frac{283}{n_0^2} K^{(3)} \operatorname{Re}[\chi^{(3)}(-\omega;\omega,-\omega,\omega)]\left(\frac{m^2}{V^2}\right) \tag{2.20}$$

$$\alpha_2\left(\frac{m}{W}\right) = \frac{3548}{n_0^2\lambda} K^{(3)} \operatorname{Im}[\chi^{(3)}(-\omega;\omega,-\omega,\omega)]\left(\frac{m^2}{V^2}\right). \tag{2.21}$$

Besides SI unit, gaussian unit is sometimes used, the following relation are useful to converting between them

$$n_2\left(\frac{cm^2}{W}\right) = \frac{12\pi^2}{n_0^2 c} 10^7 K^{(3)} \operatorname{Re}[\chi^{(3)}(-\omega;\omega,-\omega,\omega)](esu) = \frac{0.0395}{n_0^2} \operatorname{Re}\left[\chi^{(3)}(esu)\right] \tag{2.22}$$

$$\alpha_2\left(\frac{cm^2}{W}\right) = \frac{48\pi^3}{n_0^2 c\lambda} 10^7 K^{(3)} \operatorname{Im}[\chi^{(3)}(-\omega;\omega,-\omega,\omega)](esu) = \frac{0.496}{n_0^2\lambda} \operatorname{Im}\left[\chi^{(3)}(esu)\right] \tag{2.23}$$

The third-order nonlinearity $\chi^{(3)}$ can be calculated using several models which are available in the literature, for example Boyd [Boyd'08], Butcher and Cotter [Butcher'91].

2.2 Quantum-Mechanical Model of Nonresonant Electronic Nonlinearities

Third-order susceptibility $\chi^{(3)}$ which is calculated using density-matrix approach is given by Eq. (2.24) [Boyd'08]. The P_I is intrinsic permutation operator, whose meaning is that everything to the right of it is to be added up over all-possible permutations of input frequencies ω_p, ω_q and ω_r, with the Cartesian indices h, i, j permuted

simultaneously. N is density of electrons, ρ_{ll} is probability of the electrons in eigenstate l, μ_{mn} is transition dipole moment between state m and n and γ_{nl} is damping factor or linewidth.

$$\chi^{(3)}_{kjih}(\omega_p+\omega_q+\omega_r,\omega_r,\omega_q,\omega_p)=\frac{N}{\varepsilon_0\hbar^3}P_l\sum_{nm\nu\lambda}$$

$$\left\{\frac{(\rho^{(0)}_{mm}-\rho^{(0)}_{ll})\mu^k_{mn}\mu^j_{n\nu}\mu^i_{\nu\lambda}\mu^h_{lm}}{\left[(\omega_{nm}-\omega_p-\omega_q-\omega_r)-i\gamma_{nm}\right]\left[(\omega_{\nu m}-\omega_p-\omega_q)-i\gamma_{\nu m}\right]\left[(\omega_{lm}-\omega_p)-i\gamma_{lm}\right]}\right. \quad \text{(a)}$$

$$-\frac{(\rho^{(0)}_{ll}-\rho^{(0)}_{\nu\nu})\mu^k_{mn}\mu^j_{n\nu}\mu^i_{lm}\mu^h_{\nu\lambda}}{\left[(\omega_{nm}-\omega_p-\omega_q-\omega_r)-i\gamma_{nm}\right]\left[(\omega_{\nu m}-\omega_p-\omega_q)-i\gamma_{\nu m}\right]\left[(\omega_{\nu\lambda}-\omega_p)-i\gamma_{\nu\lambda}\right]} \quad \text{(b)}$$

$$-\frac{(\rho^{(0)}_{\nu\nu}-\rho^{(0)}_{ll})\mu^k_{mn}\mu^j_{\nu m}\mu^i_{nl}\mu^h_{l\nu}}{\left[(\omega_{nm}-\omega_p-\omega_q-\omega_r)-i\gamma_{nm}\right]\left[(\omega_{n\nu}-\omega_p-\omega_q)-i\gamma_{n\nu}\right]\left[(\omega_{l\nu}-\omega_p)-i\gamma_{l\nu}\right]} \quad \text{(c)}$$

$$\left.+\frac{(\rho^{(0)}_{ll}-\rho^{(0)}_{nn})\mu^k_{mn}\mu^j_{\nu m}\mu^i_{l\nu}\mu^h_{nl}}{\left[(\omega_{nm}-\omega_p-\omega_q-\omega_r)-i\gamma_{nm}\right]\left[(\omega_{n\nu}-\omega_p-\omega_q)-i\gamma_{n\nu}\right]\left[(\omega_{nl}-\omega_p)-i\gamma_{nl}\right]}\right\}. \quad \text{(d)} \qquad (2.24)$$

Eq. (2.24) could be written in compact form as Eq. (2.25) for the **nonresonant** region where $\omega_\sigma=\omega_r+\omega_q+\omega_p$ and $\rho^{(0)}_{ll}=1$. The P_F is full permutation, where the expression is to be summed over all permutation of the frequencies $\omega_p,\omega_q,\omega_r$ and $-\omega_\sigma$ - that is, over all input and output frequencies. In the case of intensity dependent refractive index we get $\omega_p=-\omega$, $\omega_q=\omega$, $\omega_r=\omega$ then $\omega_\sigma=\omega$.

$$\chi^{(3)}_{kjih}(\omega_\sigma,\omega_r,\omega_q,\omega_p)=\frac{N}{\varepsilon_0\hbar^3}P_F\sum_{lmn}\frac{\mu^k_{gn}\mu^j_{nm}\mu^i_{ml}\mu^h_{lg}}{(\omega_{ng}-\omega_\sigma)(\omega_{mg}-\omega_q-\omega_p)(\omega_{lg}-\omega_p)}, \qquad (2.25)$$

Eg. (2.25) can be arranged to visualize two excitation sequences. Eq. (2.26), which is composed of two terms: The first summation describes the sequence involving 2 intermediate states and the second involves one intermediate state only.

$$\chi^{(3)}_{kjih}(\omega,\omega,\omega,-\omega)=\chi^{(3)}_{kjih}(\omega=\omega+\omega-\omega)=\frac{N}{6\varepsilon_0\hbar^3}$$
$$\times\left(\sum_{lmn}\frac{\mu^k_{gn}\mu^h_{nm}\mu^i_{ml}\mu^j_{lg}+\mu^k_{gn}\mu^h_{nm}\mu^j_{ml}\mu^i_{lg}+\mu^h_{gn}\mu^k_{nm}\mu^i_{ml}\mu^j_{lg}+\mu^h_{gn}\mu^k_{nm}\mu^j_{ml}\mu^i_{lg}}{(\omega_{ng}-\omega)(\omega_{mg}-2\omega)(\omega_{lg}-\omega)}\right.$$
$$\left.-\sum_{ln}\frac{\mu^k_{gn}\mu^j_{ng}\mu^h_{gl}\mu^i_{lg}+\mu^k_{gn}\mu^i_{ng}\mu^h_{gl}\mu^j_{lg}+\mu^h_{gn}\mu^i_{ng}\mu^k_{gl}\mu^j_{lg}+\mu^h_{gn}\mu^j_{ng}\mu^k_{gl}\mu^i_{lg}}{(\omega_{ng}-\omega)(\omega_{lg}-\omega)(\omega_{lg}-\omega)}\right). \quad (2.26)$$

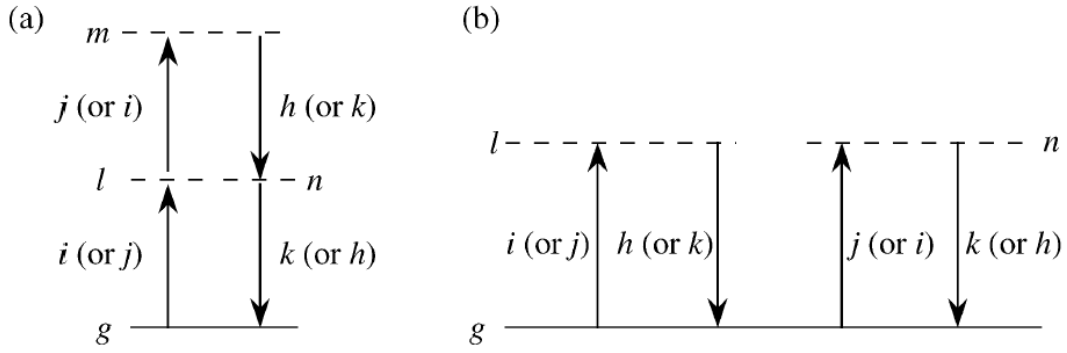

Fig. 2.1: Diagram of the first (a) and second (b) summations of Eq. 2.26. The picture is redrawn from Boyd [Boyd'08].

An isotropic medium means that $k=j=i=h=x$. In the case of conjugated polymers, we assume that only transition matrix elements parallel to the direction x of the polymer backbone dominate the $\chi^{(3)}$ [Neher'91]. The Eq. (2.27) is valid only for the **nonresonant** condition.

$$\chi^{(3)}_{1111}=\frac{2N}{3\varepsilon_0\hbar^3}\sum_{lmn}\frac{\mu^x_{gn}\mu^x_{nm}\mu^x_{ml}\mu^x_{lg}}{(\omega_{ng}-\omega)(\omega_{mg}-2\omega)(\omega_{lg}-\omega)}$$
$$-\frac{2N}{3\varepsilon_0\hbar^3}\sum_{ln}\frac{\mu^k_{gn}\mu^j_{ng}\mu^h_{gl}\mu^i_{lg}}{(\omega_{ng}-\omega)(\omega_{lg}-\omega)(\omega_{lg}-\omega)}. \quad (2.27)$$

A general three-level model was used to interpret the third-order nonlinear optical spectra of conjugated polymers [Neher'91, Ueberhofen'99]. The model involving the ground state g (with even symmetry) and two-excited states (g' with even symmetry and u with odd symmetry) is shown in Fig. 2.2.

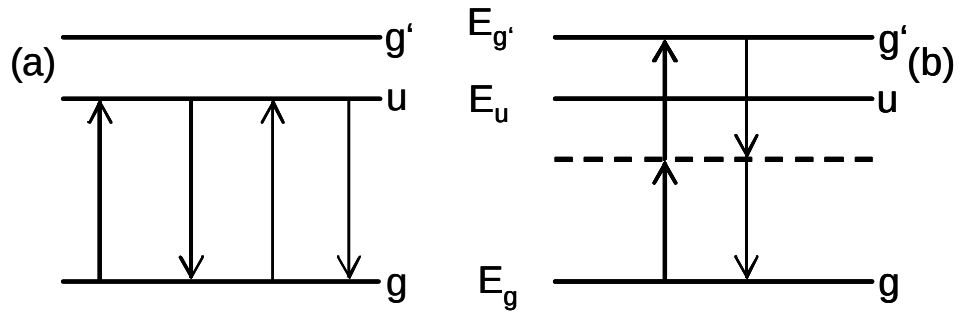

Fig. 2.2: Excitation pathways in a three-level system with real states g, u and g': (a) one-photon absorption and (b) two photon absorption.

The $\chi^{(3)}_{1111}$ is calculated using a three-level system by means of Eq. (2.28). $E_{g'g} = \hbar\omega_{g'g}$ and $E_{ug} = \hbar\omega_{ug}$ are energy level differences between ground state g, excited state g' and u, respectively. To involve resonant cases as shown in Fig. 2.2, we have to insert back the imaginary terms by replacing ω_{ng} with $\omega_{ng} - i\gamma_{ng}$, the other terms also have to be changed accordingly. The $\gamma_{g'g}$ and γ_{ug} are damping factors or line widths of transition from state g to g' and u, respectively.

$$\chi^{(3)}_{1111} = \frac{2N}{3\varepsilon_0\hbar^3}\left\{\frac{\mu^x_{gv}\mu^x_{vg'}\mu^x_{g'v}\mu^x_{vg}}{\left(\frac{1}{2}\omega_{g'g} - \omega - i\frac{1}{2}\gamma_{g'g}\right)\left(\omega_{g'g} - 2\omega + i\gamma_{g'g}\right)\left(\frac{1}{2}\omega_{g'g} - \omega - i\frac{1}{2}\gamma_{g'g}\right)}\right.$$

$$\left. - \frac{\mu^x_{gu}\mu^x_{ug}\mu^x_{gu}\mu^x_{ug}}{\left(\omega_{ug} - \omega - i\gamma_{ug}\right)\left(\omega_{ug} - \omega + i\gamma_{ug}\right)\left(\omega_{ug} - \omega - i\gamma_{ug}\right)}\right\} \tag{2.28}$$

The Eq. (2.28) can be arranged into more practical form as shown in Eq. (2.29), where we use energy $E = \hbar\omega$ as variable instead of ω, and include many constants into two constants $A_{g'g}$ and A_{gu} only, which denote transition dipole moments from g to g' and u, respectively. The damping factors $\Gamma_{g'g}$ and Γ_{ug} refer to $\hbar\gamma_{g'g}$ and $\hbar\gamma_{ug}$, respectively.

$$\chi^{(3)}_{1111} = \frac{A_{g'g}}{\left(\frac{1}{2}E_{g'g} - E - i\frac{1}{2}\Gamma_{g'g}\right)\left(E_{g'g} - 2E + i\Gamma_{g'g}\right)\left(\frac{1}{2}E_{g'g} - E - i\frac{1}{2}\Gamma_{g'g}\right)}$$

$$- \frac{A_{ug}}{\left(E_{ug} - E - i\Gamma_{ug}\right)\left(E_{ug} - E + i\Gamma_{ug}\right)\left(E_{ug} - E - i\Gamma_{ug}\right)} \tag{2.29}$$

2.3 Planar Waveguide

Eq. (2.30) is well known as one dimensional wave equation. In this case $\vec{E}(x)$ is electric field distribution along x axis. The k and $k\tilde{N}$ are wave vector and propagation constant in vacuum, respectively. Relation of k and wavelength of the laser λ is $k=2\pi/\lambda$. Distribution of refractive index n along x is given by $n(x)$, which is related with the geometry of waveguide.

$$\left(\frac{d}{dx^2}+\left[k^2n^2(x)-k^2\tilde{N}^2\right]\right)\vec{E}(x)=0 \tag{2.30}$$

We consider now a planar dielectric waveguide displayed in Fig. 2.3. It consists of a film of thickness d and refractive index n_f surrounded by media (substrate and cladding) with refractive indices n_s and n_c, respectively. In order to support the guided modes in the waveguide, it is necessary that n_f must be larger than n_s and n_c. We will show later that under these conditions, light can be confined in the waveguide by total internal reflection at the interfaces between the high and low index materials. We have a symmetric planar waveguide, if $n_s = n_c$, while for $n_s \neq n_c$ the waveguide is asymmetric. In this thesis, we study the asymmetric planar waveguides only.

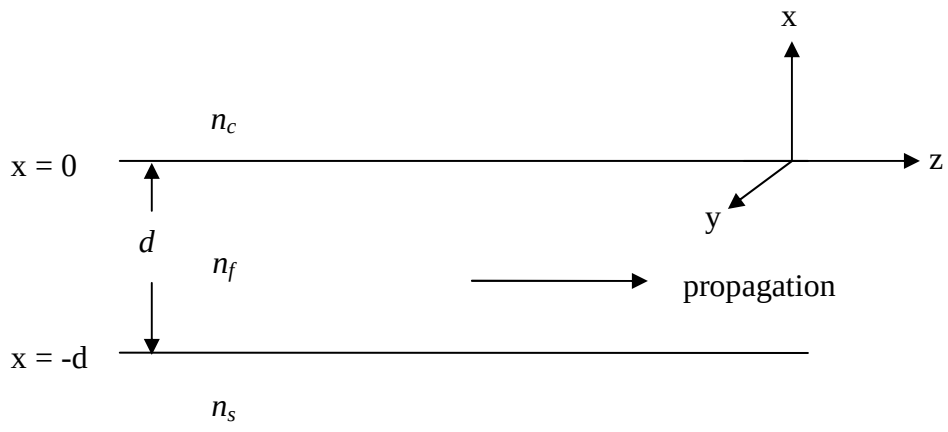

Fig. 2.3: A planar dielectric waveguide [Bahtiar'04].

Referring to Fig. 2.3, the refractive index profile n(x) is described by

$$n(x)=\begin{cases} n_c, & x>0 \\ n_f, & 0<x<-d \\ n_s, & x<-d \end{cases}. \tag{2.31}$$

We assume that $n_f > n_s > n_c$. The solution of wave equation for this refractive index profile depends on the value of $(k^2 n_i^2 - k^2 \tilde{N}^2)$, where *i* = *c*, *f*, *s*. Fig. 2.4 shows the illustration of electric field distribution for different values of propagation constant $k\tilde{N}$ at fixed frequency ω, redrawn after Yeh [Yeh'88].

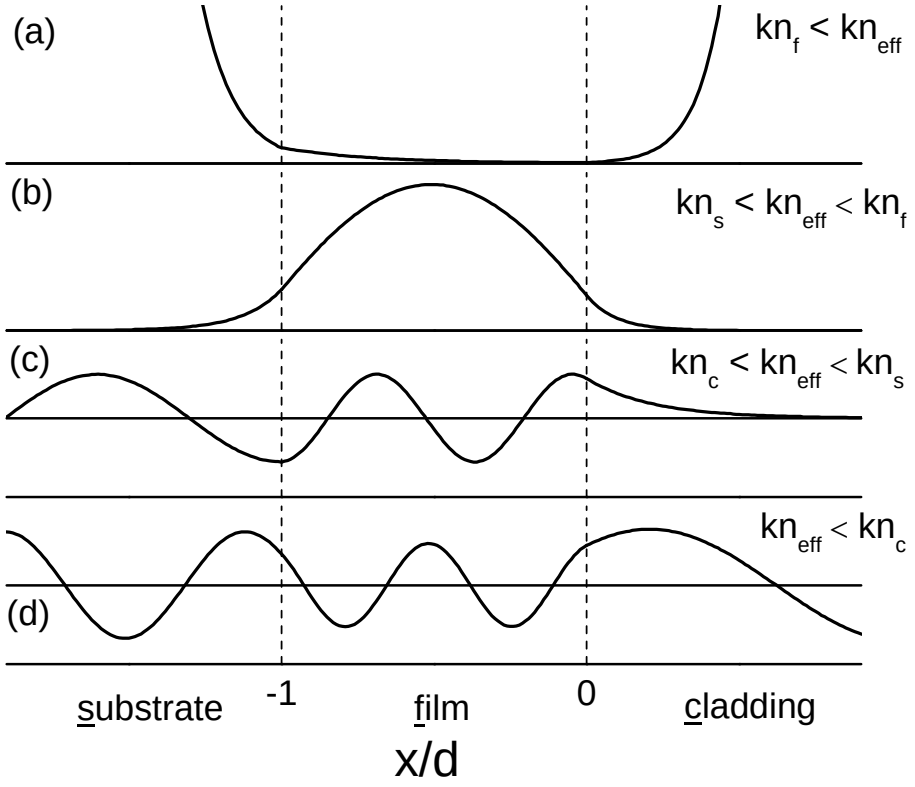

Fig. 2.4: Electric field distribution in a planar waveguide for different values of propagation constant $k\tilde{N} = kn_{eff}$, redrawn after Yeh [Yeh'88].

The electric field distribution E(x) for $k\tilde{N} > kn_f$ is exponential at all three regions, as illustrated in Fig. 2.4(a). It increases exponentially away from the waveguide. Physically, this solution is not realizable because it does not correspond to a real wave.

For $kn_s < k\tilde{N} < kn_f$, the solution is sinusoidal in the waveguide ($-d < x < 0$), but it decays exponentially in the surrounding media. It is possible to have solutions *E(x)* that satisfy the boundary conditions at the interfaces. One of the solutions is shown in Fig. 2.4(b). The energy carried by these modes is mostly confined in the guiding layer, only a small fraction is flowing into surrounding media. Therefore, these modes are referred as confined or guided modes. The confined modes are possible only if $n_f > n_c, n_s$. By applying the boundary conditions at interfaces, the values of allowed $k\tilde{N}$ are discrete. The number of confined modes depends on the thickness of waveguide, frequency or

wavelength, and the refractive indices n_c, n_f, and n_s. At a given wavelength, the number of confined modes increases with increasing film thickness.

Solutions of Eq. (2.30) for $kn_c < k\tilde{N} < kn_s$ correspond to exponential behaviour in the region $x > 0$ and to sinusoidal in the region x < 0, as illustrated in Fig. 2.4(c). These modes are referred as substrate radiation modes. Finally, the solution for $0 < k\tilde{N} < kn_c$ is sinusoidal in all three regions [Fig. 2.4(d)]. These are called as radiation modes of the waveguides.

We would like to discuss the derivation of the guided modes, which according to Fig. 2.4(b), have a propagation constant $k\tilde{N}$ ($kn_s < k\tilde{N} < kn_f$) for $n_c < n_s$. The guided modes of the planar waveguide can be classified as TE and TM modes. TE or transverse electric modes do not have a component of electrical field in the direction of wave propagation, while TM or transverse magnetic modes do not have a longitudinal magnetic field component. We will consider TE and TM modes separately.

2.3.1 Transverse Electric Modes

TE modes have their electric field perpendicular to the plane of incidence. They have only three field components: E_y, H_x, and H_z. The field component of E_y can be taken in the form [Taylor'74, Marcuse'74, Yeh'88]

$$E_y(x,z,t) = E_m(x)\exp\left[i(\omega t - k\tilde{N}z)\right] \tag{2.32}$$

$$H_x(x,z,t) = -\frac{k\tilde{N}}{\omega\mu_0}E_y \tag{2.33}$$

$$H_z(x,z,t) = \frac{i}{\omega\mu_0}\frac{\partial E_y}{\partial x} \tag{2.34}$$

By substituting Eq. (2.31) into (2.29), the function $E_m(x)$ can be written as

$$E_m(x) = \begin{cases} C\exp(-qx), & x > 0 \\ C[\cos(hx) - (q/h)\sin(hx)], & -d < x < 0 \\ C[\cos(hd) + (q/h)\sin(hd)]\exp[p(x+d)], & x < -d \end{cases} \tag{2.35}$$

where C is the normalization constant and h, q and p are given by

$$q^2 = \tilde{N}^2 k^2 - (n_c k)^2$$
$$h^2 = (n_f k)^2 - \tilde{N}^2 k^2 \qquad (2.36)$$
$$p^2 = \tilde{N}^2 k^2 - (n_s k)^2$$

The boundary conditions require that the tangential E and H fields be continuous at the interfaces $x = 0$ and $x = -d$. It means that E_y and $H_z = (i/\omega\mu_0)(\partial E_y / \partial x)$ are continuous at $x = 0$ and $x = -d$. By applying these requirements into Eq. (2.35), we obtain

$$\tan(hd) = \frac{h(p+q)}{(h^2 - pq)}. \qquad (2.37)$$

This equation is used to obtain the eigenvalues $k\tilde{N}$ for the confined TE-modes and it can be solved graphically or numerically.

2.3.2 Transverse Magnetic Modes

For transverse magnetic or TM modes, the magnetic field vector is perpendicular to the plane of incidence. The derivation of the confined TM modes is similar to that of TE modes. The nonzero field components H_y, E_x, and E_z are [Taylor'74, Marcuse'74, Yeh'88]

$$H_y(x,z,t) = H_m(x)\exp\left[i(\omega t - k\tilde{N}z)\right] \qquad (2.38)$$

$$E_x(x,z,t) = \frac{k\tilde{N}}{n_i^2 \omega\varepsilon_0} H_y \qquad (2.39)$$

$$E_z(x,z,t) = -\frac{i}{n_i^2 \omega\varepsilon_0}\frac{\partial H_y}{\partial x}. \qquad (2.40)$$

The function $H_m(x)$ for all three regions

$$H_m(x) = \begin{cases} -C\left[(h/\bar{q})\cos(hd) + \sin(hd)\right]\exp[p(x+d)], & x < -d \\ C[-(h/\bar{q})\cos(hx) + \sin(hx)], & -d < x < 0 \\ -(h/\bar{q})C\exp(-qx), & x > 0 \end{cases} \qquad (2.41)$$

where C is a normalization constant and h, q, and p are given by Eq. (2.36). The continuity of H_y and E_z components at the interfaces $x = 0$ and $x = -d$, leads to the eigenvalue equation for confined TM-modes

$$tan(hd) = \frac{h(\bar{p} + \bar{q})}{(h^2 - \bar{p}\bar{q})} \tag{2.42}$$

where

$$\bar{p} = \left(\frac{n_f}{n_s}\right)^2 p, \quad \bar{q} = \left(\frac{n_f}{n_c}\right)^2 q . \tag{2.43}$$

Again, similar to that of TE, this eigenvalue equation can only be solved graphically or numerically.

We can also solve the eigenvalue equation for both TE- and TM-modes by applying geometrical or ray optics. This is possible because the waveguide consists of layers of homogeneous dielectric materials. Wave propagation in each region can be represented by the superposition of two plane waves. One of the plane waves may be considered as the incident wave, while the other is viewed as reflected one. The total internal reflection is sufficient to assure the confinement of energy in the guiding layer. The phenomenon of total internal reflection can be found in literature [Hecht'87, Möller'88, Yeh'88]. Consider a ray of light A propagates in the film toward the film-substrate interface (x = -d) with an incident angle θ, as displayed in Fig. 2.5.

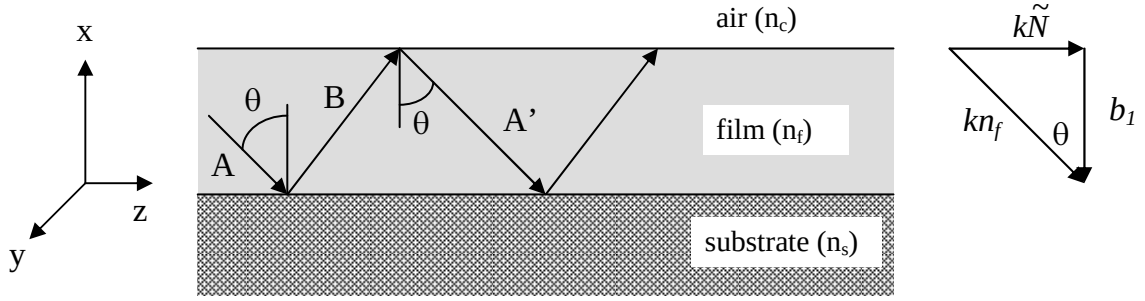

Fig. 2.5: Ray trajectory of a guided wave in a thin film waveguide. The coordinate system and wave vector are also given [Bahtiar'04].

If θ is larger than the critical angle $sin^{-1}(n_s/n_f)$, the ray A will be totally reflected into ray B at film-substrate interface. The phase of B at this interface is

$$\Phi_s = tan^{-1}\left(\frac{p}{h}\right) \tag{2.44}$$

for the TE modes and

$$\Phi_s = tan^{-1}\left(\frac{n_f}{n_s}\right)^2\left(\frac{p}{h}\right) \tag{2.45}$$

for the TM modes. Similarly, the B is reflected into A' at film-air interface (x = 0). In this case the phase changes are

$$\Phi_c = tan^{-1}\left(\frac{q}{h}\right) \tag{2.46}$$

for TE modes, and

$$\Phi_c = tan^{-1}\left(\frac{n_f}{n_c}\right)^2\left(\frac{q}{h}\right) \tag{2.47}$$

for TM modes, respectively. Here, $0 < \Phi_{ij} < \pi/2$, the constants p and h are given by Eq. (2.36).

We will use the zigzag model to derive the mode equation. As can be seen in Fig. 2.5, the ray A' follows the ray A after one zigzag path. Because the total reflection at both film-substrate and film-air interfaces, the amplitude of rays A and A' differs only by a phase Δ. After subsequent zigzags, the ray has phase differences 2Δ, 3Δ …relative to A. The superposition of such of rays is zero, except when $\Delta = 2m\pi$ with integer m. The total phase difference between A and A' is [Tien'70, Tien'77, Kogelnik'79]

$$2b_1 d - 2\Phi_s - 2\Phi_c = 2m\pi \qquad \text{m = 0, 1, 2, ...} \tag{2.48}$$

This equation is called as mode equation, where m represents the number of the mode. Equation (2.48) is valid for both TE and TM modes, but Φ_{ij} differ. According to the vector diagram in Fig. 2.5, we have

$$\begin{aligned} b_1 &= kn_f \cos\theta \\ k\tilde{N} &= kn_f \sin\theta \end{aligned} \tag{2.49}$$

For each allowed mode, the corresponding propagation constant and velocity are given by

$$\begin{aligned} kN_m &= kn_f \sin\theta_m \\ v &= c\left(\frac{k}{kN_m}\right) \end{aligned} \quad . \tag{2.50}$$

Effective refractive index can be defined as

$$n_{eff} = \frac{c}{v} = \frac{kN_m}{k} \tag{2.51}$$

which is bounded by $n_s < n_{eff} < n_f$.

2.3.3 Waveguide Propagation Losses

An important aspect of guided wave propagation in thin films is attenuation of the intensity of light along the propagation direction. Three different mechanisms can lead to propagation losses in the waveguide. The first mechanism is absorption of the electromagnetic energy by the molecules of the film. It occurs in the UV-Vis region due to electronic absorption and in the near infrared (NIR) region due to overtones of molecular vibrations. The second mechanism is volume scattering which is caused by imperfections, such as density variations, impurities, and defects within the volume of waveguide. These losses depend on the relative size of the imperfections as compared to the wavelength of the light and number of scattering centres (imperfections). The third mechanism is surface scattering loss or reflection loss. The second and the third mechanism were brought together in the paper of Ma [Ma'02] as follow:

$$\alpha_{gw}(\lambda) = a_0 + \frac{a_1}{\lambda^2} + \frac{a_2}{\lambda^4}, \tag{2.52}$$

where a_0 is representing the scattering of particles with a size, which is very large compared to λ, a_1 and a_2 are Mie- and Rayleigh-scattering coefficients, respectively. The second term in Eq. (2.52) was elaborated into more detail by Tien [Tien'71], who derived an expression for scattering due to surface roughness, based on the Rayleigh criterion. The scattering loss coefficient is defined as [Tien'71]

$$\alpha_s = \frac{A^2}{2}\left(\frac{cos^3\theta_m}{sin\theta_m}\right)\left(\frac{1}{d+\frac{1}{p}+\frac{1}{q}}\right) \tag{2.53}$$

$$A = \frac{4\pi}{\lambda}(\sigma_{cf}^2 + \sigma_{fs}^2)^{\frac{1}{2}}, \tag{2.54}$$

where d is the thickness of waveguide, θ_m is the incident angle, p and q are constants given by Eq. (2.36), σ_{fs} and σ_{cf} are the variances of surface roughness at film-substrate and film-air interfaces, respectively. We can understand from Eqs. (2.53) and (2.54) that the loss coefficient is reduced for small roughness at interfaces, thick films, long wavelengths and small mode number (large θ_m). The scattering loss of the fundamental mode (zero mode) is the smallest, because the electromagnetic fields concentrate mainly in the center of the waveguide. Therefore, the influence of the roughness at the film-substrate and film-air interfaces is not so large as compared to higher modes. A more detailed theory of surface scattering in planar waveguide has been developed by Marcuse [Marcuse'74].

To describe quantitatively the magnitude of optical loss, the attenuation coefficient is generally used. In that case, the intensity of light at any point along the length of the waveguide is given by

$$I(z) = I_0\, exp(-\alpha z) \tag{2.55}$$

where I_0 is the initial intensity. In the waveguides, the total propagation loss, α_{gw} is frequently expressed by

$$\alpha_{gw}\,[\text{dB/cm}] = 4.3\ \alpha\,[\text{cm}^{-1}] \tag{2.56}$$

2.3.4 Prism Coupling

The Prism coupling technique is reviewed by Tien [Tien'70, Tien'77] and others [Ulrich'70, Ulrich'73]. The technique has been exploited so far in many applications for example in sensing devices [Kadir'09, Descrovi'09].

Prism coupling is one of the most precise techniques used to characterize optical constants of the material layer of slab waveguide structures. The material layer usually

acts as a core layer but it is also possible as cladding layer or leaky waveguide. High refractive index prism of n_p is used to couple the light into the waveguide.

The coupling condition required to launch a mode m in a waveguide is given by Snell's law (or phase matching) [Lee'86]

$$k_p \sin \theta_i = k_f \sin \theta_{m,} \tag{2.57}$$

where k_p and k_f are wavevectors in prism and film, respectively. The angles of incidence at the prism base and mode angles are shown in Fig. 2.5 and Fig. 3.3, respectively. By adjusting θ_i properly, one can couple the light to any desirable propagating mode. The right sides of Eq. 2.30 contain the effective propagation constant kN_m of Eq. 2.42 and 2.25. Where kN_m is very unique and only determined by n_c, $n_{f,}$ n_s and d, in many cases refractive index of substrate and air gap thickness (cladding) are known. Thus by measuring several θ_i it is possible to determine n_f and d of the film.

Suppose we have two values of $\theta_{i,}$ namely θ_0 and $\theta_{1.}$ Using Eq. 2.51 we could have N_0 and N_1. Then using Eq. 2.44, one could have the following

$$n_f^2 = F\left(n_f^2\right); \quad F\left(n_f^2\right) = \left[\frac{N_0^2\psi_1^2 - N_1^2\psi_0^2}{\left(\psi_1^2 - \psi_0^2\right)}\right], \tag{2.58}$$

where

$$\psi_m = 2m\pi + 2\Phi_c + 2\Phi_s . \tag{2.59}$$

The Φ_{cf} and Φ_{fs} are defined in Eq. 2.38, 2.39, 2.40 and 2.41 for TE and TM respectively. But it can be we written in the compact form as Eq. 2.60

$$\Phi_j\left(n, N_m\right) = arctan\left[\left(\frac{n}{n_j}\right)^{2\rho}\left(\frac{N_m^2 - n_j^2}{n^2 - N_m^2}\right)\right]^{1/2}, \tag{2.60}$$

where $j=c$ and s, and $\rho = 0$ for TE polarization, $\rho = 2$ for TM polarization.

We found that the definition of ρ was misprinted in Ulrich and Torge paper [Ulrich'73], where it is written that ρ refers to "($\rho = 0$ for TE polarization, $\rho = 1$ and for TM)". The misprinted ρ =1 instead of 2 causes a wrong definition of Φ_0 and Φ_2. Ulrich and Torge [Ulrich'73] used Φ_0 and Φ_2, which are equal to Φ_s and Φ_c, respectively.

The value of n_f in Eq. 2.52 can be solved iteratively, by guessing an initial value, which inserted into the right side of Eq. 2.52 yields a new estimation for n_f. By repeating the process and using the following stopping criteria

$$\left|\frac{\partial F\left(n_f^2\right)}{\partial n_f^2}\right| < 1,$$

one could obtain the required n_f and d, which can be determined afterwards from n_f and Eq. 2.48.

The false definition of ρ for TM in Ulrich and Torge paper [Ulrich'73] led to value of n_f which is only slightly different to the true n_f. However, the misprint causes a significant difference between the thickness d_{TM} and d_{TE}, which must be identical, in principle.

2.4 Bruggeman Effective Medium Approximations

Optical response of media which consist of at least two components can be treated using the so-called Effective Medium Approximation (EMA) or Effective Medium Theory (EMT). Here we adopt the approximation, which is proposed by Bruggeman in 1935 [Bruggeman'35] because of its simplicity and advantages among others.

Consider the media consists of component a and component b, which have complex permittivity $\varepsilon^{(a)}$ and $\varepsilon^{(b)}$, respectively. The complex permittivity $\varepsilon^{(j)}$ is consists of

$$\varepsilon^{(j)} = \varepsilon_1^{(j)}(i) - i\varepsilon_2^{(j)} \tag{2.61}$$

where j=a and b. The real ε_1 and imaginary ε_2 part of permittivity are related to refractive index n and absorption coefficient α as written in Eq. 2.62a and 2.62b, respectively

$$\varepsilon_1 = n^2 - \left(\frac{\lambda\alpha}{2\pi}\right)^2, \tag{2.62a}$$

$$\varepsilon_2 = \frac{n\lambda\alpha}{\pi}. \tag{2.62b}$$

If respective volume fractions of component a and component b are δ_a and δ_b, then effective permittivity of mixture $\langle\varepsilon\rangle$ according to Bruggeman can be written as:

$$\delta_a \frac{\varepsilon^{(a)} - \langle\varepsilon\rangle}{\varepsilon^{(a)} + 2\langle\varepsilon\rangle} + \delta_b \frac{\varepsilon^{(b)} - \langle\varepsilon\rangle}{\varepsilon^{(b)} + 2\langle\varepsilon\rangle} = 0. \tag{2.63}$$

3 Experimental Methods

3.1 Spin Coating

Spin coating technique was used to prepare polymers thin films from their solutions. Thin films were prepared on fused silica substrates (Spectrosil 2000, Saint-Gobain Quartz GmbH, Germany and Precision Glass and Optics, USA) or BK7 substrates, which had a typical size of 25 mm x 35 mm and thickness of 1 mm. The substrates were cleaned by the following procedures:

- Washing with liquid soap and 10 x rinsing in purified water (Milli-Q, Millipore)
- 15 minutes cleaning in an ultrasonic bath with a solution of 1% detergent (Hellmanex, Hellma) in milli-Q water
- 10 x rinsing in purified water
- Cleaning with ethanol and subsequently drying the substrate in a flow of nitrogen.

The polymers were dissolved in appropriate organic solvents such as toluene, chlorobenzene or carbon disulfide. The solutions were filtered by means of micro-syringe filters (0.45 - 1 μm). Thin films were deposited on cleaned substrates by use of a spin coater (Headway Research Type: ECD101D) from freshly prepared and filtered solutions under a laminar flow hood to minimise dust particles. The rotation speed was varied from 500 to 9000 rpm (rounds per minute). The rotation time was set at 60 s. The film thickness d can be varied by adjusting solution concentration C_w and spinning speed ω, according to the empirical relation [Ziegler'00, Fitrilawati'02]

$$d_1 = d_0 \left(\frac{\omega_1}{\omega_0} \right)^{\alpha} \left(\frac{Cw_1}{Cw_0} \right)^{\beta} . \tag{3.1}$$

The coefficients α and β were determined experimentally. The exponent α was set to -0.5, which is typical for the spin coating process of polymers [Bornside'87, Lawrence'88]. The exponent β depends on the polymer and was determined experimentally (see chapter 4 and 5). Subsequent to the spin coating process, the films were annealed under vacuum for at least 4 hours at the elevated temperature T_a (around 45-50ºC) to let the residual solvent evaporate. The cooling process was done slowly (about 20ºC/h) to avoid stress of the polymer films.

3.2 Thickness Measurement

The thickness and the surface roughness of the polymer films were measured with a step-profilometer (KLA Tencor Coorporation Model P-10) by scanning the surface profile with a diamond tip (radius = 2 μm, force = 2 mg and sampling rate = 50 Hz). The film thickness was measured at a scratch on the film, which was made with a sharp needle. The film thickness was evaluated as the height difference between film surface and substrate surface at the scratch. The resolution of the thickness measurement was about 2 nm. The average surface roughness R_a is quantitatively determined from the average of absolute values of the profile height deviations [Tencor'98]. Surface roughness was measured with Tencor (P-10) profilometer by scanning the surface profile of the film at 1500 μm scale ranges.

3.3 UV-Vis-NIR Transmission and Reflection Spectroscopy

The dispersion of intrinsic absorption coefficient $\alpha(\lambda)$ and refractive index $n(\lambda)$ of thin polymer films ($d \approx 50 - 70$ nm) were determined from the spectra of the transmission T and reflection R. The T- and R-spectra were measured by using the UV-Vis-NIR spectrophotometer (Perkin Elmer model Lambda 900). The configurations for transmission and reflection measurements are shown in Fig. 3.1. The light was s-polarized which means that the electrical field vector was parallel to the film plane. T-spectra of thin films were measured at normal incidence [see Fig. 3.1(a)]. Part of light is reflected at interfaces such as air-film-, film-substrate- and substrate-air-interfaces, respectively. The R was measured using a reflection unit [Fig 3.1(b)] at an incidence angle of 15º, as it is not possible to measure R at normal incidence.

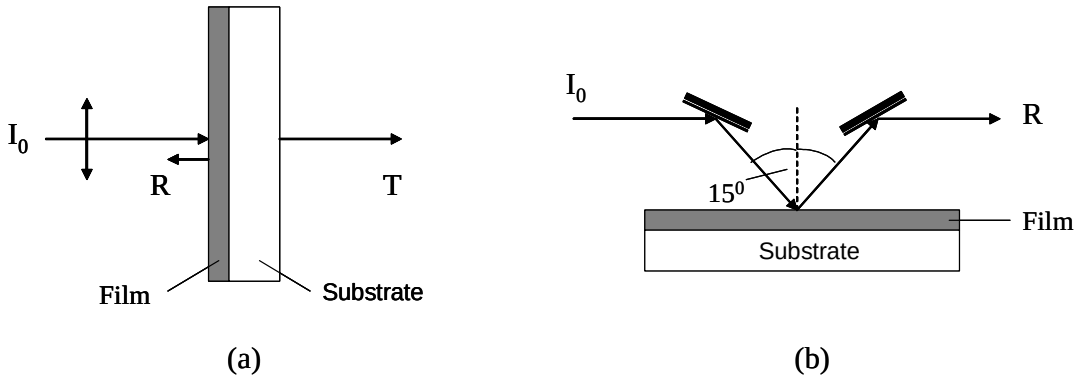

Fig. 3.1: The configuration for measurement of (a) Transmission and (b) Reflection of thin films on fused silica or BK7 substrates [Bahtiar'04].

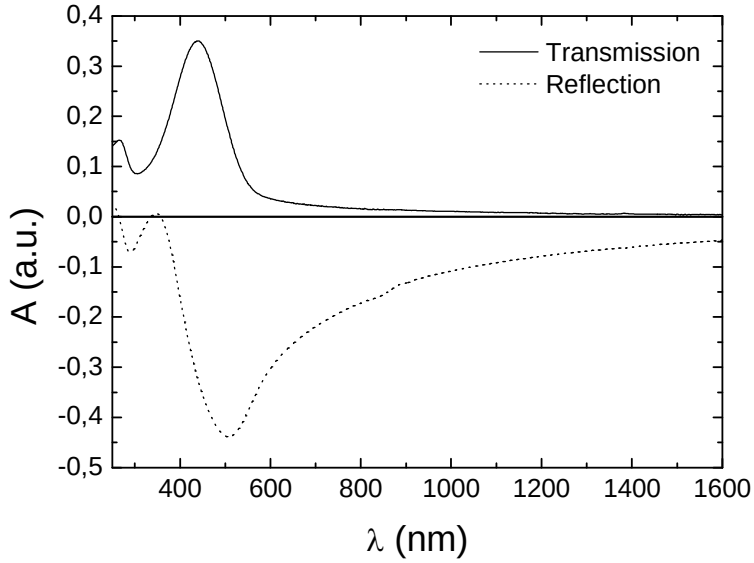

Fig. 3.2: Transmission and reflection spectra in absorbance (A) units of a regiorandom poly-3butylthiophene (P3BT-ra) thin film (P3BT-ra, see Chapter 6, d=50.7 nm) on top of a fused silica substrate.

Measurements were performed using a bare fused silica or BK7 substrate as reference depending on the kind of substrate of the sample. A typical measured transmission and reflection spectrum is shown in Fig. 3.2. From transmission and reflection one can determine the refractive index n(λ) and absorption coefficient α(λ) of the film by using equations 5-2-5 and 5-2-6 in page 110 of Yeh [Yeh'05]. This method is called reflectometry [Ueberhofen'99]. Calculation of refractive index and absorption coefficient from T and R was done by means of the available computer program (Bitrab Version 2.0, 2007). The program was developed by W. Scholdei [Scholdei'07] from earlier versions which were written by R. Schwarz [Schwarz'92a, Schwarz'92b] and K. Ueberhofen [Ueberhofen'96] in the group of C. Bubeck at MPI-P. The Program is based on the Levenberg-Marquardt Algorithm to solve the least squares curve fitting problem between experimental data points (from reflectometry) and equation of R and T in Yeh [Yeh'05]. The dispersions of n(λ) and α(λ) are depicted in Fig. 5.12 which are solutions of equations in Yeh [Yeh'05] for specific T and R in Fig. 3.2.

3.4 Prism Coupling

The prism coupling technique is well established to measure refractive index and thickness of waveguides with high precision. Theory, experimental setup and numerical

evaluation method of the prism coupler were described by Tien and Ulrich [Tien'69, Ulrich'70 and Ulrich'73]. Two setups were used in our studies, linear prism coupling and nonlinear prism coupling as described in earlier work [Ueberhofen´96, Deutesfeld´96 and Bahtiar´04].

Linear Prism Coupling Setup

The linear prism coupling setup is depicted in Fig. 3.3. Four different laser sources were used: He-Ne: (632.8 nm), continuous wave (cw) Nd:YAG: (1064 nm), Argon: (488.0 nm), and Kr: (676.4 nm).

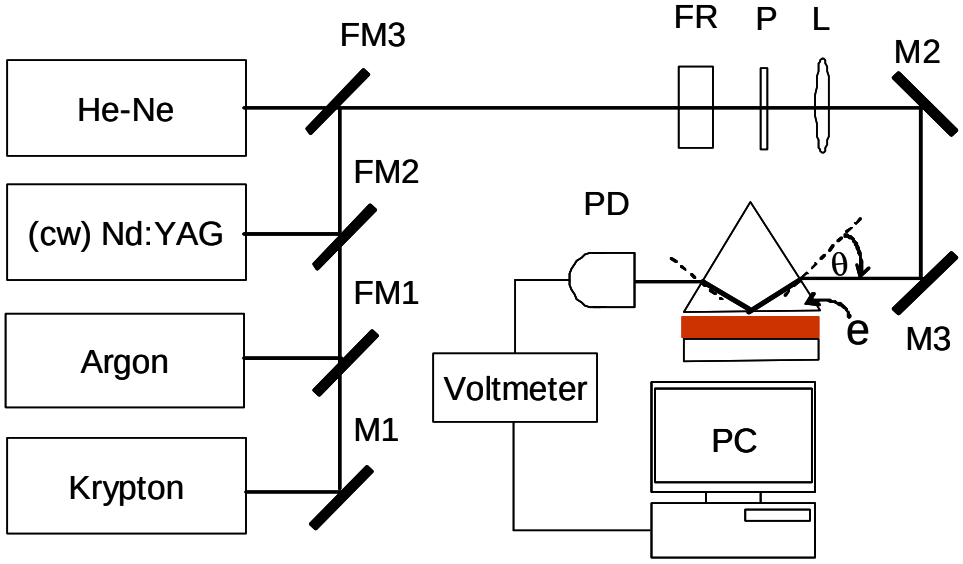

Fig. 3.3: Experimental setup of linear prism coupling. e: prism angle, cw: continuous wave, PC: computer, PD: Photodiode, P: Polarizer, L: lens, FR: Fresnel Rhomb, M1, M2 and M3: permanent mirrors and FM1, FM2 and FM3: Mirrors on flip-mounts.

A lens of focal length L = 60 cm was used to focus the polarized beam onto the base of an equilateral triangular prism, which was made from N-LaSF9 glass (Schott). The prism was mounted on a holder which is placed on a computer controlled goniometer. A slab waveguide was pressed against the prism base with the film facing the prism base. The focused laser beam was totally reflected from the prism base, then transmitted out of the prism and hits the photo-detector (PD). A Silicon photo-detector was used to convert the intensity of light to electric output signal, which is measured with the voltmeter (PREMA 5000) and recorded by computer. The plots of recorded reflected intensities I_R versus incident angles θ are called coupling curve. An example is shown in Fig. 3.4 a PVK thin film (d ≈ 1 μm) on BK7 substrate, three lowest order TE modes were excited.

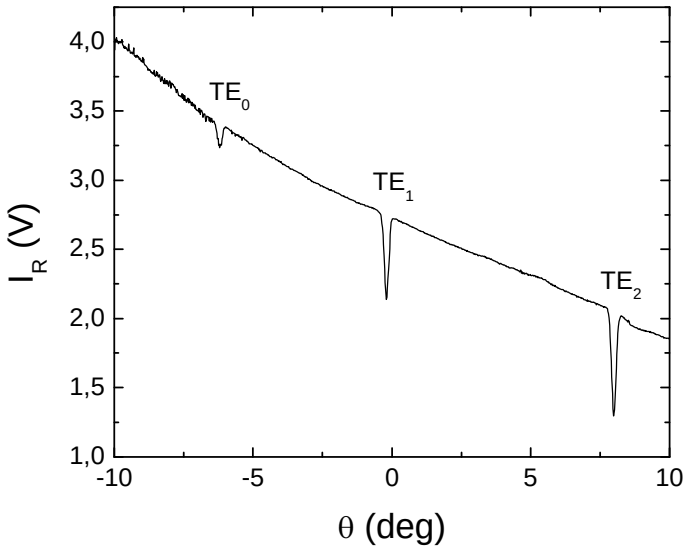

Fig. 3.4: Coupling curve of a PVK thin film of 1 μm thickness on top of BK7 excited with the He-Ne laser (λ=632.nm). Three clear TE modes were observed in the measurement range of coupling angle θ from -10 to 10 degrees.

Refractive index and thickness of the film were determined from coupling angle data of observed modes by using an available computer program prismcoupling.exe which was developed by M. Jahja from Ulrich report [Ulrich'73] and some sources [Marcuse'74 and Yeh'88].

Nonlinear Prism Coupling Setup

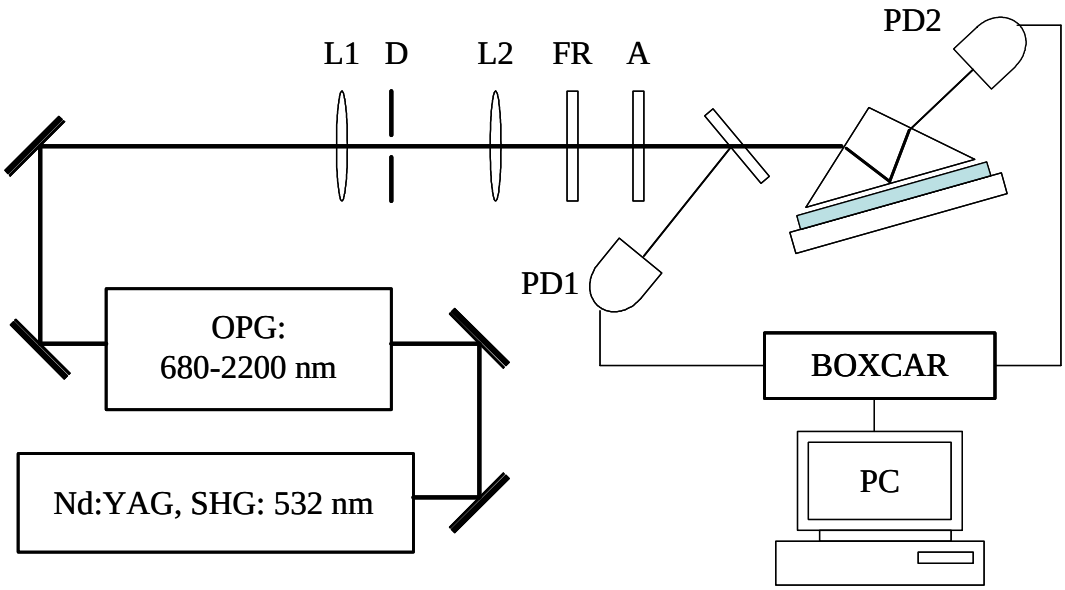

Fig. 3.5: Experimental setup of nonlinear prism coupling adopted from A. Bahtiar [Bahtiar´04]. SHG: second harmonic generation, OPG: optical parametric generation, L1, L2: lenses, D: spatial filter, FR: Fresnel Rhombus, A: Polarizer, BS: beam splitter, PD1, PD2: photodiode, PC: computer.

The second-harmonic output (SHG: 532 nm) of the Nd:YAG laser (from EKSPLA, Model 2143B) was used to pump the optical parametric generator (OPG) (from EKSPLA, Model PG), which produced variable laser wavelengths between 680 nm and 2200 nm. The laser pulse duration depends on the laser wavelength. The following typical pulse duration for 1064 nm is 28.02 ps and OPG output is 15.02 ps were observed in earlier work [Kim´08 and Bahtiar´04].

Laser pulse energy was measured with pyroelectric detector (Laser probe model RjP-735). Spatial filter D is composed of two lenses (focal length of 8 cm and 6 cm)**.** The lens L2 has a focal length of 100 cm. The Fresnel Rhomb (FR) was used in combination with the polarizer (A) to vary the intensity of the laser pulses. Photo-detector PD1 was used to compensate pulse-to-pulse energy fluctuations of the laser pulses. Photo-detector PD2 was used to measure reflected intensity from the prism base. Signals from PD1 and PD2 were collected with a BOXCAR amplifier (from Stanford Research System Model SR250) and displayed as reflected intensity versus coupling angle on the computer.

3.5 Attenuation Loss of Slab Waveguides

The prism coupling technique was employed to determine the waveguide loss as described earlier [Mathy'89]. The setup is depicted in Fig. 3.6. Two laser sources were used HeNe (λ = 633 nm) and cw-Nd:YAG (λ = 1064 nm). The laser beams were coupled to waveguide using a high refractive index prism P made from N-LaSF18A

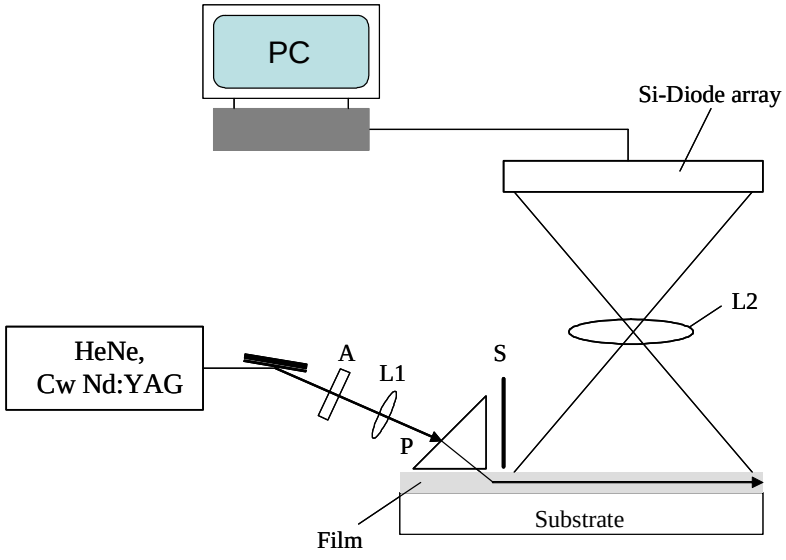

Fig. 3.6: Experimental setup for waveguide attenuation loss measurement adopted from A. Bahtiar [Bahtiar'04]. A: polarizer, L1, L2: lenses, P: prism, S: shield, PC: computer.

The film was pressed against the half-cut prism mounted on a precision rotation table. The lens L1 of focal length 60 cm was used to focus the laser beam at the coupling edge of the prism. The coupling angle was adjusted until a guided mode was launched in the waveguide.

The lens L2 (focal length = 40 mm, diameter = 40 mm) was used to image the scattered light from the waveguide onto a diode array. The black paper S was used to suppress the stray light of the coupling prism. Attenuation loss coefficients α_{gw} were determined from the scattered light intensity as function of distance from the coupling prism

$$\alpha_{gw}[dB/cm] = \frac{10}{x} log\left(\frac{I_0}{I_x}\right), \tag{3.2}$$

where I_0 and Ix are scattered light intensity at 0 position and after propagation along distance of x respectively. The distance calibration was performed by means of millimetre paper at the same position, which was imaged onto the diode array. At wavelength 1064 nm, the propagation of light in the waveguide can be observed by means of an IR-camera (Microviewer from Polytech Model 7290). The detection limit of this method is in the order of $\alpha_{gw} \approx 0.5$ dB/cm.

3.6 Photostability

There are two kinds of photostabilities that we measured, the so-called wavelength dependence of photostability and the intensity dependence photostability, i.e. the ablation threshold intensity. All of the experiments were done in ambient air.

Wavelength dependent photostability

The experiments were performed in the following way: A high pressure 450 Watt Xenon lamp (AMCO Model XBO 450 OFR) combined with a water filter and a variety of edge filters (Schott) was used to irradiate the polymer films as sketched in Fig. 3.7.

Fig. 3.7: The wavelength dependent photostability setup, WF: Water Filter, EF: Edge Filter, S: Sample.

The transmission spectra of the edge filters are shown in Fig. 3.8. First, a longer wavelength edge filter (λ_e > 665 nm) was used and then the shorter wavelength filters were employed. For each filter, the absorption of the film was measured after every 10 minutes exposure. The aim of this experiment is to find the cut-off wavelength (λ_c), where no absorption changes of the sample are observed after irradiation at $\lambda > \lambda_c$.

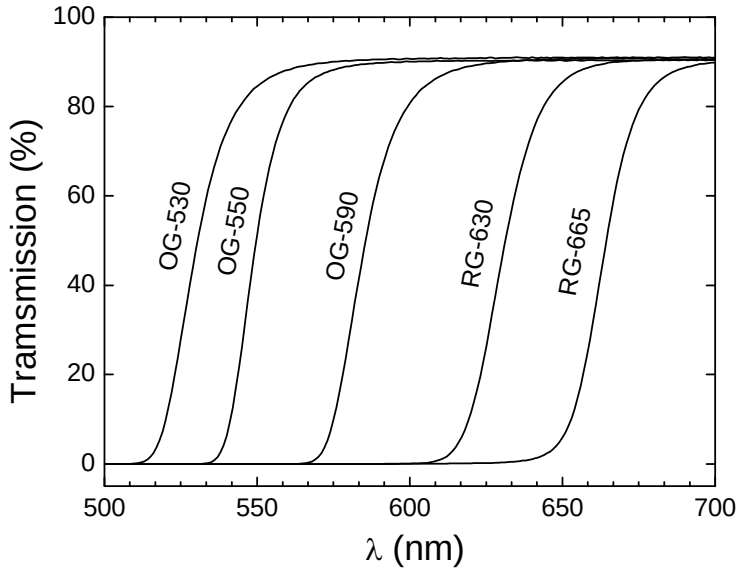

Fig. 3.8: Transmission of several edge filters, which were used in photostability experiments.

Ablation threshold intensity

The experiment was aimed to determine the so-called threshold intensity of pulsed laser ablation. Laser ablation is the process of removal material from the film surface by high intensity exposure [Chichkov'96]. The wavelength of the laser was chosen where the sample has very small absorption. Usually it was 1064 nm.

High intensity laser pulses can damage the surface of the sample, for example see Fig 3.9 as an illustration. The diameter of damaged area D was determined from optical microscopy. The damaged threshold F_{th} was determined from the linear curve fitting of square of D vs. F_0. The relation between D, F_0 and F_{th} was given by Krüger [Krüger'04] as follows

$$D^2 = 2\sigma_x^2 ln\left(\frac{F_0}{F_{th}}\right), \tag{3.3}$$

where F is fluence (J/cm^2) defined as pulse energy per cm^2, σ_x is defined as the 1/e^2-Gaussian beam radius. The determination of energy threshold does not need any information about σ_x (see eq. 3.3); even one could determine σ_x from the slope of the linear fit of plot D^2 versus *ln(E)*.

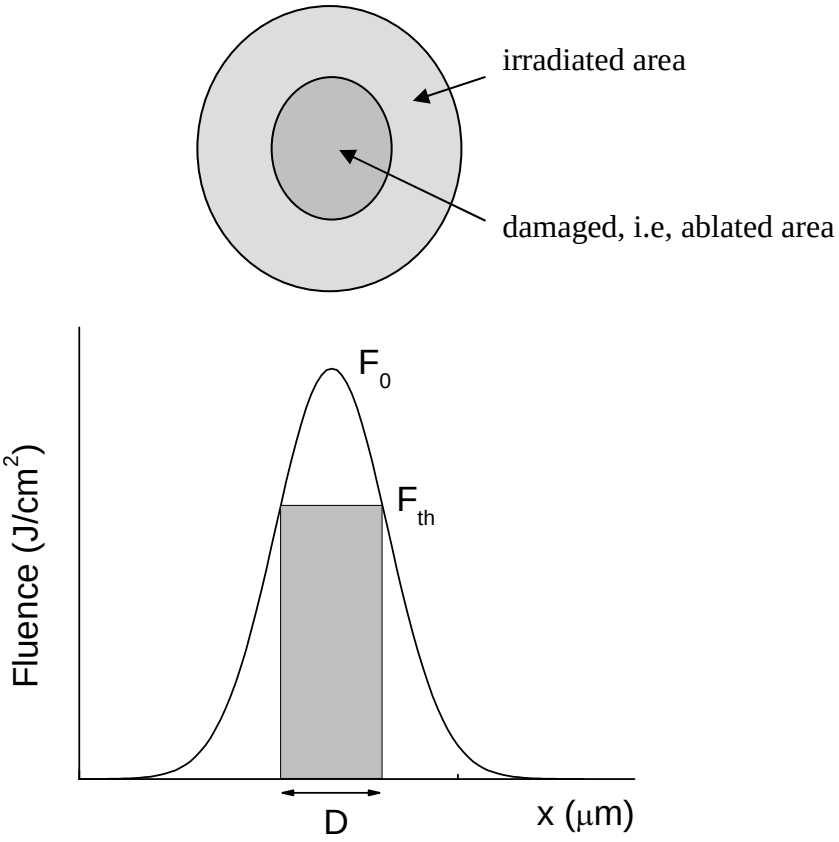

Fig 3.9 Illustration of damaged area of the sample related with gaussian beam profile of laser, redrawn from Krüger [Krüger'04].

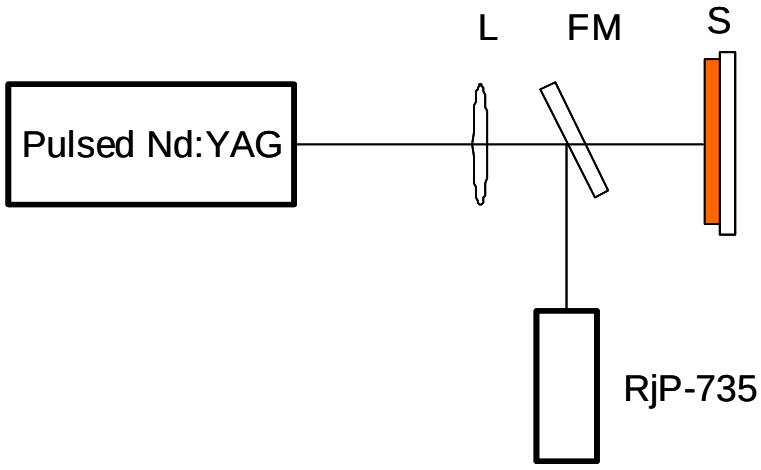

Fig. 3.10 Pulsed laser ablation setup, lens L of focal length 60 cm, FM: mirror flip-flop mount, used to reflect beam into the pyroelectric detector (Laser probe model RjP-735).

Nd:YAG (λ=1064 nm) laser pulses were focused by lens L (f= 60 cm) onto the film surface S. Some points on the sample surface were marked for exposures. A single exposure consists of 100 pulses each. Pulse energy was measured with pyroelectric detector (Laser probe model RjP-735) at the position of the sample. The beam diameter of the laser was determined by IR laser beam profiler (Newport Model LBP-2-USB).

4 Optical Constants of Polymer Thin Films – Results and Discussion

Optical constants of polymer thin films are determined by their chemical structure, substituent and molecular weight, but depend also on the preparation technique. Spin-coating is a frequently used and well-known film preparation technique. In the spin-coated films, polymers may be aligned preferably parallel to the substrate plane, depending on their chemical structure and preparation condition. Different orientations of chain segments with respect to the film plane could be indicated by optical birefringence.

Two kinds of polymers are addressed here: polyvinylcarbazole (PVK) and polystyrene (PS) and the conjugated polymer MEH-PPV. PVK and PS have anisotropic moieties (carbazole and phenyl ring of PVK and PS, respectively), which are attached to the polymer backbone. In MEH-PPV, the polymer backbone behaves like rigid rod. Although these polymers are having a different nature of anisotropy, the optical constants of the polymers usually show significant anisotropy [Prest'79, Prest'80, Zhokhavets'04, Koynov'04, Campoy-Quiles'05 and Koynov'06].

Recently, photonic crystals of PS turned out as promising all-optical switches [Hu'05, Liu'09]. Because Hu et. al. claim, that PS has very large cubic nonlinearities, we investigated the intensity dependent refractive index of PS waveguides at 532 nm.

4.1 Poly(9-vinylcarbazole) (PVK)

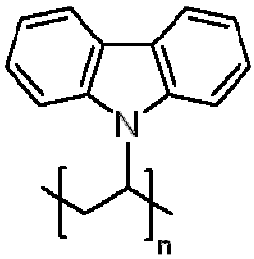

Fig. 4.1: Chemical structure of Poly(9-vinylcarbazole) (PVK).

Poly(9-vinylcarbazole) or (PVK) (chemical structure depicted in Fig. 4.1) has already found many applications because of its remarkable photoconductivity [Zhang'98], high thermal stability and good processability [Fitrilawati'99]. Its main application is photoreceptor in photocopy machines. It has found also applications in electroluminescence devices [Gebler'98, Allegrini'99], as matrix for NLO dyes and polymers [Zhang'98, Bermudez'00]. Recently, PVK and carbazole derivatives based

polymers have shown large third-order nonlinear optical susceptibility in the order of 10^{-13} esu at the wavelength of 532 nm [Fuks'02].

PVK thin films are optically anisotropic, because of the rigid carbazole moieties. Inconsistencies of optical constants of anisotropic thin films have been described in the literature [Campoy-Quiles'05 and Koynov'06], which are probably caused by different preparation conditions and measurement methods. To solve this problem, a European collaborative study was carried out in order to compare the optical constants of identical thin films, which were measured with different techniques. We were involved in this study with our prism coupling results of PVK [Campoy-Quiles'08].

PVK powder was purchased from Aldrich (M_w=1.1x10^6 g/mol, T_g = 200ºC) and used as received. Thin films were made from fresh and filtered (0.45 μm syringe driven filters) chlorobenzene solutions by means of spin coating onto freshly cleaned fused silica substrates. They were prepared at ambient atmosphere under a laminar flow hood to minimize dust particles as described in detail earlier [Koynov'06]. The spin coating parameters of PVK were available from Marcia Becker [Becker'05]: α = -0.5, β = 1.39 and d_0 = 35.8 nm for C_{w0}= 1 % and ω_0 = 1000 rpm. We used Eq. 3.1 to determine the appropriate spinning speed and concentration of the solution to produce PVK films with the desired thicknesses.

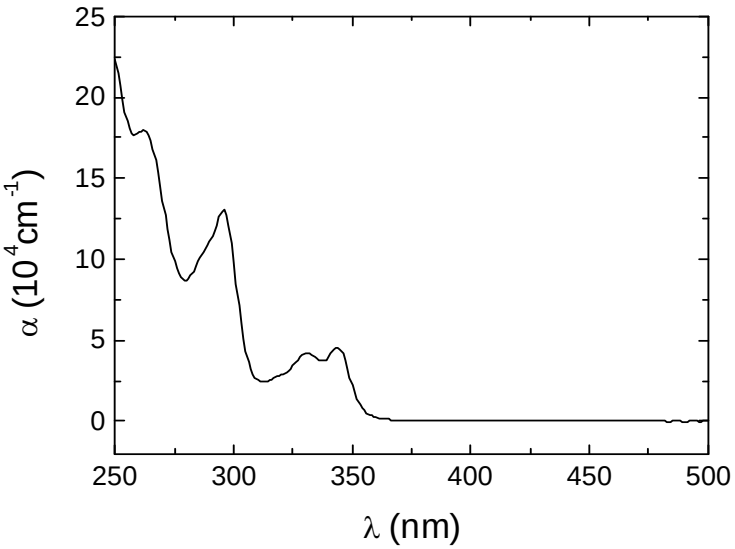

Fig. 4.2: Absorption coefficient of PVK thin film of thickness d=39.8 nm determined from reflectometry. It has some peaks at 262 nm, 296 nm, 331 nm and 344 nm which are consistent with peak positions reported by Fuks et. al. [Fuks'02].

Optical constants (absorption coefficient and refractive index, see Fig. 4.2 and 4.3, respectively) were determined by reflectometry of very thin films (d ≈ 50 nm) for TE mode polarization only. Refractive indices of both polarizations (TE and TM) at

particular wavelengths were determined by the prism coupling technique of waveguides (d=500-1000 nm).

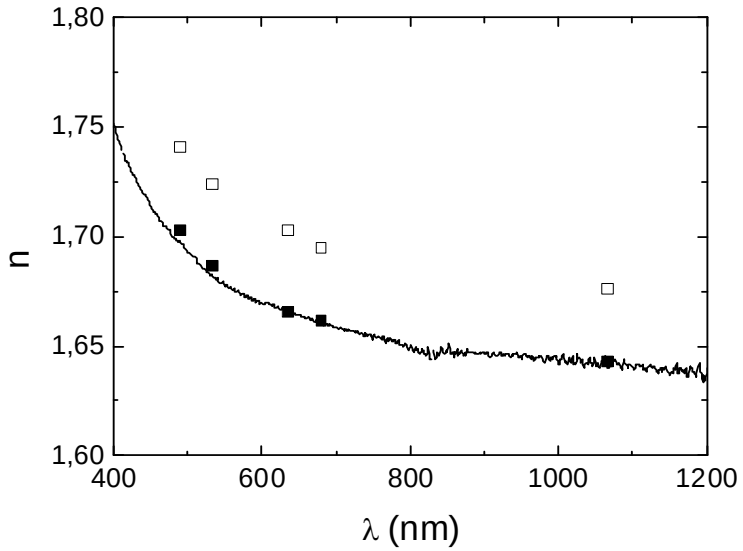

Fig. 4.3: Refractive index dispersion of PVK films measured by reflectometry (lines) and prim-coupling (TE- and TM-data are filled and open squares, respectively). There is a good agreement between n_{TE} values, which are obtained from both techniques.

It is clear from Fig. 4.2 that PVK thin films are transparent at VIS-NIR range (375 – 1600 nm) which make it possible to perform prism coupling measurements at several available laser wavelengths (488 nm, 532 nm, 633 nm, 678 nm and 1064 nm). The prism coupling measurement provides more precise data as compared to reflectometry and ellipsometry techniques [Ulrich'73 and Campoy-Quiles'08]. Table 4.1 shows the comparison between refractive indices at 633 nm from prism coupling, reflectometry and average data of ellipsometry techniques in Campoy-Quiles et al. [Campoy-Quiles'08]. Prism coupling data have precision of 4 to 3 decimal places for TE and TM respectively, which are more precise than ellipsometry results.

Table 4.1: Refractive indices of PVK thin films which are measured by different techniques at 633 nm. (a) this work, (b) from Campoy-Quiles et. al. [Campoy-Quiles'08]

PRISM COUPLING (A)		REFLECTOMETRY (A)	ELLIPSOMETRY (B)	
n_{TE}	n_{TM}	n_{TE}	n_{TE}	n_{TM}
1.6658±0.0006	1.7003±0.0010	1.66±0.01	1.677±0.007	1.73±0.02

The agreement of the refractive index data of very thin films (d≈50 nm) with waveguide results (d=500-1000 nm) reveals that there is no thickness dependence of the refractive index of PVK films in the thickness range studied here. This confirms the

earlier report that PVK ($M_w \approx 1.5x10^6$ g/mol) does not show a strong thickness dependence of the refractive index [Prest'80]. However, the optical birefringence $\Delta = n_{TE} - n_{TM}$ of PVK thin films depends on boiling point (T_{BP}) of the solvents, see Fig. 4.4.

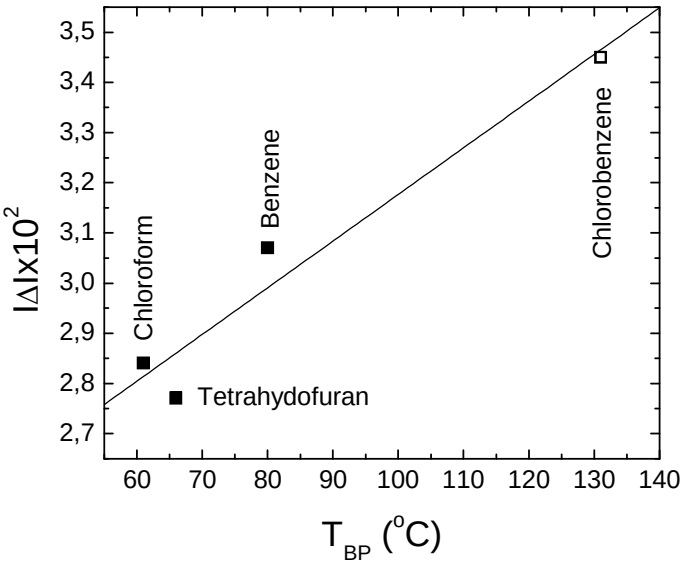

Fig. 4.4: Absolute values of optical birefringence Δ of PVK films (filled squares are from Prest et.al. [Prest'80] and open square is from this work) plotted versus boiling temperature T_{BP} of solvents.

Refractive indices and thicknesses of waveguide were calculated from coupling angles, which were obtained from prism coupling measurement. Coupling angles are extracted from the minima of the coupling curve. An example of PVK films on fused silica (FS) substrates, which were excited with 632.8 nm He-Ne laser and studied with LaSF18A prism (prism angle e = 60˚; refractive index n_P=1.907738) is listed in Table 4.3. Calculations were done using two different programs which are available in group of C. Bubeck of MPI-P Mainz. The computer program: INDEX01.exe (program A) was developed by Hansjörg Menges [Mathy'89] based on Eq. 10 of Ulrich report [Ulrich'73] and the program prismcoupling.exe (program B) developed in this work is based on Eq. 6.30 of Lee [Lee'86], see Eq. 2.58.

Table 4.2: Coupling angles of a particular PVK film on fused silica substrate.

MODE	θ_M (DEG)	
	TE	TM
0	0.15	4.05
1	-3.95	-0.85
2	-10.20	-8.35
3	-18.35	-17.50

Refractive indices and thicknesses were calculated from coupling angles in Table 4.2. They are displayed in Table 4.4 and 4.5 for TE and TM respectively. For TE polarization there is no significant difference of both equations concerning n_{TE} and d_{TE}. But for TM polarization, the thickness d_{TM} differs significantly, see Tab. 4.4. Clearly, the thicknesses d_{TE} and d_{TM} should agree within the experimental error. The data shown in Tab.4.3 and 4.4 indicates that the evaluations based on Eq.2.58 show closer agreement as compared to Eq. 10 [Ulrich'73]. Obviously, the misprint of ρ for Eq. 10 [Ulrich'73] causes a still small, but visible discrepancy of the data at TM polarization.

Table 4.3: Comparison of n_{TE} and d_{TE}, which were calculated from Eq. 10 of Ulrich and Eq. 2.58

	ρ=0 (PROGRAM A)		ρ=0 (PROGRAM B)	
TE_n & TE_m	n_{TE}	d_{TE}(μm)	n_{TE}	d_{TE} (μm)
TE_0 & TE_1	1.665662	1.3700	1.665663	1.369983
TE_0 & TE_2	1.665459	1.3833	1.665459	1.383252
TE_0 & TE_3	1.665593	1.3745	1.665593	1.374488
TE_1 & TE_2	1.664359	1.3913	1.664360	1.391324
TE_1 & TE_3	1.665313	1.3756	1.665314	1.375614
TE_2 & TE_3	1.668060	1.3647	1.668060	1.364644
average	**1.666 (0.001)**	**1,377 (0.009)**	**1.6657 (0.0008)**	**1,377 (0.007)**

Table 4.4: Comparison of n_{TM} and d_{TM} which were calculated from Eq. 10 of Ulrich and Eq. 2.58

	ρ=1 (PROGRAM A)		ρ=2 (PROGRAM B)	
TM_n & TM_m	n_{TM}	d_{TM} (μm)	n_{TM}	d_{TM} (μm)
TM_0 & TM_1	1.700151	1.3189	1.700154	1.350590
TM_0 & TM_2	1.700190	1.3169	1.700211	1.347604
TM_0 & TM_3	1.700155	1.3187	1.700269	1.344568
TM_1 & TM_2	1.700400	1.3157	1.700517	1.345804
TM_1 & TM_3	1.700170	1.3187	1.700731	1.343013
TM_2 & TM_3	1.696504	13120	1.701355	1.340919
average	**1.7001 (0.0003)**	**1.318 (0.002)**	**1.7005 (0.0003)**	**1.345 (0.003)**

The prism coupling technique can be used also to measure the waveguide propagation loss α_{gw}, which is an important parameter in integrated optics. It contains information about intrinsic absorptions and scattering losses, which are related strongly with the morphology of thin polymer films. Figure 4.5 shows the scattered intensity of TE_0, TE_1 and TE_2 modes in a PVK waveguide excited with He-Ne (633 nm) laser. The value of α_{gw} is caused mainly by scattering losses of the surface and the interior of the

film, because at this wavelength intrinsic absorption of PVK is negligible. Effects of surface roughness to α_{gw} of PVK films have been reported earlier [Firilawati'99, Ziegler'00].

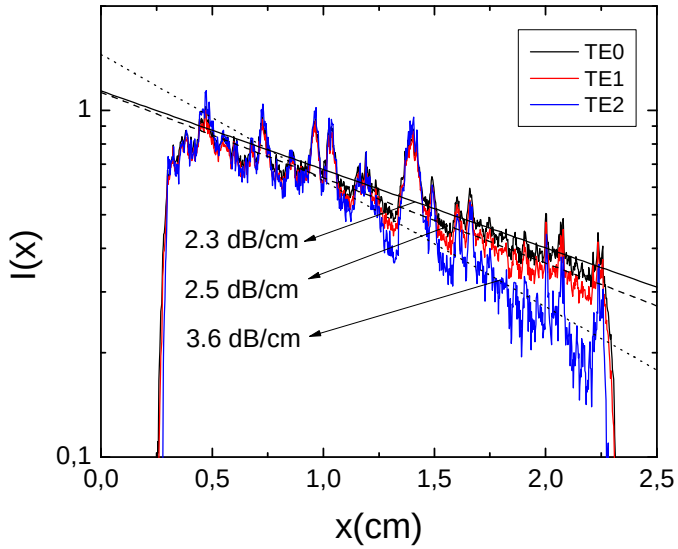

Fig. 4.5: Scattered intensity (I) of TE_0, TE_1 and TE_2 modes of guided wave in a PVK waveguide measured along propagation distance (X) obtained from waveguide loss setup at 633 nm (lines). The film thickness is 1.15 ± 0.05 µm. Waveguide loss (α_{gw}) of 2.3 dB/cm=0.4 cm^{-1}, 2.5 dB/cm=0.6 cm^{-1} and 3.6 dB/cm=0.8 cm^{-1} was determined from the slope the linear fit (straight lines).

PVK waveguide (PVK film of thickness d=1133 nm coated onto BK7 substrate) was measured with prism-coupling setup (LaSFN9 prism) and excited with He-Ne laser (λ = 632.8 nm). Three TE modes (TE_0, TE_1 and TE_2) and two TM modes (TM_1 and TM_2) were excited in the waveguide. Reflected intensity from the waveguide is plotted against coupling angle θ. This plot is also called coupling curve in the following. Refractive index and the optical thickness of the waveguide were determined from the minima positions of coupling curves. The laser beam diameter d_b = 175 µm was measured with a beam profiler. The only parameter, which has been varied for each mode is the waveguide propagation loss α_{gw} which is tabulated and compared to experimental values obtained from the waveguide loss setup (see Table 4.5). Both results agree very well and prove that the fit of the coupling curves provides valuable results.

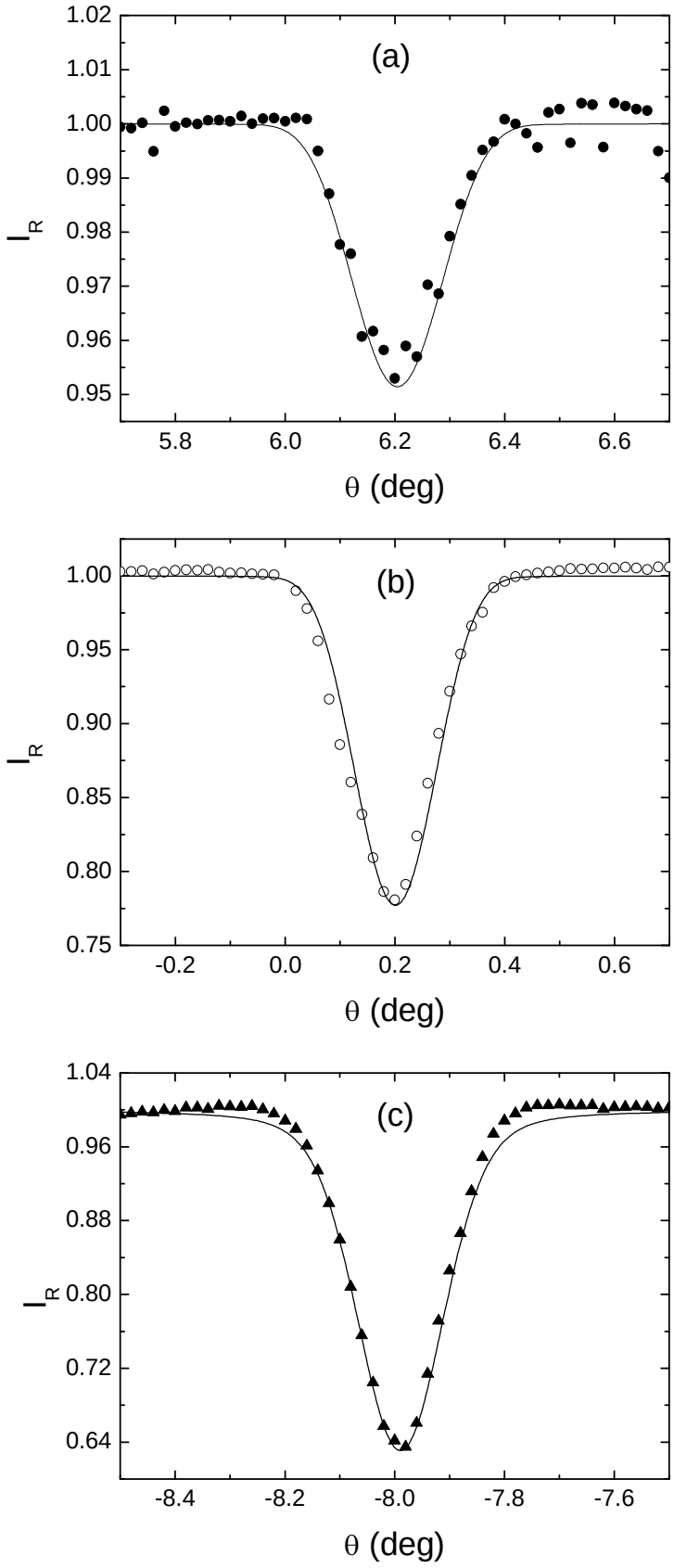

Fig. 4.6 Coupling curves of PVK waveguide (d=1133 nm excited with 633 nm He-Ne laser) from prism coupling (symbols) and their fits (lines) for (a) TE_0 (b) TE_1 and (c) TE_2 mode. More detail about fitting parameters could be found in the text.

Table 4.7: Comparison between α_{gw} obtained from fitting and experiment.

MODE NUMBER	α_{GW} (CM^{-1})	
	From fit	Experiment
TE_0	0.5	0.5 ± 0.2
TE_1	0.6	0.6 ± 0.2
TE_2	1.0	0.8 ± 0.2

Before performing intensity dependent nonlinear prism coupling, we determine the air gap thickness by measuring coupling curves at different clamping pressures as shown in Fig. 4.7. The coupling curves of TE_0 mode of PVK film on BK7 substrate were excited using 633 nm laser and measured at different clamping pressures (p_1, p_2 and p_3). Symbols are experimental results and lines are numerical fits. As the clamping pressures increases from p_1 to p_2, the coupling curve shifted to the smaller angle of incidence θ and is becoming deeper. The I_R change continues as clamping pressure increases from p_2 to p_3. The change of I_R, is only related to change of distance between prism and film or air gap thickness (d_a). As d_a decreases, the amount of light which couples to the waveguide mode increases, as can be seen as decrease of I_R. But when d_a is continuing to decrease, the amount of light coupled into the waveguide is not increasing as much as resulted in the former change because the amount of light coupled back from the waveguide into the prism is also increasing [Ulrich'70, Moneret'00, and Koynov'02].

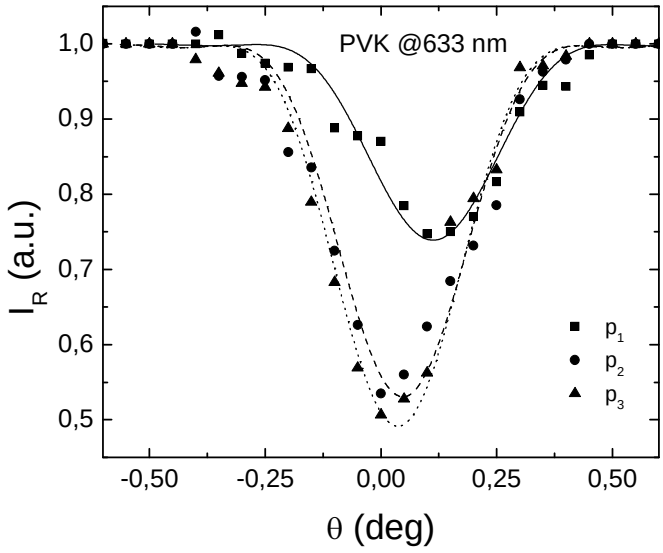

Fig. 4.7: The TE_0 coupling curves of PVK film on a BK7 substrate (film thickness 1159 nm, laser wavelength 632.8 nm) with different clamping pressures (p_1, p_2 and p_3 where $p_3 > p_2 > p_1$). Symbols are experimental data and lines are numerical fits. Some fitting parameters were kept constants (d_b=120 μm, n=1.6689 and α_{gw}=0.25 cm^{-1}) and only the air gap thickness was varied (d_{a1}=145, d_{a2}=115 and d_{a3}=110 nm).

Intensity dependent prism coupling has been applied to determine the $n_{2,}$ α_2 and α_{gw} of PVK film. The SHG beam (λ=532 nm) of Nd:YAG laser was used to excite the PVK waveguide of thickness 1164 nm. The coupling curve I_R vs. θ is depicted in Fig. 4.8. A consistent slight shifting of minima θ_m of the coupling curve to larger θ is seen as pulse energy E_p increases. The shifting is related to the change of refractive index of the film. The minimum values of $I_R(\theta_m)$ also consistently become smaller as the pulse energy E_p increases, which is related to a change of the absorption coefficient of the film.

The refractive index n_f and absorption coefficient α_f of the film at corresponding pulse energy E_p were determined using a curve fitting procedure, which was explained in detail by Koynov et.al [Koynov'02] and Bahtiar [Bahtiar'04].

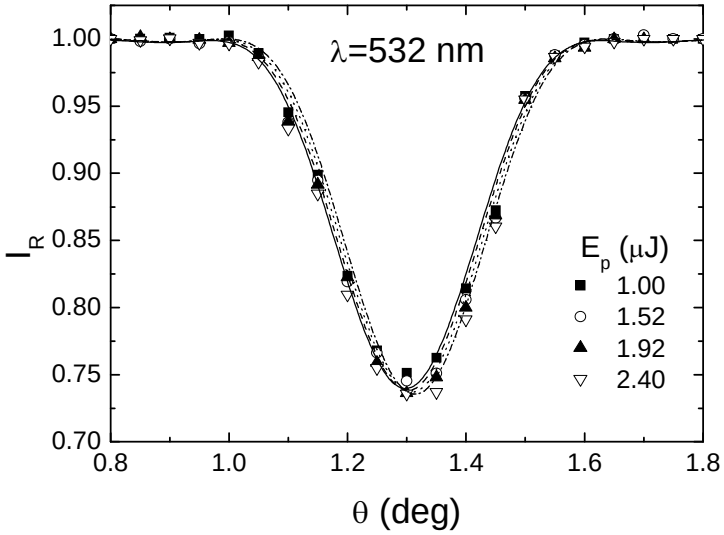

Fig. 4.8: Coupling curve of a PVK waveguide on a BK7 substrate (film thickness 1164 nm, laser wavelength λ = 532 nm). The TE_0 mode was excited at different pulse energies given in the inset. Symbols represent the experimental data and lines are the numerical fits. The air gap thickness d_a = 110 nm was held constant. Only n_f and α_f of the film were varied to fit the measurements at different energies (1.00 μJ: n_f =1.688064, α_f = 2.0 cm^{-1}; 1.52 μJ: n_f =1.68810, α_f = 3.0 cm^{-1}; 1.92 μJ: n_f =1.68815, α_f = 4.0 cm^{-1}; 2.40 μJ: n_f =1.68820, α_f = 5.0 cm^{-1}).

To determine the n_2 and α_2 we plot n_f and α_f versus $<I_{gw}>$ as depicted in Fig. 4.9a and 4.9b, respectively. The average guided wave intensity $<I_{gw}>$ is calculated according to Eq. 3.12 of Bahtiar thesis [Bahtiar'04]. Using linear fit to n_f and α_f vs. $<I_{gw}>$, one can determine n_2 and α_2, respectively. The values of n_2 and α_2 are $(1.2 \pm 0.5)\cdot 10^{-14}$ cm^2/W and $(3.2 \pm 1)\cdot 10^{-10}$ cm/W, respectively. The corresponding $\chi^{(3)}$ values which can be

calculated using Eq. (2.22) is $(8.7 \pm 0.4)\cdot 10^{-14}$ esu or $(1.2 \pm 0.5)\cdot 10^{-20}$ m^2/V^2. The value of $\chi^{(3)}$ is about 10 times larger compared to the value reported earlier [Fuks'02].

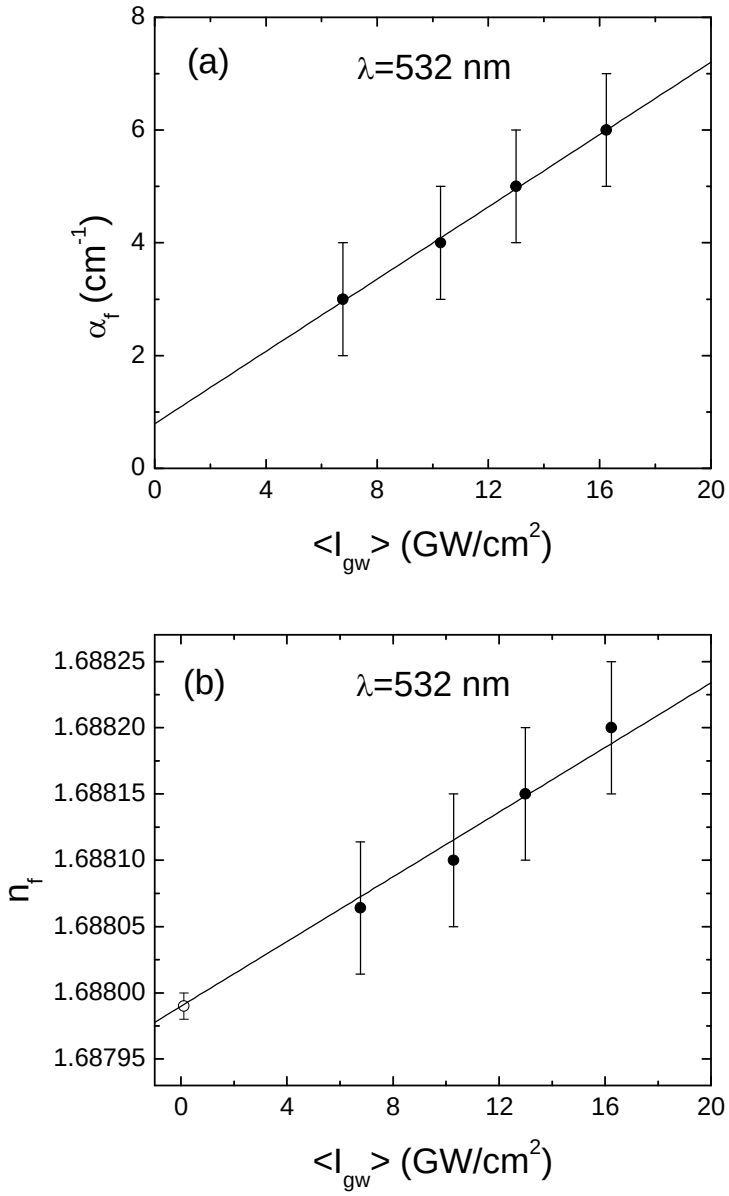

Fig. 4.9: Plot of absorption coefficient (a) and refractive index (b) vs. average guided wave intensity $<I_{gw}>$. The slope of fit in (a) and (b) corresponds to nonlinear absorption coefficient $\alpha_2 = (3.2\pm1)\cdot 10^{-10}$ cm/W and nonlinear refractive index $n_2=(1.2\pm0.5)\cdot 10^{-14}$ cm^2/W respectively. The open symbol in (b) at low $<I_{gw}>$ represents the linear refractive index as derived from m-line technique using several modes.

4.2 Polystyrene (PS)

The chemical structure of polystyrene (PS) is depicted in Fig. 4.10. PS has found applications in integrated optics as passive waveguide [Sosnowski'72, Prest'79, and Prest'80] and also as active waveguide, for example doped with organic dyes like rhodamine 6G [Ulrich'72]. It is transparent in the visible and NIR range and also has an ultralow waveguide loss of 0.1 dB/cm and small birefringence of $4.7x10^{-3}$ [Sosnowski'72, Prest'79, and Prest'80]. Hu et al. [Hu'05a, Hu'05b and Liu'05] demonstrated an all-optical-switching process in a polystyrene photonic crystal (PC). These reports have stimulated research on nonlinear optical properties of PS to verify the linear and nonlinear optical constants of PS.

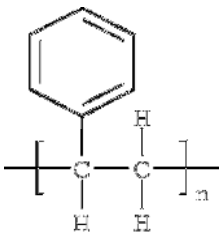

Fig. 4.10: Chemical structure of Polystyrene (PS).

Polystyrene (PS) powder (M_w=1.3·10^6 g/mol) was commercially available and was used as received. The PS films were made from toluene solution by means of spin coating onto fused silica (FS) glasses as substrates. The optical properties of PS films were measured by means of reflectometry of very thin film (d=48 nm) and by prism-coupling of waveguides (d=1000 nm) at several laser wavelengths (532 and 633 nm), as described in the experimental part (see chapter 3.3 and 3.4).

The spin coating parameters of PS were determined experimentally from four samples with combinations of two concentrations and two rotation speeds. Those parameters are α = -0.49±0.1, β = 1.86±0.1 and d_0 = 58±2 nm which were calculated from data in Table C1.1 in Appendix C by using Eq. (3.1). (C_{w0}=1 % , ω_0 = 1000 rpm).

The spectrum of the absorption coefficient of PS thin film measured at s-polarized light by reflectometry is depicted in Fig. 4.11. The PS film is completely transparent in the spectral range from 300 – 1600 nm and has a peak around 260 nm. The values of α agree qualitatively with earlier data of Inagaki et al. [Inagaki'77]. From reflectometry we also get spectra of n as depicted in Fig. 4.12, which are in agreement with n_{TE} data as measured using prism coupling of PS waveguides. The optical anisotropy in PS film is

significant and $n_{TM} > n_{TE}$ which is caused by preferred perpendicular orientation of the phenyl ring with respect to the substrate plane [Prest'79].

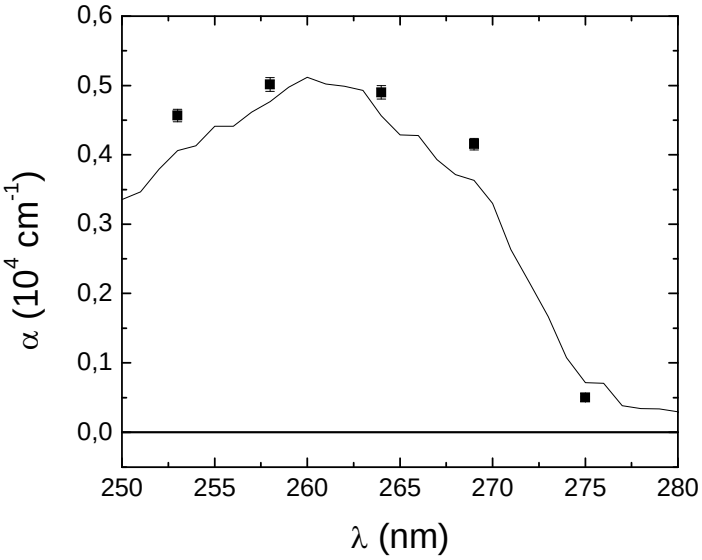

Fig. 4.11: Dispersion of the absorption coefficients of PS film (d=48 nm) measured by reflectometry (line) and data taken from Inagaki [Inagaki'77] (symbols).

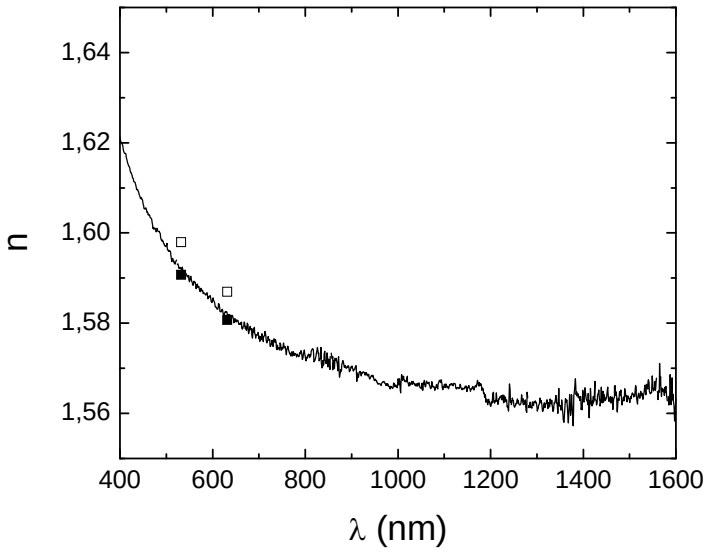

Fig. 4.12: Refractive index dispersion of a PS film (d=48 nm) which is measured using reflectometry (lines) and prim-coupling of waveguides (symbols); open square (TM modes) and full square (TE modes).

We performed nonlinear prism coupling to determine the n_2 and α_2 of PS waveguide at 532 nm. The intensity dependent coupling curves of PS waveguide are shown in Fig. 4.13. We do not observe any significant change on experimental I_R (symbols) for E_p of 0.39, 0.70 and 1.13 μJ. A significant shift of I_R appears when E_p

reaches 2.02 μJ. The lines in Fig. 4.13 are fitting curves (full and dashed) for experimental data and a simulation curve (dotted) for refractive index change according to Hu et. al. [Hu'05].

The fitting curves (1 and 2) which were applied to determine the refractive index and absorption coefficient change induced by applied intensity changes are shown in the same graph as lines. The fitting procedure is mentioned before in the page 40, when we were dealing with PVK.

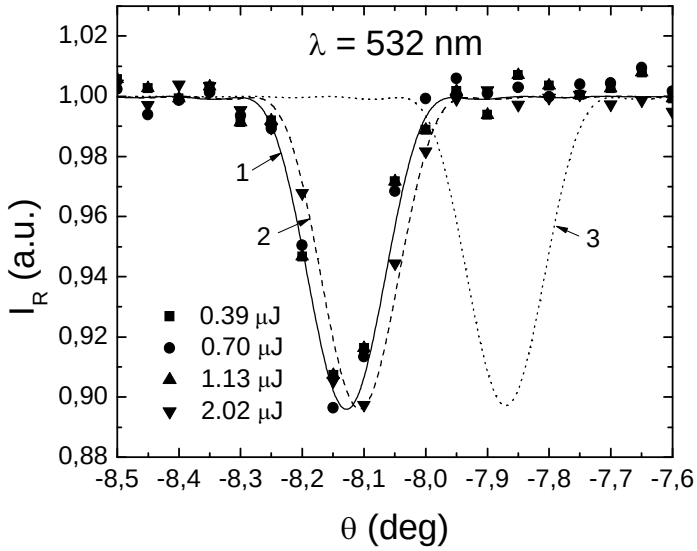

Fig. 4.13: Prism coupling of a PS film on a fused silica substrate (film thickness 2002 nm, laser wavelength λ = 532 nm). The TE_0 mode was excited at different pulse energies given in the inset. Symbols represent the experimental data and lines are the numerical fits. The airgap thickness d_a = 128 nm was held constant. Only n_f and α_f of the film were varied to fit the measurements at different energies (0.39 μJ: n_f =1.59459, α_f = 0.38 cm^{-1}; 2.02 μJ: n_f =1.59480, α_f = 1.00 cm^{-1}). There are three lines shown. The fit line number 1 corresponds to three first pulse energies E_p=0.39, 0.70 and 1.13μJ . The fit line number 2 corresponds to E_p=2.02 μJ. The line number 3 corresponds to simulated I_R if we considered the change of n according to the n_2 value of Hu et.al. [Hu'05] and E_p = 2 μJ.

The absorption coefficient and refractive index values at corresponding average guided intensities are plotted in Fig. 4.14a and b respectively. Values of n_2 and α_2 which were derived from the linear fitting curves in Fig. 14a and b are considered as maximum possible values at 532 nm. The n_2 and α_2 values are $(2.6\pm0.5)\cdot10^{-14}$ cm^2/W and $(1.5\pm0.5)\cdot10^{-10}$ cm/W respectively.

We could try to compare n_2 at 532 nm from our measurement with the values of n_2 which we could deduced from shift of defect mode of PS photonic crystal under irradiation of high intensity laser pulses. If we consider the photonic crystal as a Bragg

grating, which has effective refractive index n_{eff} and grating period Λ then Bragg wavelength $\lambda_0 = 2n_{effr}\Lambda$ [Bahtiar'04]. Since refractive index of material are intensity dependent according to Eq. (1.1) then n_{eff} is intensity dependent. Any shift of transmittance minima $\Delta\lambda_0$ of photonic crystal is purely caused by refractive index change of the constituent materials Δn_{eff}. In the case of photonic crystal which is composed of polymer slab waveguides and air filled submicron cylindrical holes, one can assume $\Delta n_{eff} = \Delta n_{polymer}$ then $\Delta\lambda_0 = 2\Delta n_{polymer}\Lambda$.

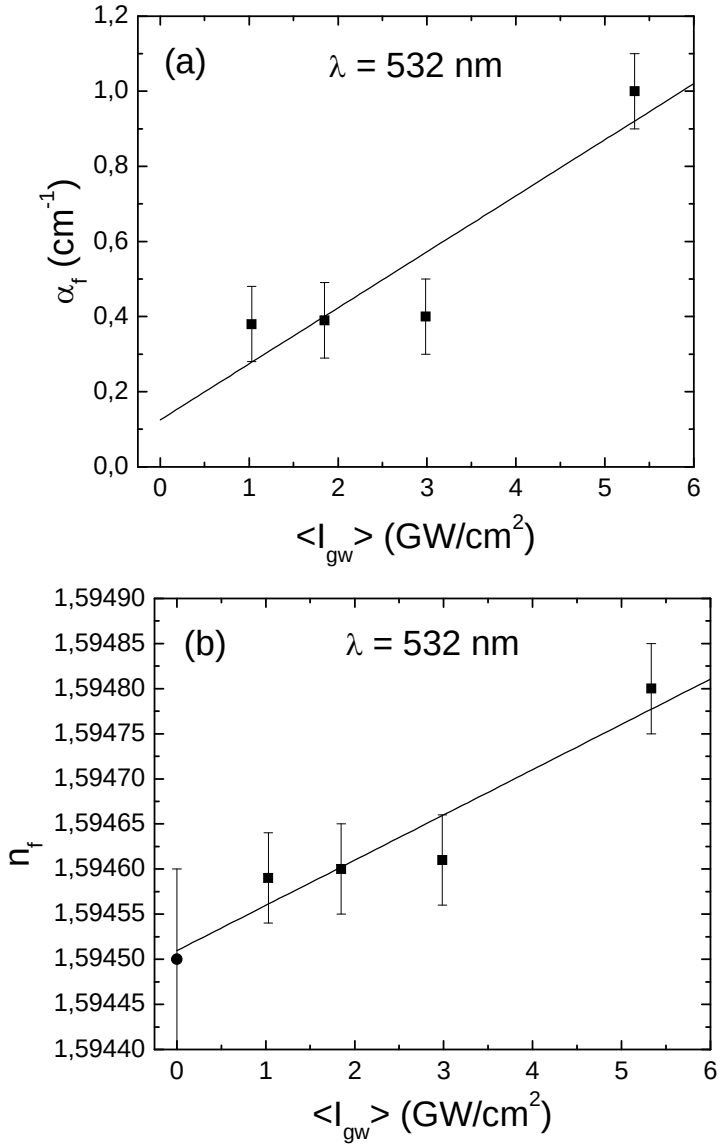

Fig. 4.14: Absorption coefficient α_f (a) and refractive index n_f (b) of PS film at laser wavelengths 532 nm (symbols) as a function of the average intensity in the waveguide $\langle I_{gw} \rangle$. Values of α_2 and n_2 are equal to slopes of linear fits of α_f and n_f respectively. The n_2 and α_2 values are $(2.6\pm0.5)\cdot10^{-14}$ cm^2/W and $(1.5\pm0.5)\cdot10^{-10}$ cm/W respectively. For comparison, data from reflectometry of very thin films is shown (full circle).

Hu et.al. [Hu'05] reported that the shift of 5 nm was induced by 18.7 GW/cm^2 which means $\Delta n_{PS}=5/(2\cdot220)=0.011$ which corresponds to $n_2 = 5.9\cdot10^{-13}$ cm^2/W. The value of n_2 is 23 times of the maximum value of n_2 of our sample. The reason is not fully clear yet. The M_w of their PS is almost 8 times higher than our PS. These facts are observed already as M_w dependence on $\chi^{(3)}$, which are reported elsewhere [Kishida'05 and Koynov'06]. But such a strong dependence on molecular weight is unlikely. We assume that the high repetition rate (76 MHz) of the laser system used by Hu, et. al. [Hu'08] could cause thermal nonlinearities.

The simulation was performed as follows: we assume refractive index changes induced by pulse energy change from 0.39 to 2.02 mJ. The value of $n_2 = 5.9\cdot10^{-13}$ cm^2/W according to Hu et.al. [Hu'05], then $\Delta n=5.9\cdot10^{-13}\times(5.34\text{-}1.03)\cdot10^9=0.0025$. Using the Δn, we expected the minima of I_R shifts from -8.13 deg to -7.87 deg correspond to the change of n from 1.59459 to 1.5971. But we observe shifts of minima only from -8.12 deg to -8.10 which is related to relatively small Δn of 0.0002 or 8% of Δn expected according to n_2 of Hu [Hu'05].

4.3 Poly[2-methoxy-5-(2'-ethyl-hexyloxy)-1,4-phenylene vinylene] (MEH-PPV)

Investigation of MEH-PPV (see Fig. 4.15) waveguides were performed in collaboration with Mardiyati [Mardiyati'10], who provided the waveguide samples for the intensity dependent prism coupling experiment reported here. The sample of MEH-PPV was obtained by fractionation experiments of Mardiyati [Mardiyati'10] (sample batch number **P3*,** M_w=53,000 g/mol, Mn=19,000 g/mol). The MEH-PPV waveguide was prepared from toluene solution and had thickness of 511.8±2 nm.

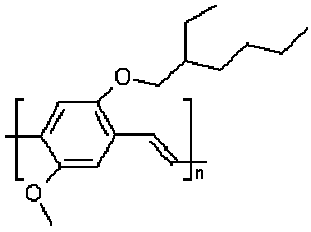

Fig. 4.15: Chemical structure of MEH-PPV

We performed nonlinear prism coupling at the wavelengths 1064 nm and 1100 nm in order to reproduce the nonlinear optical constants of MEH-PPV from earlier work [Koynov'02 and Bahtiar'04]. In Figs 4.16 and 4.18, the coupling curves at different pulse

energies are shown, which consist of experimental data (symbols) and numerical fits (lines). Subsequently, Fig. 4.17 and Fig. 4.19 show the pair of α_f and n_f data versus $\langle I_{gw} \rangle$. The α_2 and n_2 values which were obtained are listed in Table 4.5 together with the values of α_2 and n_2 at nearest λ of earlier work [Bahtiar'04, Koynov'02].

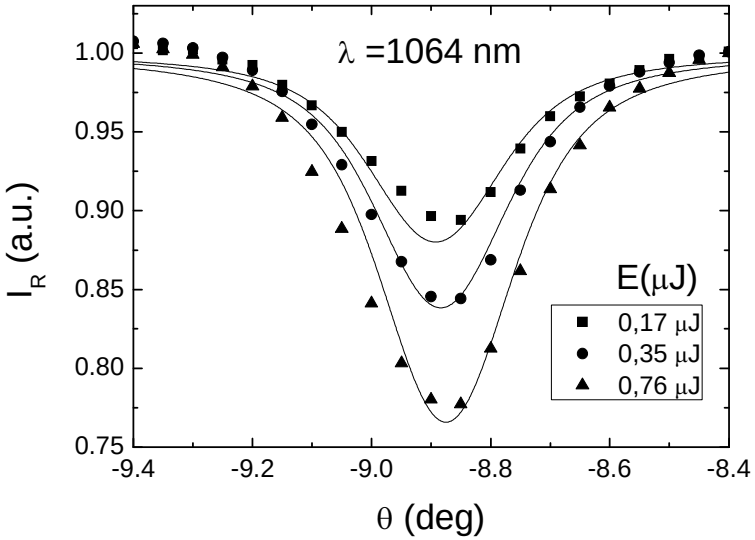

Fig. 4.16: Coupling curve of a MEH-PPV waveguide on a fused silica substrate (film thickness 511.8 nm, laser wavelength λ = 1064 nm). The TE_0 mode was excited at different pulse energies given in the inset. Symbols represent experimental data and lines are numerical fits. The air gap thickness d_a=300 nm was held constant. Refractive index and waveguide loss of the film were the only parameters, which were varied at different pulse energies (0.17 μJ, n_f=1.6625 α_{gw}=2.2 cm^{-1}; 0.35 μJ, n_f=1.6626 α_{gw} =3 cm^{-1}; 0.76 μJ, n_f=1.6627, α_{gw}=4.5 cm^{-1}).

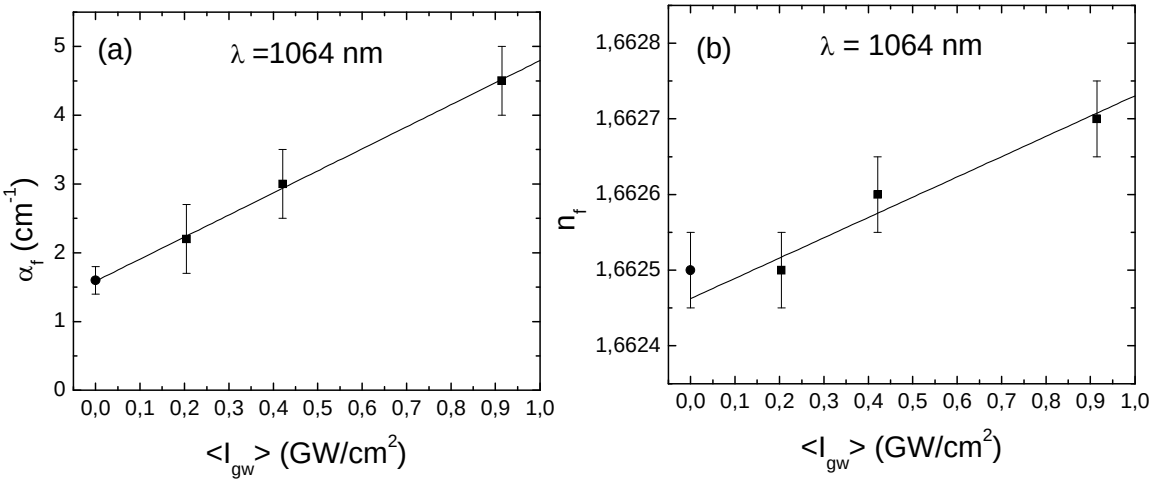

Fig. 4.17: Absorption coefficient α_f (a) and refractive index n_f (b) of a MEH-PPV film at laser wavelength 1064 nm (full squares) as a function of the average intensity in the waveguide $\langle I_{gw} \rangle$. Values of α_2 and n_2 are equal to slopes of linear fits of α_f and n_f respectively. The n_2 and α_2 values are $(2.7 \pm 0.6) \cdot 10^{-13}$ cm^2/W and $(3.2 \pm 0.2) \cdot 10^{-9}$ cm/W. For comparison, the results of linear prism couplings using a cw Nd:YAG laser are shown (full circles).

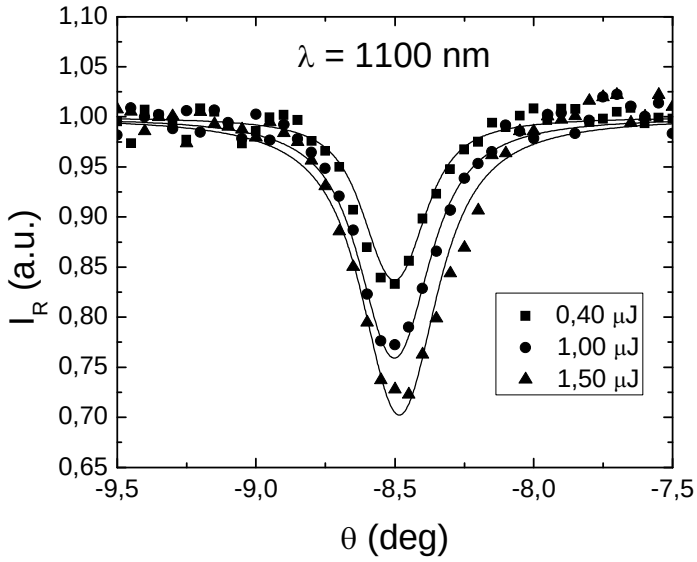

Fig. 4.18: Coupling curve of a MEH-PPV waveguide on a fused silica substrate (film thickness 511.8 nm, laser wavelength λ = 1100 nm). The TE_0 mode was excited at different pulse energies given in the inset. Symbols represent experimental data and lines are numerical fits. The air-gap thickness d_a=400 nm was held constant. Refractive index and waveguide loss of the film were the only parameters which were varied at different pulse energies (0.40 μJ, n_f=1.6508 α_{gw}=1.25 cm^{-1}; 1.00 μJ, n_f=1.6510 α_{gw} =3 cm^{-1}; 1.50 μJ, n_f=1.6512, α_{gw}=4.5 cm^{-1}).

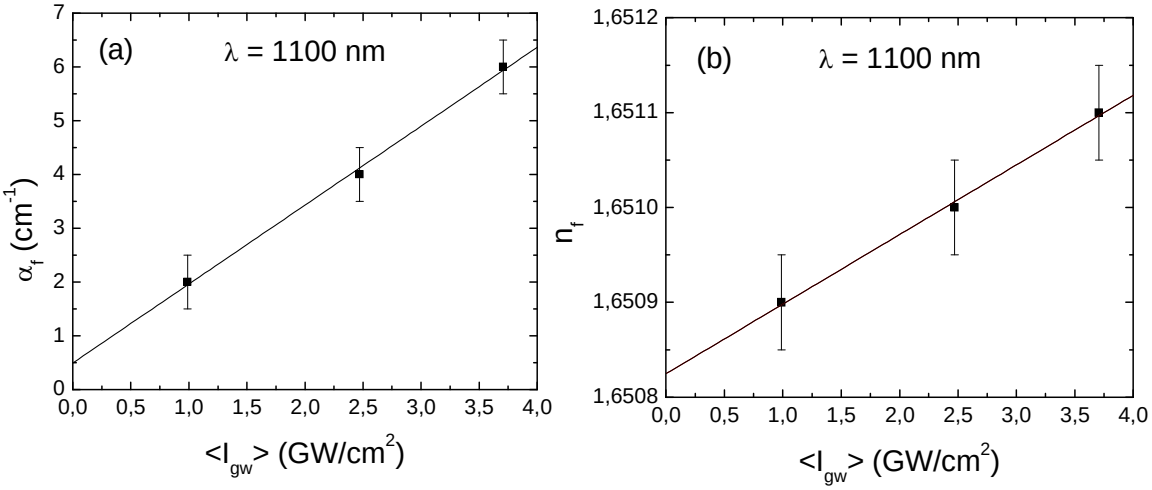

Fig. 4.19: Absorption coefficient α_f (a) and refractive index n_f (b) of MEH-PPV film at laser wavelength 1100 nm (full squares) as a function of the average intensity in the waveguide $<I_{gw}>$. Values of α_2 and n_2 are equal to slopes of linear fits of α_f and n_f respectively. The n_2 and α_2 values are $(7.3 \pm 0.4)\cdot 10^{-14}$ cm^2/W and $(1.5 \pm 0.1)\cdot 10^{-9}$ cm/W.

Comparison with nonlinear spectra of MEH-PPV at TE polarization

Table 4.5: Comparison of optical constants of MEH-PPV

λ [NM]	N_0 ±0.0002	α_0 CM^{-1}	N_2 10^{-13} CM^2/W	α_2 10^{-9} CM/W	REFERENCE
1064	1.6625	1.6±0.2	2.70±0.60	3.20±0.2	This Work
1064	1.6531	0.2±0.5	1.84±0.36	3.00±7.00	Bahtiar'04
1100	1.6508	0.5±0.2	0.73±0.40	1.47±0.10	This Work
1130		0.2±0.2	0.80±0.30	3.20±7.00	Bahtiar'04

The nonlinear spectra of MEH-PPV are already published. They were measured with intensity dependent prism coupling [Koynov'02], two-photon excitation of fluorescence [Bader'02] and z-scan of solution [Bahtiar'06] and using different molecular weight (M_w) of samples. Here, we compare our data with 3 spectra reported earlier in Fig. 4.20, where the data are consistent with the trends of all spectra from earlier report.

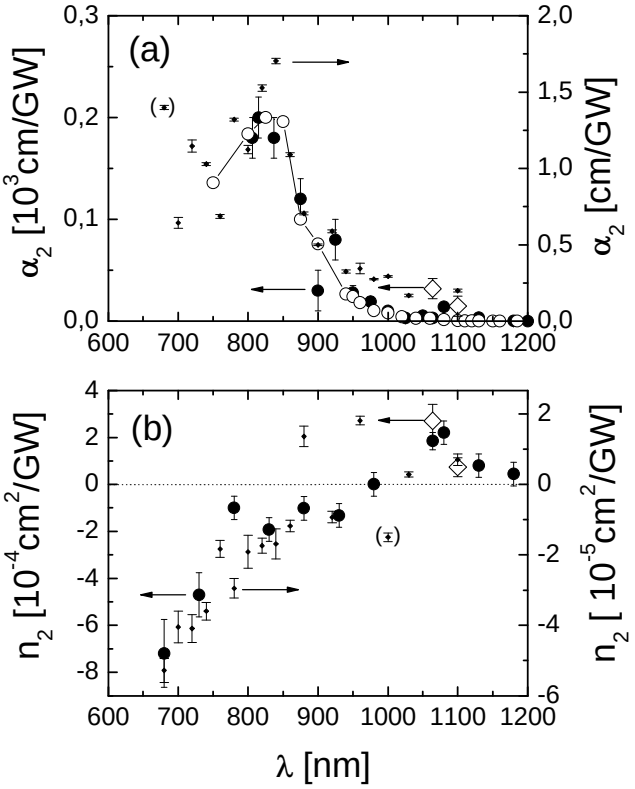

Fig. 4.20: Comparison of own data (diamonds) with earlier work [Bahtiar'06]. Nonlinear optical spectra of MEH-PPV measured at the laser wavelength λ. (a) Comparison of data α_2 from nonlinear prism coupling (full large dots, left scale; own data of **P3***, open diamonds, left scale), from two-photon excitation spectra of fluorescence (open circles, arbitrary scaled to the peak of film data, error bars are smaller than symbol size), and from z-scan (small dots, right scale). (b) Dispersion of n_2 from nonlinear prism coupling (full large dots, left scale; own data of **P3***, open diamonds, left scale), and z-scan (small dots, right scale).

By using the quantum mechanical model of $\chi^{(3)}$ which is written in Eq. 2.29 and relation of n_2 and α_2 with $\chi^{(3)}$ in Eq. 2.18 and 2.19, respectively, one could fit experimental data of the dispersion of n_2 and α_2. Fig. 4.21 shows the currently available data of prism coupling studies of MEH-PPV by Bahtiar et.al. [Bahtiar'04, Koynov'02] and from own work.

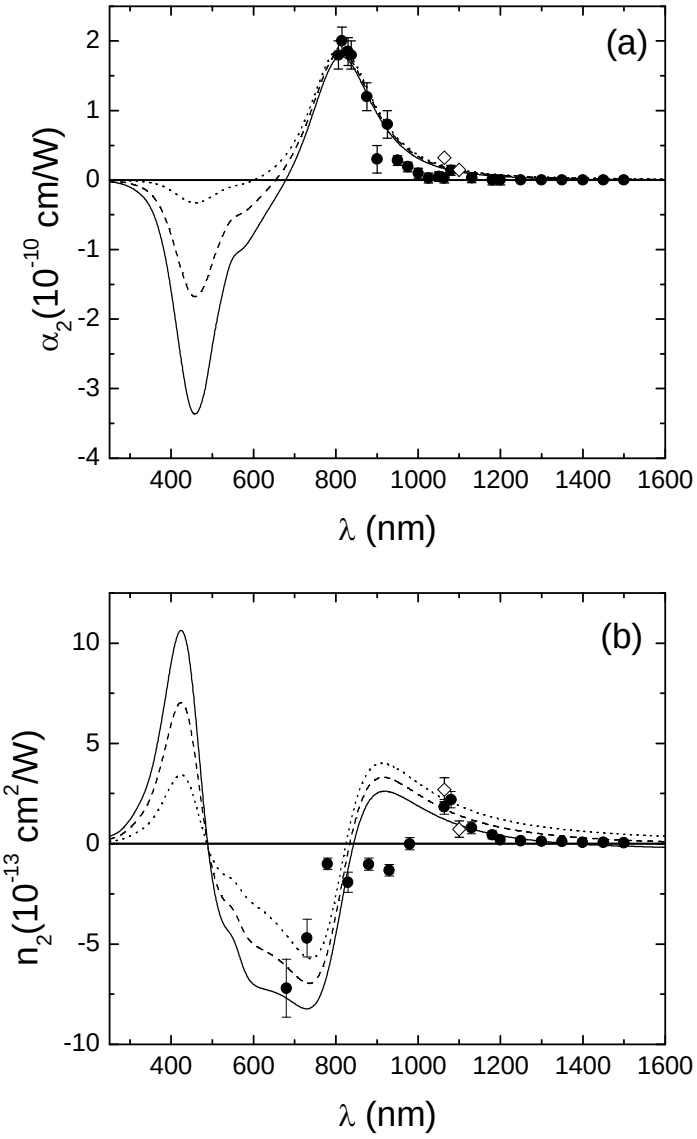

Fig. 4.21: Nonlinear spectra α_2 (a) and n_2 (b) of MEH-PPV films measured using nonlinear prism coupling (symbols) and calculated (lines) using Eq. (2.29). The full circles are from Bahtiar'04 and the open diamonds are from this work. The parameters were $E_{gg'}$=3.04 eV, $\Gamma_{gg'}$=0.4 eV, $A_{gg'}$=4.0 and E_{gu}=2.53 eV, Γ_{gu}=0.6 eV, A_{gu}=1.0 (dotted), A_{gu}=2.0 (dashed), A_{gu}=4.0 (full).

The fit parameters E_{gu}=2.53 eV and Γ_{gu}=0.6 eV of saturable absorption (SA) corresponds to λ_{max} and Full Width Half Maximum (FWHM) of absorption coefficient dispersion $\alpha(\lambda)$ of Polymer 4 in Fig. 2 of Koynov et.al. [Koynov'06]. The parameters

$E_{gg'}$=3.04 eV and $\Gamma_{gg'}$=0.4 eV were determined from two-photon absorption (TPA) spectra of MEH-PPV solutions [de Boni'04, Bahtiar'06]. Those parameters were kept constant and the fitting process was done by using $A_{gg'}$ and A_{gu} only.

The lines shown in Fig. 4.21 are calculated nonlinear optical spectra. They consist of normalized n_2 and α_2 of one-photon and two-photon processes with weighted constants $A_{gg'}$ and A_{gu}, respectively. Since we do not have experimental data of the one-photon resonance (saturable absorption, SA), we present lines with different A_{gu} values. Obviously, the model can fit TPA region of α_2. The zero crossing of α_2 according to this model is probably in the range of 600 to 680 nm, which is red shifted from 570 nm according to de Boni et.al. [de Boni'04]. But the fit to n_2 is still poor, especially in the range of 800 to 1064 nm. Theoretical values of n_2 in TPA region (λ > 800 nm) are strongly affected by n_2 of SA region, because the Γ_{gu} of SA is quite large.

The maximum value of n_2 of TPA region according to the theoretical fit is happen to be at around 900 nm, which should be red-shifted to around 1100 nm according to the experimental data. The reasons of large discrepancies between model and experimental data points of n_2 in the range of 800 – 1000 nm might be caused by the large experimental error and also the lack of data points in SA region, which were not accessible experimentally because wavelengths at λ < 680 nm were not available in our laser system. Another reason is the limitation of the theory, which was discussed by Hutchings et. al. [Hutchings'92].

The linear and nonlinear data that measured in this work are consistent with the data from former work of Koynov et. al. [Koynov'02]. In general the data are also consistent with the spectra measured by z-scan [Bahtiar'06] and two-photon excitation of fluorescence [Bader'02]. The model seems to fit the spectra of α_2 quite well but it fails to fit spectra of n_2 in the range of 800 < λ < 1064 nm, which is probably caused by limitation of the model.

The spectrum of the linear waveguide loss α_{gw} of MEH-PPV is depicted in Fig. 4.22 and shows a monotonous decrease toward longer wavelengths. This behavior can be interpreted by Rayleigh and Mie type light scattering of the guided modes [Ma'02]. By using Eq. 2.52 to fit experimental data in Fig. 4.22 we have found a_0, a_1 and a_2 parameters as follows: $a_0=5.08\times10^{-17}$ cm^{-1}, $a_1=1.08\times10^{-24}$ cm and $a_2=2.48\times10^{-16}$ cm^3. The Rayleigh contribution is dominant, can be seen when we put a_2=0 which means the only α_{gw} is contributed by Mie scattering only. The curve obtained by setting a_2=0 is close to the line

at α_{gw}=0 and not shown explicitly in Fig. 4.22. This means the size of the scattering object is smaller than the wavelength. The theoretical line is not valid anymore as it is approaching 600 nm, where the tail of absorption coefficient is dominant.

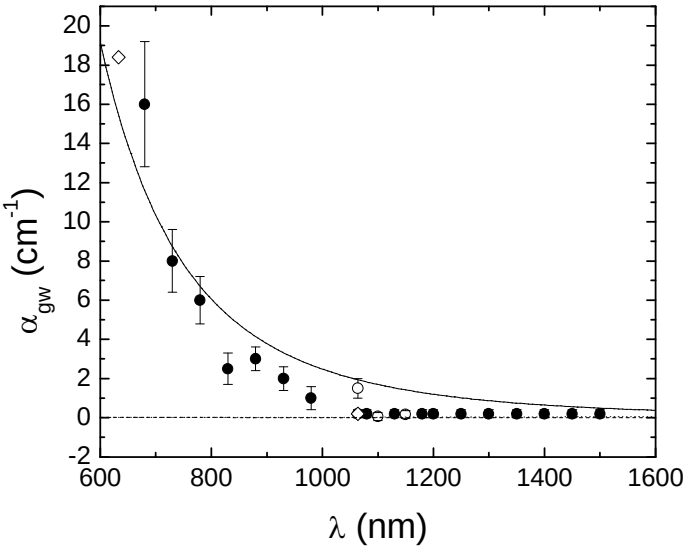

Fig. 4.22: Waveguide loss dispersion of MEH-PPV waveguide determined from coupling curve at low intensity (filled circles are taken from Bahtiar [Bahtiar'04], open circles are from this study) and from waveguide-loss experiments (open diamonds) taken from Bahtiar. Empirical law fit (line) (a_0=5.08×10^{-17} cm^{-1}, a_1=1.08×10^{-24} cm a_2=2.48×10^{-16} cm^3).

5 Material Properties of Poly(3-Alkylthiophene)s

Some poly(3-alkylthiophene)s or P3ATs have good waveguiding properties [Rau'06, Messaad'08]. Large third-order nonlinearities of P3ATs have been reported, most of them determined by third-harmonic generation (THG) [Neher'90, Mathy'96 and Kishida'05] and degenerate four wave mixing (DFWM) [Bubeck'91, Schrof'98].

The properties of P3ATs are depending on intrinsic properties of constituents (thiophene rings backbone and its alkyl substitutions) and their interactions. In this chapter, linear optical properties of P3ATs thin films and thermal properties of powder samples of P3ATs are presented. Effects of alkyl chain length and alkyl chain distribution along the polymer backbone will be discussed. The best candidate among P3ATs for photonics application will be selected and its optical properties will be studied in more detail.

Unsubstituted polythiophene (PT) has thiophene rings in coplanar orientation. The properties of P3ATs depend on its regioregularity, which is defined as their head-to-tail ratio HT ratio. The HT ratio is defined as [Chen'93]:

$$\text{HT ratio} = \frac{\text{number of } (\text{HT - HT})}{\text{number of } ((\text{HT - HT}) + (\text{HT - TH}) + (\text{HT - HH}) + (\text{TT - HH}))}, \qquad (5.1)$$

where HH and TT refer to head-head and tail-tail couplings, respectively. Regioregular P3AT or P3AT-rr (see Fig.5.1 left) has only HT-HT linkage or 100 % HT ratio compared to the right side where P3AT-ra has all types of coupling possibilities (HT, TH, HH and TT).

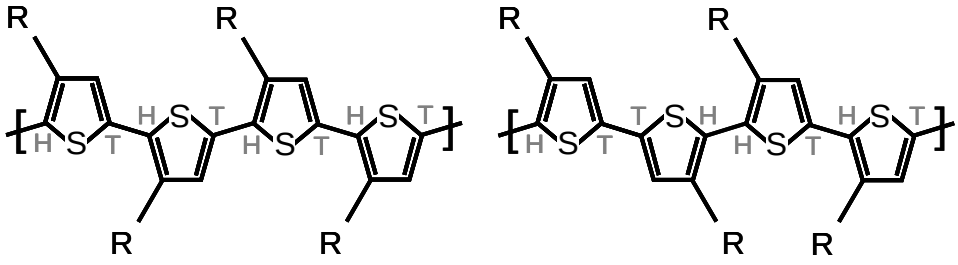

Regioregular P3AT or P3AT-rr Regiorandom P3AT or P3AT-ra

Fig. 5.1: Chemical structure of P3AT-rr and P3AT-ra, R is alkyl (C_nH_{2n+1} where n=1, 2, 3,…) chain. Head (H) and Tail (T) are specified in order to make clear difference between isomerism. Head to tail (HT) coupling between two adjacent monomers is an important factor which is used to distinguish between regioregular and regiorandom P3ATs.

Alkyl chains may cause steric problems and a tilted backbone structure at some positions. In regiorandom P3AT, positions of alkyl chains at thiophene rings are randomly distributed along the chain, which is contrast to the regioregular one. Effects of alkyl chain positions will be explained in more detail with the help of the following scheme depicted in Fig. 5.2. A fish bone like structure of P3AT-rr (see Fig. 5.2 left) allows coplanar dense packing formation, which favours aggregate formation [Hugger'04]. Randomly oriented alkyl chains in P3AT-ra (see Fig. 5.2 right) permit the entanglement between two repulsive chains (top) which twists two adjacent thiophene rings to each other and produces a round brush like formation (bottom). The so-called brush formation of P3AT prevents a closely packed structure of P3AT chains, which leads to an amorphous morphology. Twisted thiophene rings will reduce co- planarity of thiophene rings. This increases the optical band gap, reduces conductivity and other crucial properties for electronic applications [McCullough'93a].

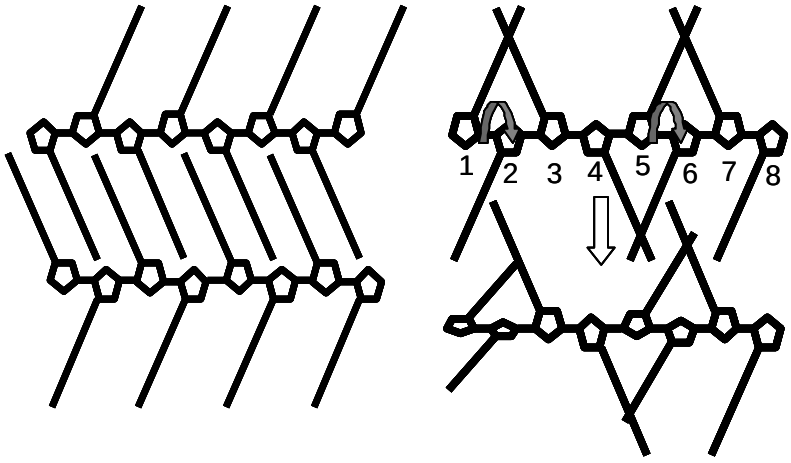

Regioregular P3AT or P3AT-rr Regiorandom P3AT or P3AT-ra

Fig. 5.2: Fish bone like structures of P3AT-rr (left) and P3AT-ra (right), which show three couples (1-3, 4-6 and 5-7) of entangled alkyl chains (top) and twisted thiophene rings (bottom) between adjacent rings (2-3, 4-5 and 6-7).

5.1 Materials and Film Preparation

P3ATs were bought from various suppliers (Aldrich Chem. USA, ADS Canada and Rieke Metals Inc. USA) and used without further purification. Regioregularity degrees (HT ratios) are between 90 and 93 % for regioregular P3ATs and 50 % for regiorandom. Four kinds of alkyl substituted PT were used and each of them has two kinds of regioregularities. The names of these polymers include information on length of alkyl chain and regioregularity, respectively. Their properties are listed in Table 5.1a and 5.1b, respectively.

Table 5.1a : Name and Abbreviation of P3ATs, which are used in this work.

ALKYL SIDE CHAIN	NAME	ABBREVIATION	
		Regiorandom (ra)	Regioregular (rr)
Butyl	Poly(3-Butylthiophene)	P3BT-ra	P3BT-rr
Hexyl	Poly(3-Hexylthiophene)	P3HT-ra	P3HT-rr
Octyl	Poly(3-Octylthiophene)	P3OT-ra	P3OT-rr
Decyl	Poly(3-Decylthiophene)	P3DT-ra	P3DT-rr

Table 5.1b : Molecular weight data measured at MPI-P and suppliers of P3ATs.

P3AT-RA/-RR	M_W (10^4 G/MOL)	M_N (10^4 G/MOL)	PDI	REGIOREGULARITY (% HT)	SUPPLIER AND COUNTRY
P3BT-ra	3.09	1.02	3.03	HH:HT = 1:1	Rieke Metal Inc, USA
P3BT-ra	3.18	1.14	2.8	HH:HT = 1:1	Aldrich, USA
P3BT-rr	n. a.	n. a.	n. a.	> 98.5 %	Aldrich, USA
P3HT-ra	6.94	1.50	4.62	HH:HT = 1:1	Aldrich, USA
P3HT-rr	5.80	2.91	2.00	n.a.	ADS, Canada
P3HT-rr	5.43	2.91	1.87	> 98.5 %	Aldrich, USA
P3OT-ra	5.60	1.70	3.29	HH:HT = 1:1	Aldrich, USA
P3OT-rr	n. a.	n. a.	n. a.	> 98.5	Aldrich, USA
P3DT-ra	9.05	1.09	8.35	HH:HT = 1:1	Aldrich, USA
P3DT-rr	4.20	3.00	1.40	> 98.5	Aldrich, USA

"n.a" : not available

All thin films of P3ATs used in this study were prepared by spin coating from their fresh and filtered chlorobenzene solutions. Spin coating parameters were determined by means of equations (3.1) using C_{w0} = 1 % and ω_0 = 1000 rpm. They are displayed in Table 5.2 and Table 5.3 for P3AT-ra and P3AT-rr respectively. The spin coating parameter α is decreasing as the alkyl chain length increases for both cases.

Table 5.2 Spin coating parameters of P3AT-ra.

P3AT-RA	α	B	D_0 (NM)	RANGE OF CONCENTRATION
P3BT-ra	-0.54	1.57	31.10	2-4 %
P3HT-ra	-0.48	1.67	39.70	2-5 %;
P3OT-ra	-0.45	1.68	40.20	2-4 %
P3DT-ra	-0.42	1.79	40.10	2- 4 %

Table 5.3 Spin coating parameters of P3AT-rr.

P3AT-RR	α	B	D_0 (NM)	RANGE OF CONCENTRATION
P3BT-rr	-	-	-	2 %
P3HT-rr	-0.60	1.46	40.80	2-4 %;
P3OT-rr	-0.51	-	-	2 %

P3DT-rr	-0.47	-	-	2 %

"-" : not measured

5.2 Linear Optical Properties

5.2.1 Results

Spectra of optical constants at TE polarization of very thin films (d=56nm) of regioregular P3HT were determined from reflectometry. They are depicted on Fig. 5.3. The absorption spectrum (a) of P3HT-rr has maximum at 518 nm, which is followed by two shoulders at 550 nm and 600 nm, which are typical for P3AT-rr [McCullough'93b and McCullough'98]. The maximum position appears at shorter wavelengths and indicates that this film has lesser regioregularity compared to the films studied by McCullough et.al. [McCullough'98]. The spectrum of refractive index (b) of P3HT-rr also shows a shoulder at 576 nm and followed by a maximum at 616 nm.

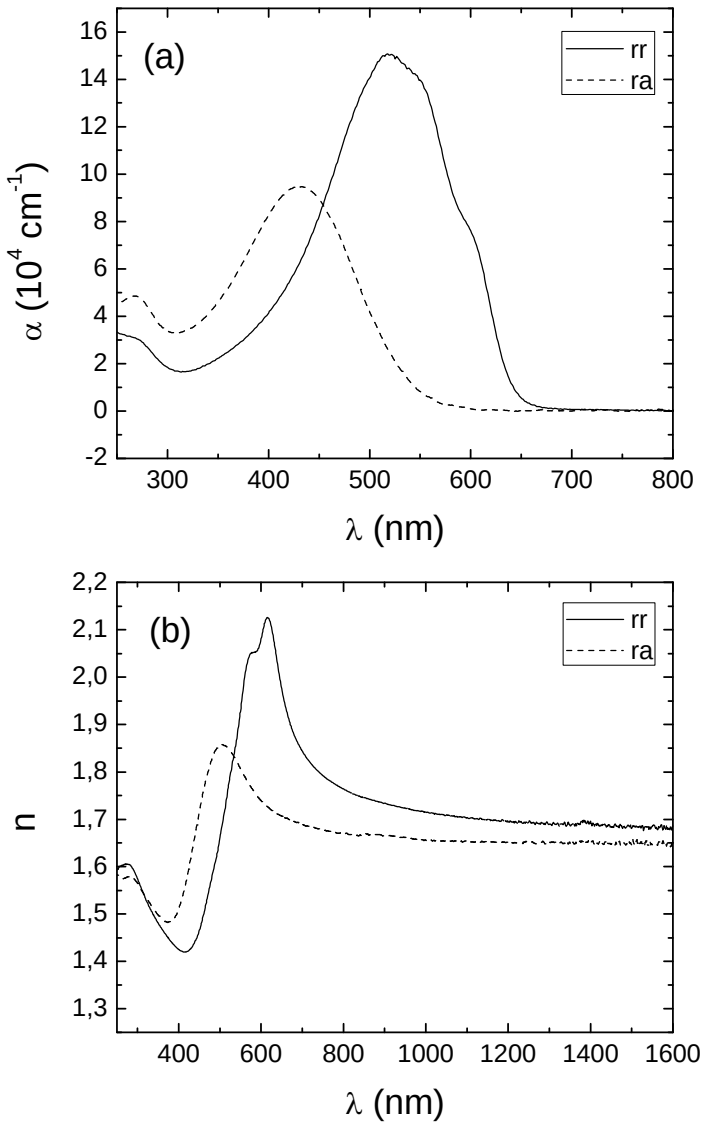

Fig. 5.3: Spectra of optical constants: absorption coefficient (a) and refractive index (b) of P3HT-rr (full line) and P3HT-ra (dashed line) thin film (d=50 - 70 nm) at TE polarization determined by reflectometry technique.

The spectra of absorption coefficient and refractive index spectrum of poly(3-alkylthiophene) thin films are strongly dependent on the morphology of the films. The morphology of P3ATs thin films depends on molecular weight, thickness of film and preparation conditions (boiling temperature of solvents T_{BP}, casting temperature T_c, casting pressure P_c and annealing temperature T_a) [Lanzi'08, Lu'07, Lu'08 and Ma'07, Zen'06]. We prepared thin films at the same condition to avoid possible variations of the film morphology.

Effects of regioregularity

Major differences between regioregular and regiorandom P3ATs are seen in their absorption spectra. Regiorandom P3AT has a broad peak only as compared to regioregular P3AT, which has a fine structure composed of three peaks. The maximum peak position is strongly dependent on thickness of the film and degree of regioregularity [Chen'93 and Chen'95]. Peak positions are related to the so-called effective conjugation lengths of P3ATs, which are increasing from regiorandom to regioregular P3ATs.

Chen et. al. [Chen'95] have shown that regioregularity (HT-HH linkage) plays an important role on absorption spectra of P3AT where the positions of absorption maxima are red shifting as the regioregularity is increasing. The fine structure (three peaks splitting) occurs only when regioregularity is high (HT ratio > 90 %). Effects of regioregularity on optical absorption and refractive index will be demonstrated here, where we have P3HT-ra (HT ratio is 50%) and P3HT-rr (HT ratio is 90%) and blend (50 % < HT ratio < 90 %). Blend films were made as follows: first we mixed regioregular and regiorandom P3HT with composition of 10:90 by weight, then the mixture was solved using chlorobenzene with composition by weight of 2 and 6 % for very thin films (d=50-70 nm) and waveguide (d=500-1000 nm) respectively. The solutions were used to prepare films by means of spin coating. Subsequently, the films were annealed in vacuum oven at 45-50˚C.

The colour of blend P3HT film compared to P3HT-ra and P3HT-rr is shown in Fig. 5.4. Chromic effect of regioregularity is demonstrated in Fig. 5.4 where colours of the films are blue shifting as regioregularities increasing. It is related to the optical absorption spectra which are depicted in Fig. 5.5. Absorption maximum of blended film

adopts major feature of P3HT-ra plus small portion of fine structure of P3HT-rr. Small fraction of P3HT-rr in blended P3HT film could change the film colour from orange to yellow. Homogenous colour and transparent films means that P3HT polymer strands are uniformly distributed in side the films.

Fig. 5.4: Photographs of very thin (d=50-70 nm) films of P3HT: regiorandom (left), regioregular (right) and blend of 10% regioregular and 90 % regiorandom (centre).

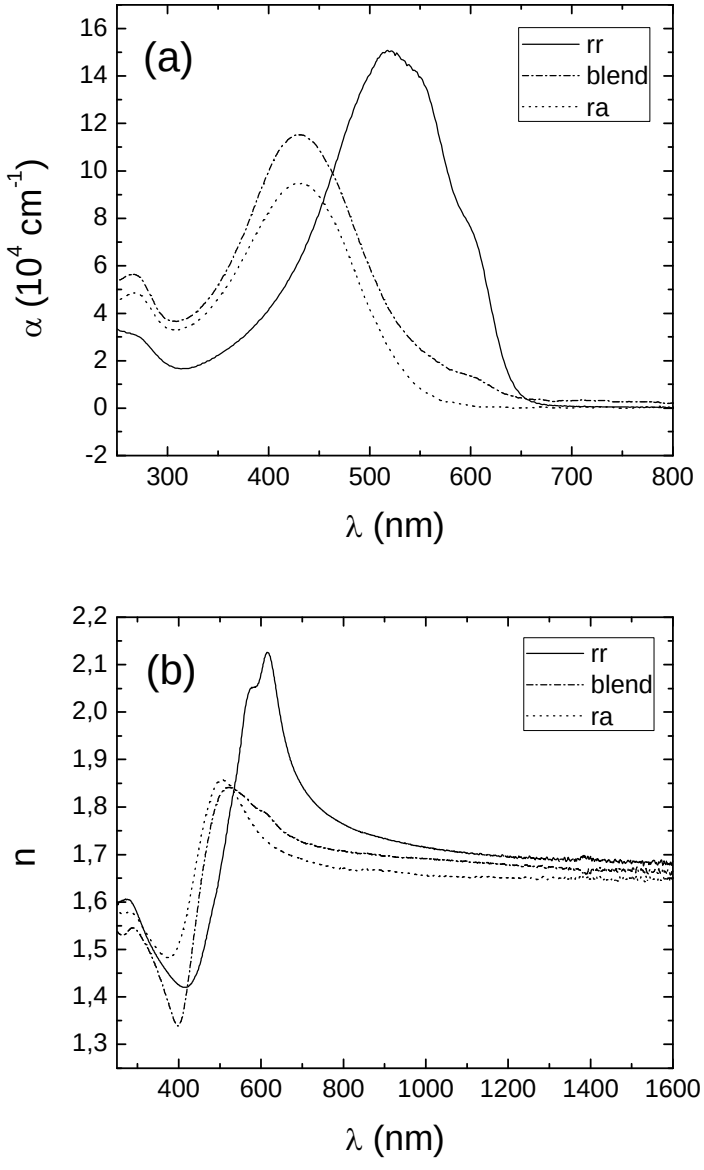

Fig. 5.5: Absorption coefficient (a) and refractive index (b) spectra of P3HT. Effects of regioregularity, regioregular (full lines), regiorandom (dotted lines) and blend of 10 % regular and 90% random (dashed and dotted lines).

Absorption coefficient and refractive index spectra of P3HT films (d=50-70 nm) were determined from reflectometry and are shown in Fig. 5.5 (a) and (b) respectively. In the range of $450 < \lambda < 650$ nm absorption coefficients of blended P3HT are between P3HT-rr and P3HT-ra. Refractive index dispersion of blended P3HT is smaller than P3HT-rr but larger than P3HT-rr in the range of λ from 650 to 1600 nm.

For quantitative specification of refractive index dispersion, we have fitted the spectra in the range of 620 – 1600 nm by Sellmeier equation [Lines'91], which are defined as Eq. 5.2. As a limit of λ approaches to infinity or $\lambda >> C_1$ and C_2, values of $n \approx n_\infty$ ($n_\infty = \sqrt{1 + B_1 + B_2}$). The n_∞ values of P3AT films, which are listed in Table 5.4 increasing from increasing from 1.636 to 1.668 with increasing HT ratio.

$$n^2 - 1 = \frac{B_1 \lambda^2}{\lambda^2 - C_1} + \frac{B_2 \lambda^2}{\lambda^2 - C_2}. \tag{5.2}$$

Table 5.4: Sellmeier coefficients of P3HT are varied with HT ratios.

HT RATIO (%)	B_1	B_2	$B_1 + B_2$ (N_∞)	C_1 (NM^2)	$(C_1)^{1/2}$ (NM)	C_2 (NM^2)	$(C_2)^{1/2}$ (NM)
> 90	0.295 ±0.006	1.487 ±0.005	1.782 (1.668)	330843 ±739	575 ±27	10000 ±2776	100 ±53
50 - 90	0.10 ±0.03	1.65 ±0.03	1.746 (1.657)	269223 ±1405	519 ±38	36000 ± 4942	190 ±70
50	0.24 ±0.02	1.44 ±0.02	1.676 (1.636)	201736 ± 2569	449 ±51	10000 ± 3559	100 ±60

Behaviour of absorption coefficient and refractive index spectra of blend P3HT will be examined using the Effective Medium Approximation (EMA) [Bruggeman'34]. Bruggeman's EMA approach is expressed in equation (2.63). Dielectric permittivity (ε) of blend is approximated using EMA where medium 1 and medium 2 are P3HT-rr and P3HT-ra respectively, f is volume fraction of medium 1. Since the fraction of P3HT-rr to P3HT-ra is known (1:9), then one can calculate the dielectric permittivity (real part ε_1 and imaginary part ε_2) of blend P3HT as depicted in Fig.5.6. The experimental ε_1 and ε_2 of blend P3HT, P3HT-rr and P3HT-ra are depicted also in Fig. 5.6. Discrepancies between EMA and experimental curves are probably caused by non-homogenous distribution of

P3HT-rr in the P3HT-ra matrix; the similar behaviour was found in another P3AT blend [Zen'06].

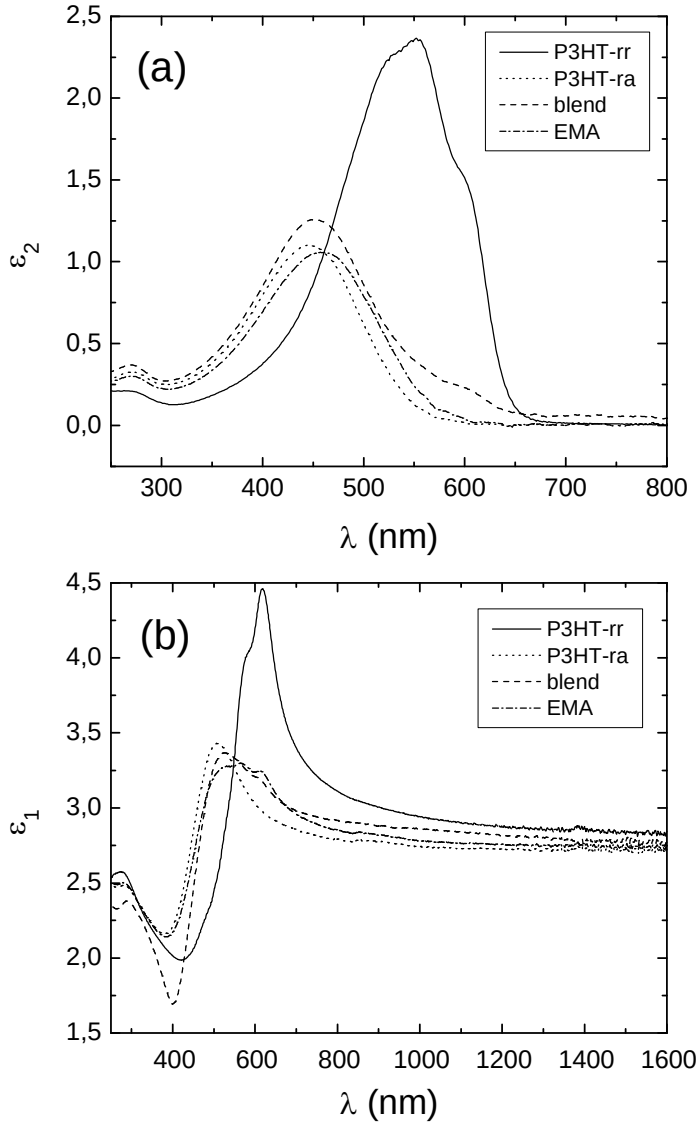

Fig. 5.6: The imaginary part ε_2 (a) and real part ε_1 (b) of dielectric permittivity spectrum of regioregular, regiorandom, blended P3HT and its EMA approximation.

Effects of alkyl substitutions

Optical constants of P3ATs are influenced by two constituents (thiophene ring backbones and alkyl side chains) [Lee'92]. In polythiophenes, the backbones are rich of π-electrons, which are delocalized along coplanar thiophene rings. Alkyl chains do not absorb light in the visible range. Attachment of alkyl chains to thiophene rings causes a dilution of π-electron density of the polymer, which is indicated by reduction of absorption peaks heights. The role of alkyl substitutions on optical properties of P3ATs

thin films were studied using reflectometry of very thin films (d=50-70 nm). Effects of alkyl chain length on optical spectra of P3AT-rr are displayed on Fig. 5.7.

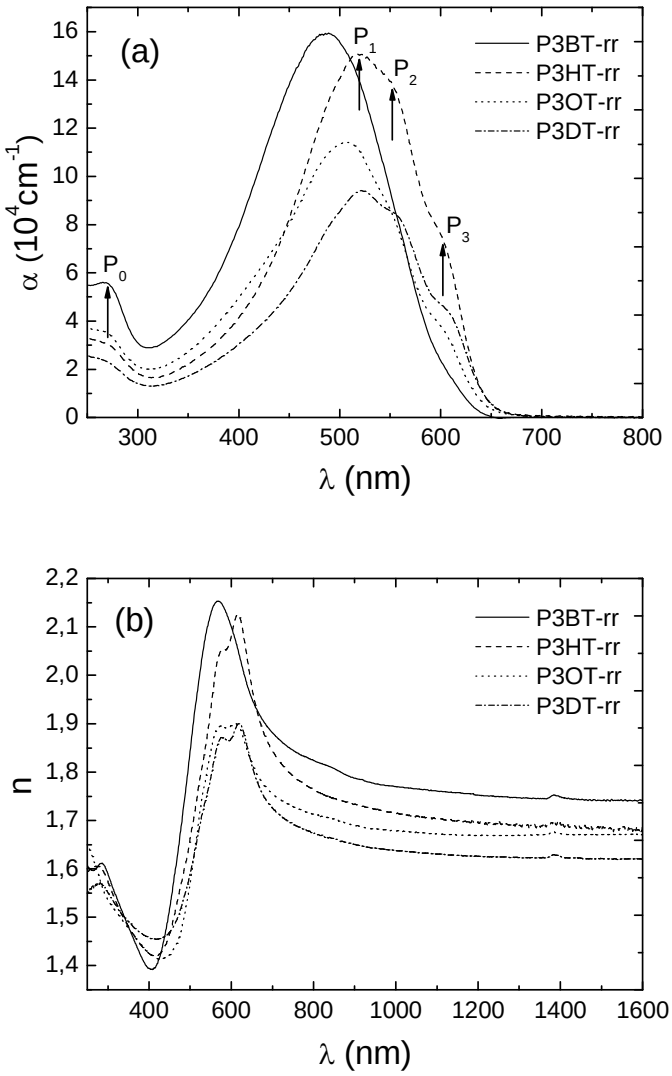

Fig. 5.7 Spectra of (a) the absorption coefficient after correction of reflection losses and (b) the refractive index of thin films of P3AT-rr at transverse electric (TE) polarization. Peaks positions of absorption coefficient spectra denoted by P_0, P_1, P_2 and P_3 and their values were listed in table 5.5.

Some optical absorption parameters are extracted from spectra in Fig. 5.7 (a) and are listed in Table 5.5. The λ_{max} (UV) values are slightly red shifted as alkyl chain length increases but λ_{max}(Vis) values vary and depend on the film morphology [McCullough'93]. The α_{max} (UV) and the peaks of α_{max} (Vis) are decreasing as the alkyl chain length is increasing. Correspondingly, the refractive indices of P3AT-rr at $\lambda > 700$ nm are decreasing at increasing alkyl chain length. Obviously, the π-electron density in P3AT-rr is diluted by alkyl chain attachment.

Table 5.5: Linear optical absorption parameters of P3AT-rr

P3AT-RR	α_{MAX} (UV) [10^4 CM^{-1}] ± 5 %	λ_{MAX} (UV) [± 2 NM]	λ_{MAX} (VIS) [± 2 NM]			α_{MAX} (VIS) [10^4 CM^{-1}] ± 5 %		
	P_0		P_1	P_2	P_3	P_1	P_2	P_3
P3BT-rr	5.61	266	486	560	611	15.93*	7.80	1.63
P3HT-rr	3.54	268	522	551	602	15.06*	13.10	7.43
P3OT-rr	3.02	271	506	555	610	11.42*	8.15	3.09
P3DT-rr	2.24	273	523	563	612	9.39*	8.00	4.11

*) the maximum among peaks

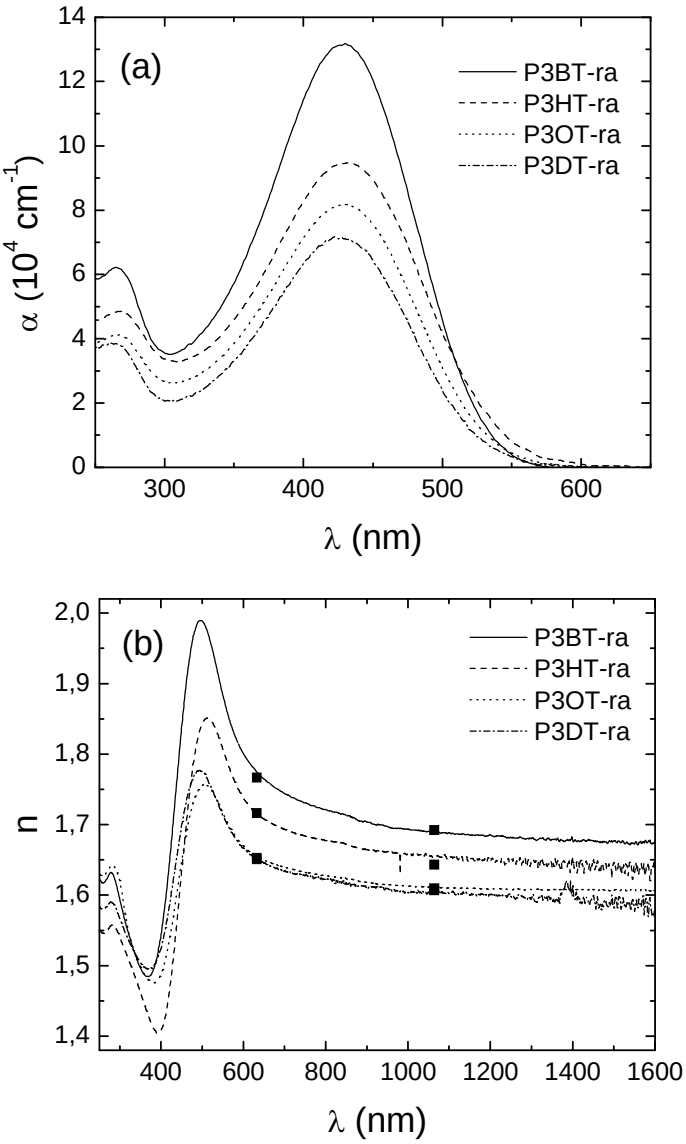

Fig. 5.8: Spectra of (a) α and (b) n of thin films of P3AT-ra at transverse electric (TE) polarization. Symbols are n of P3AT-ra waveguide at TE polarization which were obtained from prism coupling experiment.

Spectra of n and α of P3BT-ra thin films, which were obtained using reflectometry, are depicted in Fig. 5.8. The dilution effect is also clearly visible as the

alkyl chain length increases from P3BT to P3DT. Then magnitude of absorption coefficient maxima and refractive index at $\lambda > 600$ nm of the film are decreasing also. The same trend as in P3AT-ra also occurred in P3AT-rr.

Effects of alkyl chain lengths on optical properties of regiorandom P3ATs waveguides were also investigated using prism coupling technique. Refractive indices of regiorandom P3ATs waveguides which were measured using prism coupling at λ=633 and 1064 nm are presented in Fig. 5.8. Some optical absorption parameters which are extracted from spectra in Fig. 5.8 (a) are listed in Table 5.6. The λ_{max} values are almost constant for all P3ATs but values of α_{max} are decreasing as alkyl chain length increasing.

Table 5.6: Linear optical absorption parameters of P3AT-ra

P3AT-RA	α_{MAX} (UV) [10^4 CM^{-1}] ± 5 %	λ_{MAX} (UV) [± 2 NM]	α_{MAX} (VIS) [10^4 CM^{-1}] ± 5 %	λ_{MAX} (VIS) [± 2 NM]
P3BT-ra	6.2	265	13.2	430
P3HT-ra	4.9	268	9.5	432
P3OT-ra	4.1	267	8.2	431
P3DT-ra	3.9	265	7.2	423

5.2.2 Conclusion

The λ_{max} (Vis) values which are related with π-π^* transitions are strongly dependent on regioregularity. The absorption coefficients of P3AT-rr show strong vibronic features, which are typical for polycrystalline materials. The absorption coefficients of P3AT-ra are showing a structureless band and are blue shifted as compared to the corresponding P3AT-rr. This typical band of P3AT-ra is interpreted by its more amorphous morphology. Effects of alkyl side chain length on optical constant of P3ATs are caused mainly by dilution of the π-electron density. The λ_{max} (UV) values are independent from alkyl chain length and their distribution along thiophene backbone, since their values of P3AT-ra and P3AT-rr are similar.

5.3 Thermal Properties

The glass transition temperatures (T_g) and melting point (T_m) of all studied regiorandom and regioregular P3ATs were determined with Differential Scanning Calorimetry (DSC) method by the Polymer Analytic group at MPI-P Mainz. The T_g and T_m of regiorandom and regioregular P3ATs respectively are tabulated in Table 5.7.

Table 5.7: The T_g of P3AT-ra and T_m P3AT-rr.

P3AT	T_G (ºC)	T_M (ºC)
P3BT	60	242
P3HT	-3	238
P3OT	-37	200
P3DT	-60	150

At room temperature, only regiorandom P3BT-ra is in the glassy state. This phenomenon has been realized also during prism coupling experiment. In the prism coupling experiment, the polymer waveguide is pressed against the prism base. All regiorandom P3ATs were adhering to the prism except P3BT-ra. Therefore, P3BT-ra turned out as the as only useful regiorandom material of all P3ATs for prism coupling experiments.

5.4 Summary of Optical and Thermal Properties of P3ATs

In Fig. 5.9 we plot optical properties and thermal properties in a single graph. We conclude that the most promising material for integrated optic application is regiorandom P3BT-ra. Therefore, in the last section of this chapter, we will elaborate the properties of regiorandom P3BT waveguides in more detail.

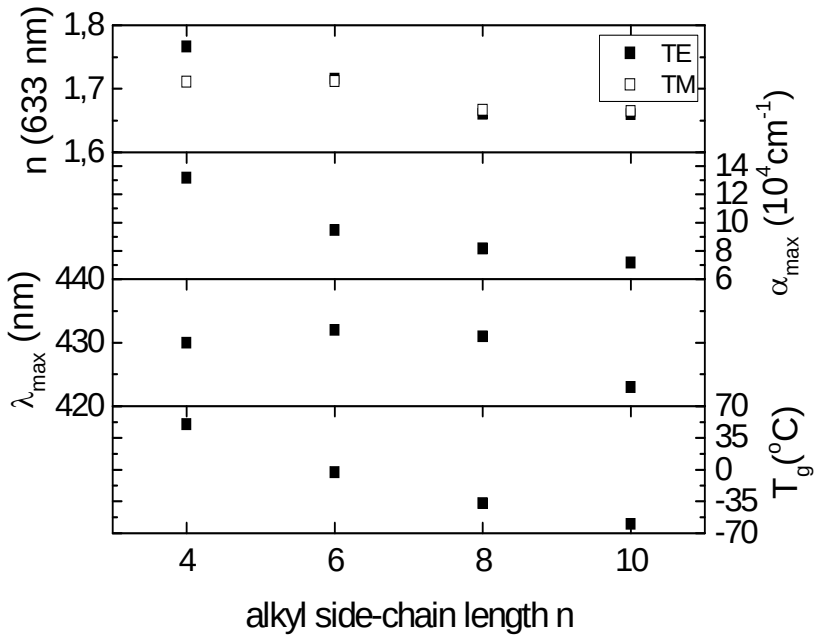

Figure 5.9: Summary of optical properties and glass transition temperatures of regiorandom P3ATs plotted against alkyl side chain length n (n is number of carbon atoms in alkyl chain).

5.5 Regiorandom Poly(3-Butylthiophene)

5.5.1 Waveguide Properties

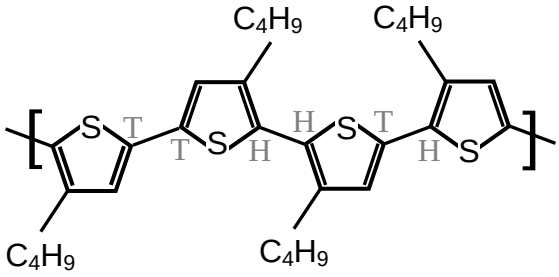

Fig. 5.10: Molecular structure of regiorandom poly(3-butylthiophene-2,5-dyl) denoted P3BT-ra. H: head and T: tail positions of the thiophene rings, respectively.

The chemical structure of P3BT-ra is depicted in Fig. 5.10. It has been purchased from Rieke Metals Inc. with the specification given in their catalogue as 4006 poly(3-butylthiophene-2,5-diyl), regiorandom, which is displayed in Tab. 5.1. In this section, some additional properties of P3BT-ra films will be presented.

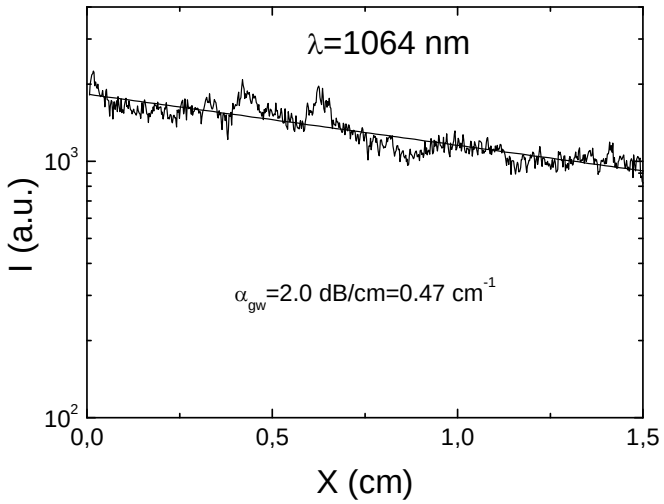

Fig. 5.11: Waveguide loss of P3BT-ra film spin coated d ≈ 1μm from toluene solvent, of TE_1 mode.

Fig. 5.11 shows the trace of scattered light of TE_1 mode guided light of 1064 nm cw-Nd:YAG laser in P3BT-ra film. We observe following waveguide losses, which depend on polarization and mode: $\alpha_{gw}(TE_0)$= 1 dB/cm, $\alpha_{gw}(TE_1)$= 2 dB/cm. The α_{gw} < 1 dB/cm of TE_0 mode is accepted as a critical values of losses that could be tolerated for low-loss waveguides [Bahtiar'04].

Fig. 5.12a again shows the absorption coefficient $\alpha(\lambda)$ of P3BT-ra, which has features of one strong and broad absorption band with a maximum around 430 nm and additional maxima in the UV range. The position where the absorption reaches its

maximum value is denoted as λ_{max} and it has a precision of ± 2 nm because of the broad absorption band. Fig. 5.12b shows the refractive index dispersion. Precisions of n and α are 0.005 and 4%, respectively, which are mainly dependent on the experimental error of the film thickness. Linear refractive indexes of P3BT-ra as shown in Fig. 5.12b are in general between reflectometry and prism coupling, but specifically there are small discrepancies between them for example at 633 and 1064 nm.

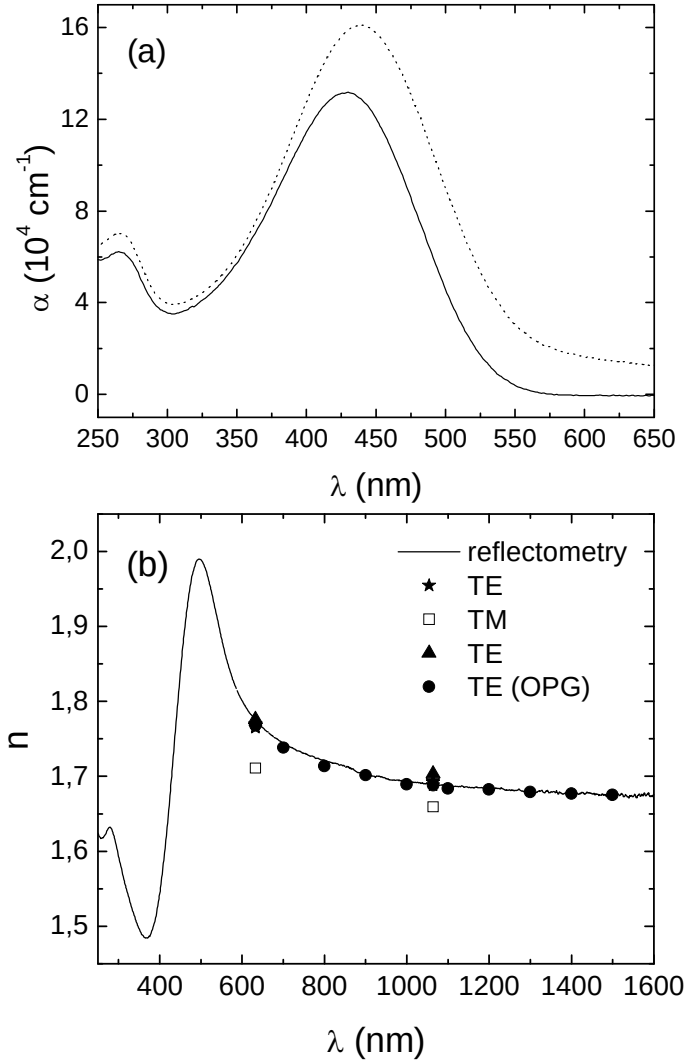

Fig. 5.12: Spectra of absorption coefficient α and refractive index n of a thin film of ra-P3BT-ra at TE polarization prepared by spincoating of toluene (line and ●) and chlorobenzene (★, □ and ▲) solutions. (a) Dispersion of α of a thin film (d = 48 nm) on fused silica substrate measured relative to fused silica (dashed line) and after correction of reflection losses at interfaces (full line). (b) Dispersion of n determined from reflectometry (line) and waveguides (symbols), OPG refers to Optical Parametric Generator.

We conducted an experiment to study the discrepancies in n of films with different thicknesses. Films with different thicknesses were prepared from chlorobenzene

solutions using spin coating. Prism-coupling was used to measure refractive indexes (n_{TE} and n_{TM}) and thicknesses (d_{TE} and d_{TM}) of the films. We measured the thicknesses d also using the α-step profilometer, since the thicknesses from d_{TE} and d_{TM} are slightly different. The data of n_{TE} and n_{TM} represented by symbols ∫ and ∫, respectively, as depicted in Fig. 5.13a. As d is increasing, both n_{TE} and n_{TM} are increasing and become constant when d reached about 2 μm. Besides the values n_{TE} and n_{TM}, it is also important to see how the $\Delta n = n_{TE}-n_{TM}$ is changing respect with d. The Δn could be related to orientation of polymers in thin film respect to substrate plane [Prest'80, Koynov'06].

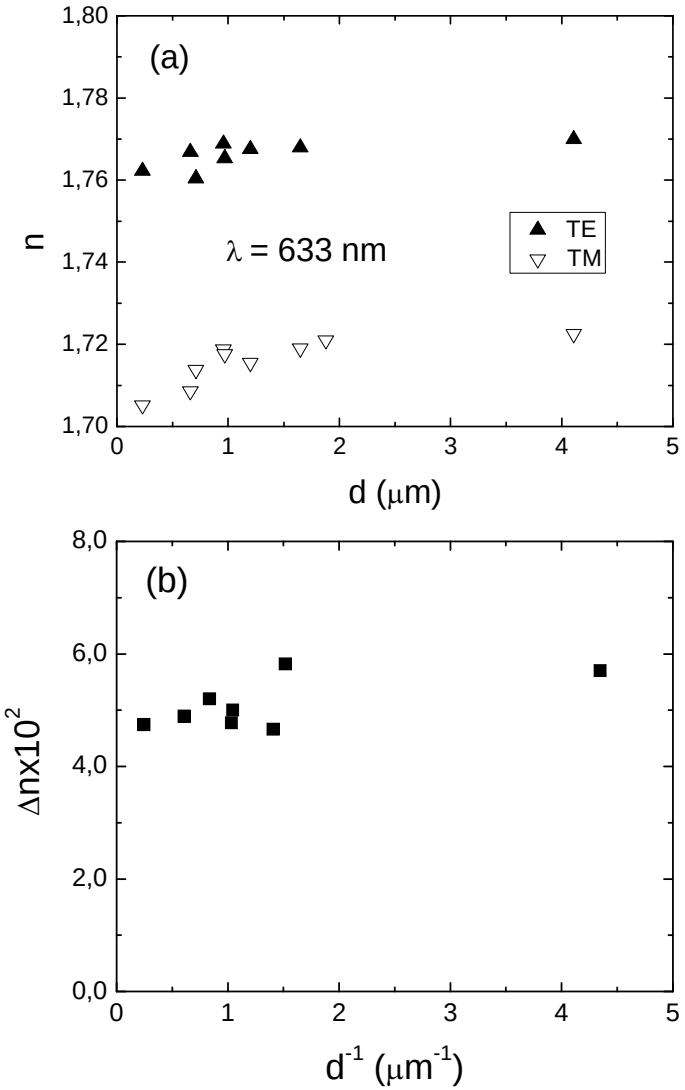

Fig. 5.13: Thickness d dependence of refractive index n (a) and optical birefringence Δn (b) of P3BT-ra films prepared from chlorobenzene solutions.

The thickness d dependence of Δn of polymer thin films could be related with orientation correlation function f, which was used by Cordeiro [Cordeiro'07] to explain the dependence of birefringence Δn of several polymers thin films with film thickness d.

According to Cordeiro [Cordeiro'07], several flexible and low molecular weight polymer shows that $\Delta n \propto d^{-1}$. In Fig. 5.13b we plotted the Δn of P3BT-ra versus d^{-1}. There is a small but significant change of Δn with d^{-1} is observed. Optical anisotropies of the polythiophene films with thickness range of 40 – 160 nm can be strongly dependent on thickness as reported by Zhokhavets [Zhokhavets'06]. The combination of our data and Zhokhavets's is confirming that, polythiophene orientations in the thin films are thickness dependent. This behaviour has not been observed in other conjugated polymers (MEH-PPV and polyfluorene), as these polymers have thickness independent optical constants.

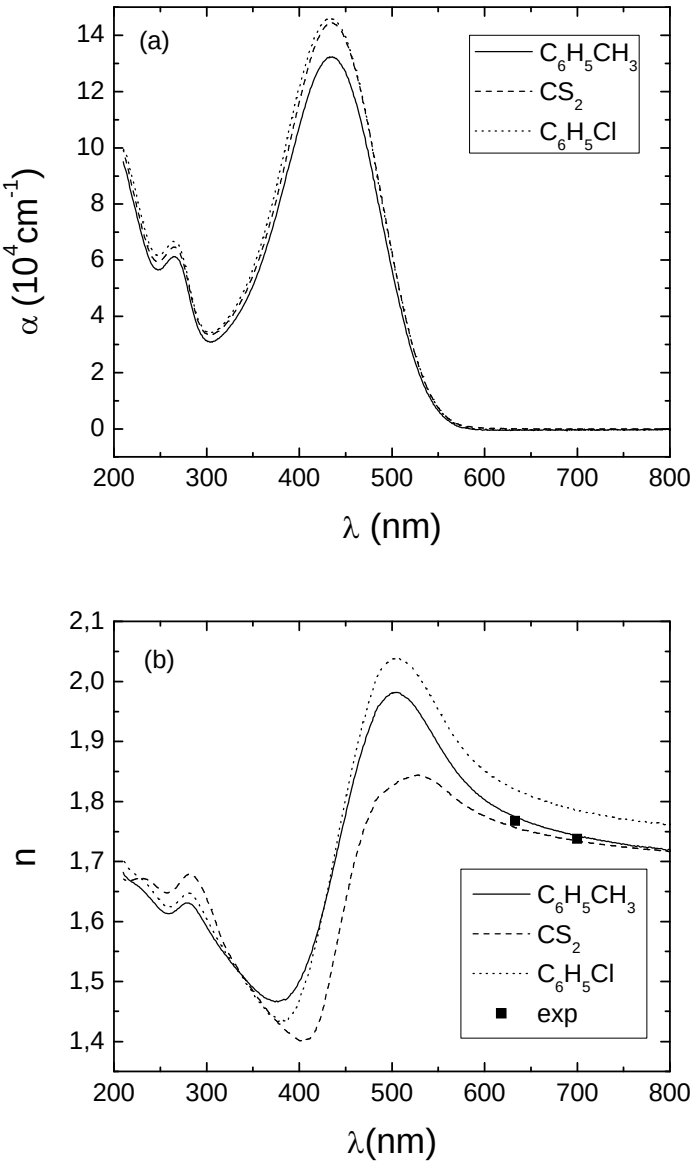

Fig. 5.14: Optical constants of thin films of P3Bt-ra measured by reflectometry and prism coupling. Optical absorption coefficients (a) and refractive indices (b) of P3BT-ra films spin coated from solutions using different solvents: CS_2 (dashed-line, T_{BP}=46°C), $C_6H_5CH_3$ (solid-line, T_{BP}=111°C) and C_6H_5Cl (dotted-line, T_{BP}=132°C).

It is also important to see the effects of solvent on optical constants of P3BT-ra films. Solvents which have different boiling points (BP) were used to prepare solutions. The following solvents were used: chlorobenzene (C_6H_5Cl, T_{BP} = 132°C), toluene ($C_6H_5CH_3$, T_{BP} = 111°C) and carbon disulfide (CS_2, T_{BP} = 46°C). Films were prepared with the same spin-coating parameters (casting temperature T_c, spinning speed ω and annealing temperature T_a). The prism-coupling measurement showed that spin-casted waveguides from toluene have the lowest waveguide loss.

Effects of T_{BP} on linear optical (α and n) spectra of P3BT-ra are shown in Fig. 5.14a and Fig.5.14b, respectively. Fig. 5.14b shows the effect of T_{BP} on n, which has a clear trend to larger n_{TE} data with increasing T_{BP}. We measured also refractive index (n_{TE} and n_{TM}) of waveguides of thickness d about 1 μm, which were prepared from solvents of different boiling temperatures T_{BP}. The plot of n_{TE} and n_{TM} of P3BT-ra film versus T_{BP} is depicted in Fig. 5.15. The n_{TE} and n_{TM} increases strongly with T_{BP} from CS_2 to toluene. But the general trend is not fully clear yet. The role of T_{BP} on refractive index (n_{TE} and n_{TM}), can be seen more clear using birefringence $\Delta n = n_{TE} - n_{TM}$, which could be related to orientation of polymer respect to substrate plane [Prest'79, Campoy-Quiles'05 and Koynov'06].

We do not have an answer, why Δn does not systematically increase with T_{BP}. Our tentative interpretation is that the solubility parameters of the solvents for P3BT-ra may differ. However, more investigations would be needed to solve this question.

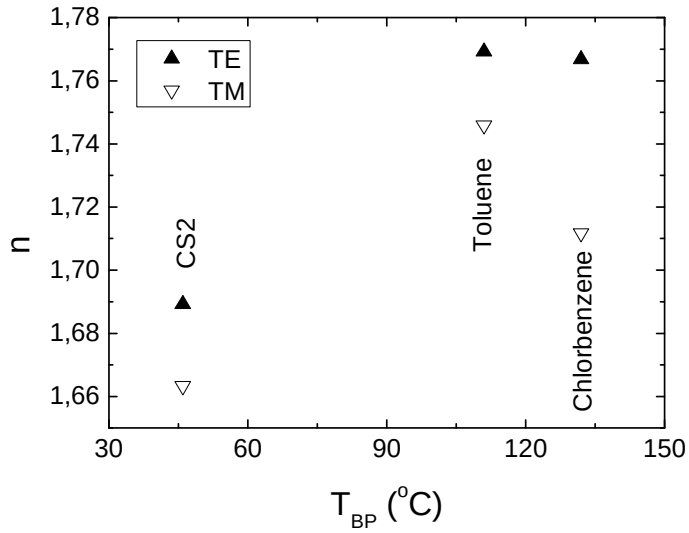

Fig. 5.15: The refractive indices of P3BT-ra film plotted against boiling-point temperatures (T_{BP}) of solvents.

5.5.2 Stability Investigations

Under photo-irradiation in ambient air, a polymer film could undergo degradation because of photo-oxidation. Chemical changes and molecular weight reductions are results of photo-oxidation. It is important to know the stability of the polymer waveguides against photo-oxidation upon irradiation in air environment. There are two kinds of photostabilities we will address here: (1) are the threshold wavelength (λ_c) and (2) the threshold intensities (I_{th}), which were defined in section 3.6. Fig. 5.16 shows the maximum of absorbance (A_{max}) of P3BT-ra thin film (d=48 nm) after irradiation with a xenon high pressure arc and at several cut-off wavelengths λ_c. It is clear that P3BT-ra film is stable for irradiation for $\lambda > 550$ nm, but at $\lambda < 550$ A_{max} decreases with higher slope.

In the case of P3AT, photo-irradiation causes photochemical reactions including photobleaching, chain scission and cross-linking [Holdcroft'91 and Abdou'91]. There are some mechanisms of photodegradation of P3AT, which have been proposed in solutions [Abdou'93] and in solid-state [Abdou'95 and Manceau'09]. In general, it can be summarized as follows: Oxidation can take place in alkyl side chain and in thiophene backbone. The backbone oxidation was initiated by alkyl chain oxidation [Manceau'05].

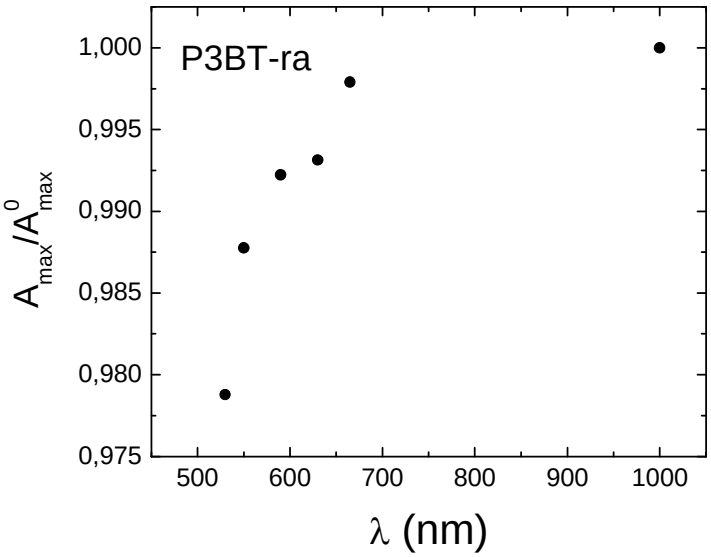

Fig. 5.16: The maximum absorbance (A_{max}) of a P3BT-ra thin film (d=54 nm) after irradiation at $\lambda > \lambda_c$ plotted against cut-off wavelength λ_c of the filter. The A^0_{max} is absorbance maximum of un-irradiated sample.

We did laser photoablation on surface P3BT-ra thin film in ambient air environment with the setup as explained in section 3.6. The experiment aim was to create some ablation holes with different pulse energies. We started with low energy where there

was no ablation hole detected, and then increased the energy for the next ablation. We repeated the processes till we have created several holes of different sizes corresponds to different pulse energies. We observed some ablation holes at several locations on the film surface using optical microscope, but the holes sizes were measured using step-profilometer (KLA Tencor Cooperation Model P-10). Fig. 5.17 show square of diameters of three holes plotted against pulse energies.

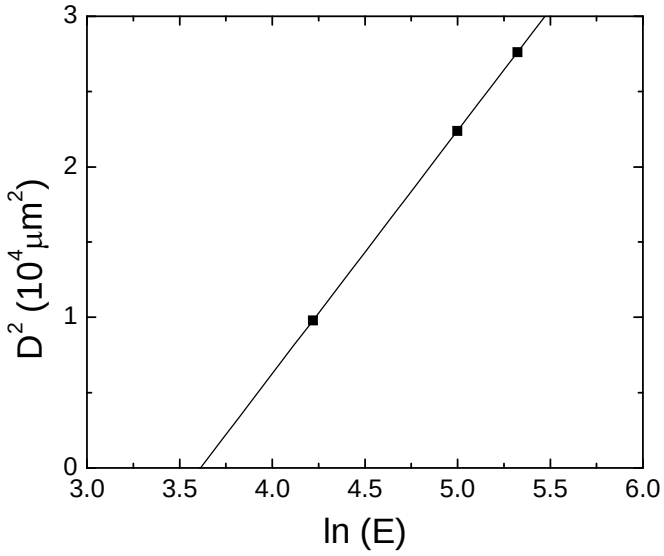

Fig. 5.17: Square of diameter D^2 of holes on P3BT-ra thin film (d=550 nm) surface after irradiation with high intensity (50 pulses) pulsed laser (λ=1064 nm; τ_{FWHM}=28.02 ps) which was focused with a f = 200 mm lens. The linear fit refers to $D^2 = -58313 + 16141\ln(E)$.

The threshold intensity (I_{th}) of pulsed laser could be determined from threshold energy (E_{th}), using Eq.3.3 and linear fit equation. The value of E_{th} was determined from interception between the line fit and ln(E) axis, where ln(E_{th})=58313/16141 = 3.6, E_{th} = exp(3.6)=36.6 μJ. The σ_x^2 is determined from the slope value, where σ_x^2 is 16141/2=8070.5 μm^2. The threshold fluence (F_{th}) of 1.8 Jcm^{-2} is calculated from values of E_{th} and σ_x^2. The I_{th} value is 22.8 $GWcm^{-2}$ and has been calculated from the values of E_{th} and σ_x^2. Typical F_{th} for polyethylene (PE) is 1 Jcm^{-2} under irradiation of femtosecond (fs) laser pulses (λ=620 nm, 100 pulses and τ_{FWHM} =300 fs), absorption coefficient of PE at 620 nm is less than 20 cm^{-1} [Krüger'04]. Threshold fluence of P3BT-ra under irradiation of picosecond pulse laser is higher compared to the typical F_{th} of non conjugated polymers, most probably because of longer pulse duration. The comparisons of the damage threshold of P3BT-ra with other conjugated polymers are given in Table 5.8,

where P3BT-ra has I_{th} a little bit more than MEH-PPV which was reported by Bader et. al [Bader'02].

Table 5.8: The I_{th} of P3BT-ra and some conjugated polymers.

	I_{TH} ($GWCM^{-2}$)	REF.
PPV	5	Fitrilawati'02
MEH-PPV	> 12	Fitrilawati'02
MEH-PPV	21	Bader'02
P3BT-ra	22.8	This work

6 Intensity Dependent Prism Coupling of P3BT-ra

In this chapter, we will present the nonlinear optical properties of regiorandom poly(3-butylthiophene) abbreviated P3BT-ra, which turned out in chapter 5 as most suitable candidate among P3ATs for all optical switching applications. The P3BT-ra was bought from Rieke Metals Inc., USA. The molecular weights were M_w=30.9 kg/mol and M_n=10.2 kg/mol as determined at MPI-P with gel permeation chromatography (GPC) using polystyrene standards and THF as eluent. Third-order nonlinear optical constants (absorption coefficient α_2 and refractive index n_2) of P3BT-ra waveguides were measured by intensity dependent prism coupling technique at several wavelengths in the NIR range (700 – 1500 nm). Spectra of figure of merit (FOM) W and T as described in chapter 1 will be determined from spectra of $\alpha_{gw}(\lambda)$, $\alpha_2(\lambda)$ and $n_2(\lambda)$. From spectra of W and T, we can find the spectral regions where requirements of all-optical switching applications are fulfilled.

6.1 Results

The s-polarized laser beam was used to excite the TE_0 mode of a waveguide. The reflected light intensity I_R is measured as function of the angle of incidence θ and displayed in Fig. 6.1. The coupling curve has a minimum at the coupling angle (θ_m) if the waveguide mode m is excited (see chapter 3). To obtain a set of intensity dependent curves, we used the following procedure. First, we measure the coupling curve at low intensity. The coupling parameters are: air-gap thickness d_a, air-gap length l_a and incident beam diameter d_b. The procedure of determination of l_a was discussed earlier [Koynov'02]. Second, d_a is adjusted to reach a slightly overcoupled condition [Koynov'02], where I_R is sensitive to changes of the absorption coefficient α. Finally, $I_R(\theta)$ was measured at gradually increasing energy of incident laser pulses. The coupling angle θ_m shifts with increasing energy of the incident laser pulses, which is directly related to a refractive index change Δn_f of the film. The depth of resonance curve is increasing as absorption coefficient α_f of the films is increasing. The reversibility of the I_R curves was controlled by applying laser pulse energy below a certain limiting value, which was approximately 3 μJ for 1064 nm < λ < 1600 nm and < 1 μJ for λ < 1064 nm. The limiting values were determined as follows: we measured I_R curves at several energies (E_1, E_2, …, E_n) where we start at very low energy E_1 then followed by

measurement at E_2 (E_2>E_1), E_3 (E_3 >E_2) and so on. After measurement at E_2, E_3, … and E_n we perform measurement at E_1 again, which is used to control the reversibility of I_R. If I_R curves at E_1 after and before measurement at E_n are different (not reversible) that E_{n-1} is the limiting value at certain λ.

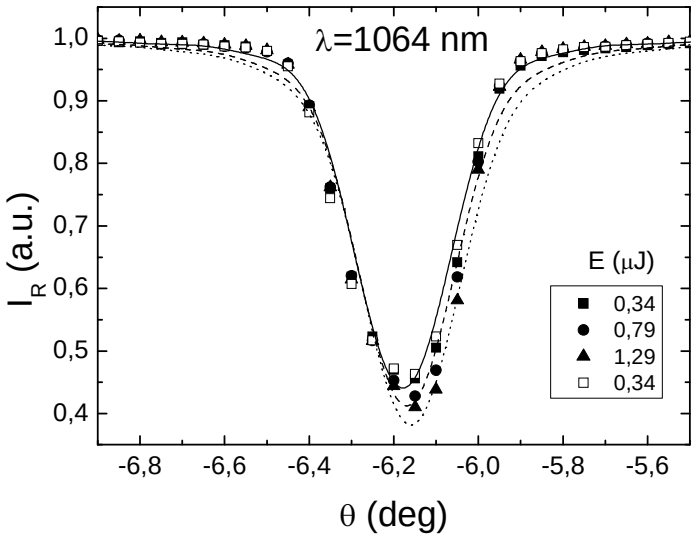

Fig. 6.1: Coupling curves (IR vs. θ) of TE_0 mode of 535 nm thick P3BT-ra waveguide were measured at 1064 nm and different pulse energies (see inset). Lines are numerical fits to the experimental points. Air gap thickness d_a = 264 nm was held constant. Only n_f and α_f of the film were varied to fit the measurements at the three energies (0.34 μJ: n_f = 1.6862, α_f = 1.7 cm^{-1}; 0.79 μJ: n_f = 1.6863, α_f = 3.7 cm^{-1}; 1.29 μJ: n_f = 1.6864, α_f = 5.7 cm^{-1}). A complete reversibility of the coupling curves was observed at 1064 nm (open squares symbols which were measured after 1.29 μJ are in coincidence with filled squares symbols).

The distributions of guided wave intensities of a waveguide in the mode-propagation direction and the direction perpendicular to the film plane are following a bell-shaped and a $\cos^2$ function (for TE_0 mode), respectively [Marcuse'74]. Since the guided wave intensities are not uniformly distributed in the waveguides, the optical constants n_f and α_f change according to these distributions. For small changes Δn_f and $\Delta\alpha_f$ (small nonlinearities) and moderate input intensities, a uniform approximation is used instead of the distribution functions and written in the form

$$\Delta n_f = n_2 \langle I_{gw} \rangle \tag{6.1}$$

$$\Delta \alpha_f = \alpha_2 \langle I_{gw} \rangle . \tag{6.2}$$

The average guided wave intensity $\langle I_{gw} \rangle$ is calculated by means of Eq. (3.12) in Bahtiar [Bahtiar'04] or Eq. (27) in Ueberhofen [Ueberhofen'99].

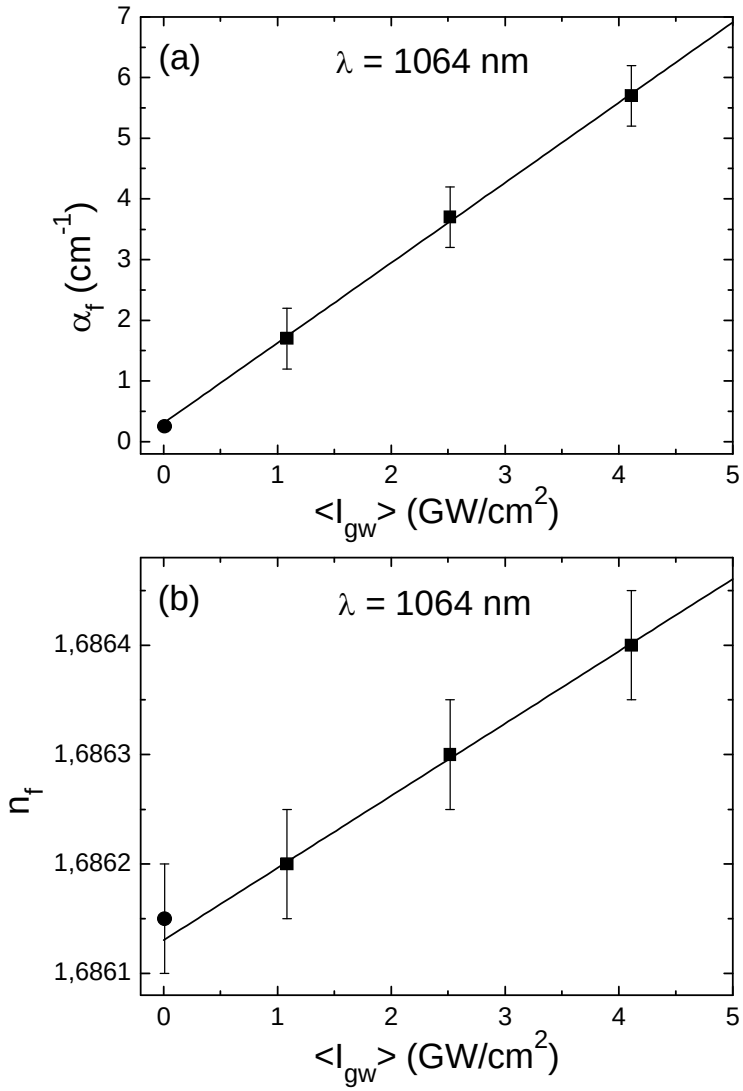

Fig. 6.2: Absorption coefficient α_f (a) and refractive index n_f (b) of the film at laser wavelength 1064 nm (full squares) as a function of the average intensity in the waveguide $<I_{gw}>$. Values of α_2 and n_2 are equal to slopes of linear fits of α_f and n_f respectively. The n_2 and α_2 values are $(6.6 \pm 0.9)10^{-14}$ cm^2/W and $(1.3 \pm 0.1)10^{-9}$ cm/W. For comparison, the results of linear prism couplings using a cw Nd:YAG laser are shown (full circles).

Since the intensity dependencies of $\beta_m(I_{gw})$ and $\alpha_{gw}(I_{gw})$ in Eq. (3.4) are neglected, the fits in Fig. 6.1 are calculated using two parameters only, namely n_f and α_f. Fig. 6.2 shows examples of the linear dependencies of absorption coefficient α_f and refractive index n_f on the average intensity in the film $<I_{gw}>$. Values of α_2 and n_2 are equal to the slopes of linear fits in Fig. 6.2 (a) and (b), respectively. The intercept of the linear fits to vertical axis α_f ($<I_{gw}>=0$) and n_f ($<I_{gw}>=0$) corresponds to the low intensity limit, i.e., the linear waveguide loss (α_{gw}) and refractive index (n_0) respectively. Both experimental methods show good agreement. All of experimental linear and nonlinear data of P3BT-ra

which were determined using nonlinear prism coupling are presented in the Table 6.1 and plotted in Fig. 6.3.

Table 6.1: Linear and non-linear optical constants of P3BT-ra were determined using non-linear prism-coupling.

λ [NM]	N_0 $\pm$ 0.0001	α_0 [CM^{-1}]	N_2 [CM^2/W]	α_2 [CM/W]
700	1.7384	3.0 ± 1.0	$(-1.5 \pm 0.5)10^{-13}$	$(3.0 \pm 1.0)10^{-10}$
800	1.7138	2.0 ± 0.1	$(-3.0 \pm 0.3)10^{-14}$	$(7.0 \pm 1.0)10^{-10}$
900	1.6996	1.0 ± 0.1	$(4.0 \pm 1.0)10^{-14}$	$(2.0 \pm 0.5)10^{-9}$
1000	1.6921	0.48 ± 0.3	$(5.6 \pm 0.1)10^{-14}$	$(7.0 \pm 2.0)10^{-10}$
1000	1.6921	0.48 ± 0.2	$(2.0 \pm 0.1)10^{-14}$	$(2.0 \pm 2.0)10^{-10}$
1100	1.6835	0.2 ± 0.1	$(1.0 \pm 0.1)10^{-13}$	$(1.0 \pm 0.3)10^{-9}$
1064	1.68615	0.25 ± 0.1	$(7.0 \pm 1.0)10^{-14}$	$(1.3 \pm 2.0)10^{-9}$
1064	1.6861	0.3 ± 0.1	$(0.4 \pm 0.3)10^{-14}$	$(0.3 \pm 0.1)10^{-9}$
1150	1.6830	0.22 ± 0.1	$(1.56 \pm 0.3)10^{-13}$	$(1.2 \pm 0.2)10^{-9}$
1150	1.6830	0.2 ± 0.1	$(1.04 \pm 0.3)10^{-13}$	$(1.0 \pm 0.3)10^{-9}$

1170	1.6820	0.2 ± 0.1	$(5.5 \pm 1.0)10^{-14}$	$(2.0 \pm 2.0)10^{-10}$
1200	1.6810	0.1 ± 0.1	$(2.3 \pm 0.8)10^{-14}$	$(2.0 \pm 1.0)10^{-10}$
1300	1.6792	0.1 ± 0.1	$(1.5 \pm 1.0)10^{-14}$	$(1.0 \pm 0.5)10^{-10}$
1400	1.6768	0.1 ± 0.1	$(1.0 \pm 1.0)10^{-14}$	$(0.5 \pm 2.0)10^{-10}$
1500	1.6753	0.1 ± 0.1	$(0.7 \pm 1.0)10^{-14}$	$(0.5 \pm 2.0)10^{-10}$

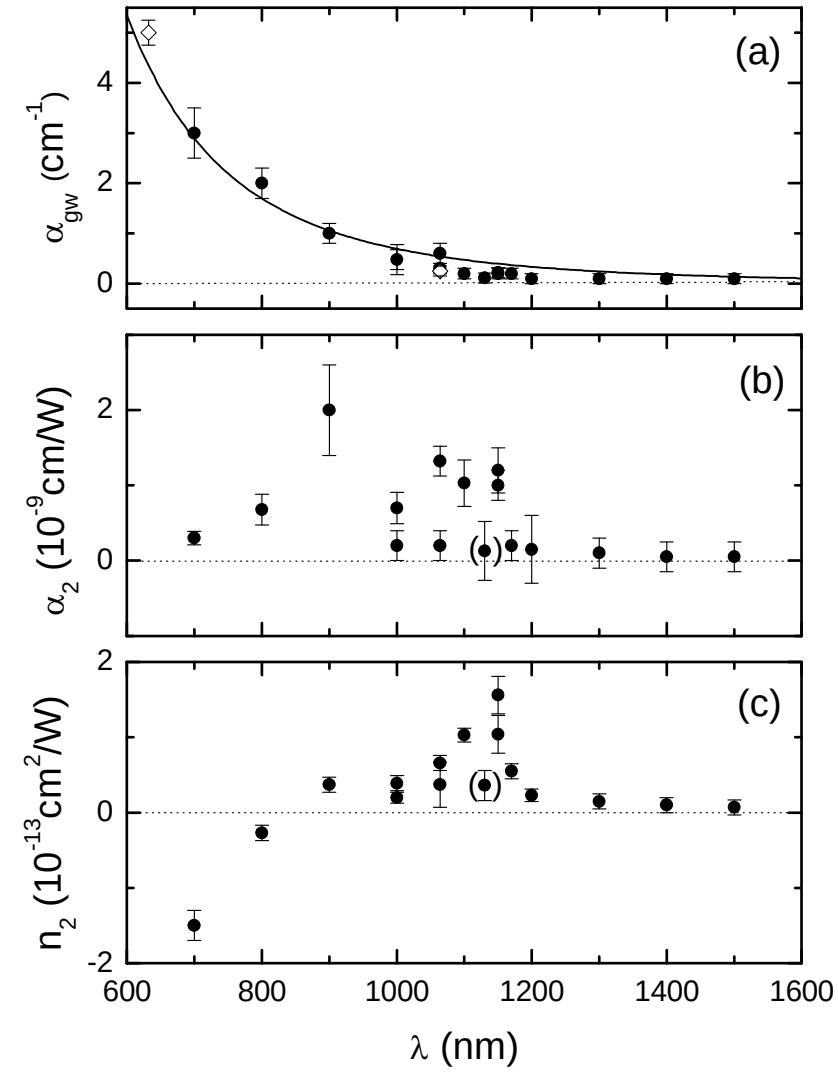

Fig. 6.3: Comparison of linear and nonlinear optical spectra of P3BT-ra measured at laser wavelengths λ. (a) Linear attenuation loss $\alpha_{gw}(\lambda)$ determined from coupling curves at low intensity (full circles) and from waveguide loss experiments (open diamonds). The fitting curve (full line) describes contributions of Rayleigh- and Mie-scattering, see text. Dispersions of α_2 and n_2 are shown in (b) and (c) respectively. Brackets are used to indicate the data points which are uncertain.

The spectrum of the linear waveguide loss α_{gw} of P3BT-ra is depicted in Fig. 6.3a and shows a monotonous decrease toward longer wavelengths. This behavior can be interpreted by Rayleigh and Mie type light scattering of the guided modes [Ma'02], which is given by Eq. 2.52. By using Eq. 2.52 to fit experimental data in Fig. 6.3a we have found a_0, a_1 and a_2 parameters which are listed in Table 6.1. The Rayleigh contribution is dominant, as can be seen when we put a_2=0 which means the only α_{gw} is contributed by Mie scattering only. The curve obtained by setting a_2=0 is close to the line at α_{gw}=0 and not shown explicitly in Fig. 6.3a. This means the size of the scattering object is smaller than the wavelength. The theoretical line is not valid anymore as it is approaching 600 nm, where the tail of absorption coefficient is dominant.

Table 6.2: Fitting parameters of Eq. 2.52

A_0 (CM^{-1})	A_1(CM)	A_2 (CM^3)
$4.99x10^{-19}$ -$1.05x10^{-16}$	$(0.35\text{-}5.81)x10^{-16}$	$(6.94\pm0.01)x10^{-17}$

The spectrum of nonlinear absorption coefficient α_2 of P3BT-ra depicted in Fig. 6.3b shows large two-photon absorption (TPA) excited at 900 – 1100 nm, which refers to a TPA energy level at 2.26 eV – 2.76 eV. The spectrum of nonlinear refractive index n_2 is shown in Fig. 6.3c. Values of n_2 were observed at $\lambda < 850$ nm are negative and become positive at $\lambda \geq 900$ nm. The maximum of $n_2 = (1.03 \pm 0.09) \times 10^{-13}$ cm^2/W was observed at $\lambda = 1100$ nm and decreases monotonically at longer wavelengths. At shorter wavelengths, n_2 becomes zero at approximately λ=850 nm and gets negative at $\lambda < 850$ nm.

6.2 Discussion

6.2.1 Comparison of the nonlinear optical spectra of polythiophenes

The nonlinear spectra of P3BT-ra, which are depicted in Fig. 6.3b and Fig. 6.3c, will be compared to experimental spectra of polythiophene which are reported earlier. Third-order nonlinear optical spectra of polythiophene have been measured with different

methods: THG [Torruellas'90, Kishida'05], two-photon absorption (TPA) spectroscopy [Periasamy'92, Sakurai'97, and Meyer'97], Kerr ellipsometry [Pfeffer'93] and DFWM [Bubeck'91].

The spectrum of nonlinear absorption coefficient α_2 of P3BT-ra depicted in Fig. 6.3b shows large two-photon absorption (TPA) excited at 900 – 1100 nm, which refers to a TPA energy level at 2.26 eV – 2.76 eV. This is in good agreement with earlier reports of TPA in polythiophenes. Using the oligomer α-sexithienyl, Periasamy et al. observed several distinct TPA energy levels at 2.25-2.48 eV [Periasamy'92], which are close to the TPA level of poly(3-octylthiophene) thin films located at 2.5 eV as reported by Sakurai et al. [Sakurai'97]. At $\lambda > 1100$ nm, α_2 decreases strongly and does not show any other significant resonance and has values smaller than 10^{-10} cm/W.

The spectrum of nonlinear refractive index n_2 is shown in Fig. 6.3c. We interpret this dispersion of n_2 by considering the joint occurrence of two electronic processes: TPA as described above and saturable absorption, which happens if the laser wavelength approaches the tail of the electronic absorption band. Saturation of the exciton absorption in polythiophenes at high laser pulse intensities was already observed earlier [Dorsenville'89, Bubeck'91, Van Keuren'99 and Yang'92].

6.2.2 Modelling of the Third-Order Nonlinear Optical Spectra with a Three-Level Model

We use a three level model [Ueberhofen'99 and Stegemann'97] including two-photon absorption (TPA) and saturable absorption (SA) to interpret the third-order nonlinear spectra of P3BT-ra. We perform a curve fitting procedure to the experimental spectra of n_2 and a_2. The α_2 and n_2 spectra are related to each other. We present two attempts to fit the experimental data n_2 and α_2. The first one is using the expression of $\chi^{(3)}$ (see Eq. 2.29) directly and second one is using a band-gap scaling model, respectively.

Using $\chi^{(3)}$ expression

The calculation is based on the general formula of $\chi^{(3)}$ (Eq. 2.29) which can be found in the basic literature of nonlinear optics [Boyd'08, Butcher'90]. Relations between n_2, α_2 and $\chi^{(3)}$ are given by (Eq. 2.20) and (Eq. 2.21) respectively. E_g is the energy of ground state g, $E_{g'}$ and E_u are energies of excited-states g' and u, respectively. There are two kinds of allowed electronic transitions between states: namely first is between g and u

and the second one is between g and g'. The transition of electron between state g and u is related to the process of linear absorption. The energy difference between E_g and E_u was chosen equal to hc/λ_{max}, λ_{max} is the wavelength of the absorption maximum or $\alpha_{max}=\alpha(\lambda_{max})$. The transition of electron from g and g' is forbidden for one-photon absorption, but it is allowed for two-photon absorption. There are six parameters, which are contained in Eg. (2.29) and used to fit the spectra of n_2 and a_2 (see Table 6.3).

Table 6.3: Fitting parameters in Eq. 2.29.

PROCESS	ENERGY LEVEL	SPECTRAL WIDTH	AMPLITUDE
TPA	$E_{g'g}= E_{g'} - E_g$	$\Gamma_{g'g}$	$A_{g'g}$
SA	$E_{ug} = E_u - E_g$	Γ_{ug}	A_{ug}

Fig 6.4 shows the calculated spectra of α_2 and n_2 for a three-level system, which consists of ground state g and excited states u and g'. One-photon absorption is a transition from the ground-state g to the excited-state u. At high intensity, the excited-state becomes more populated, resulting in the decrease of the absorption coefficient. As consequence, α_2 is negative. It has maximum at wavelength $\lambda_1 = hc/E_{ug}$. The n_2 is positive at the higher energy side ($\lambda < \lambda_1$) and negative at the lower energy side ($\lambda > \lambda_1$) of the resonance. The second process is two-photon absorption, which is the transition from the ground state g to the lowest excited state g' [see Fig. 6.4b]. It is characterized by $\alpha_2 > 0$ and a maximum at $\lambda_2 = 2hc/E_{g'g}$. The n_2 is negative at the higher energy side and positive at lower energy side of the resonance. In the non-resonant region at long wavelengths, both processes can have different strength. Therefore, the sign of n_2 is determined by the dominant mechanism.

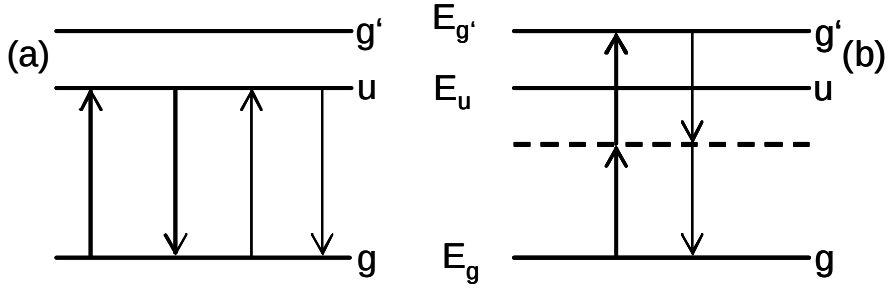

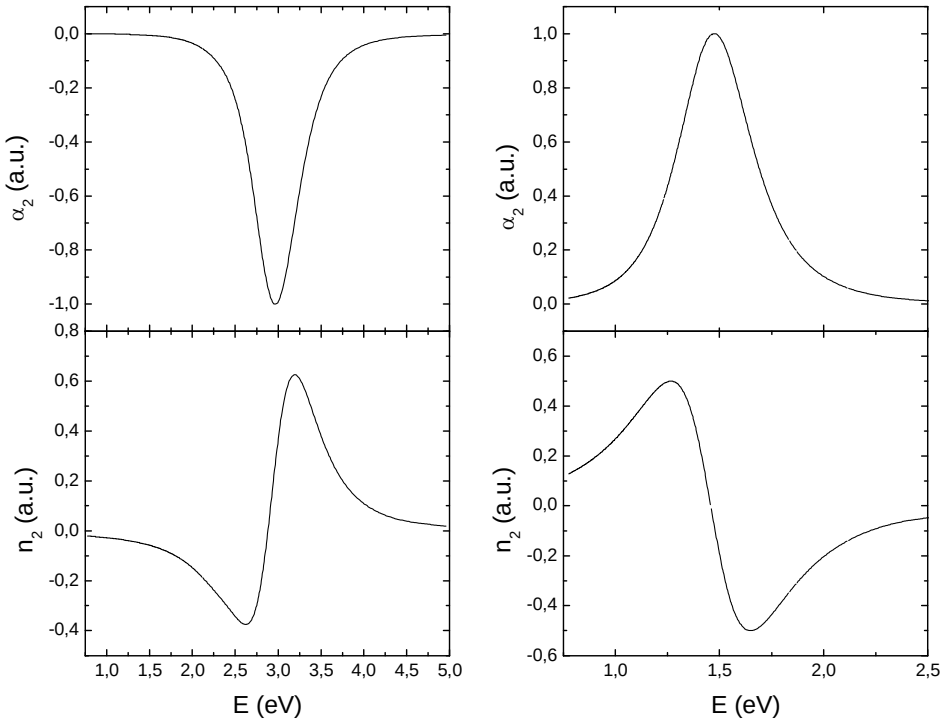

Fig. 6.4: Normalized calculated spectra of α_2 and n_2 of (a) one-photon and (b) two-photon resonances with a three-level system. The parameters were used are follows E_{ug} =2.88 eV, Γ_{ug}=0.4 eV, $E_{g'g}$=2.92 eV and $\Gamma_{g'g}$=0.5 eV.

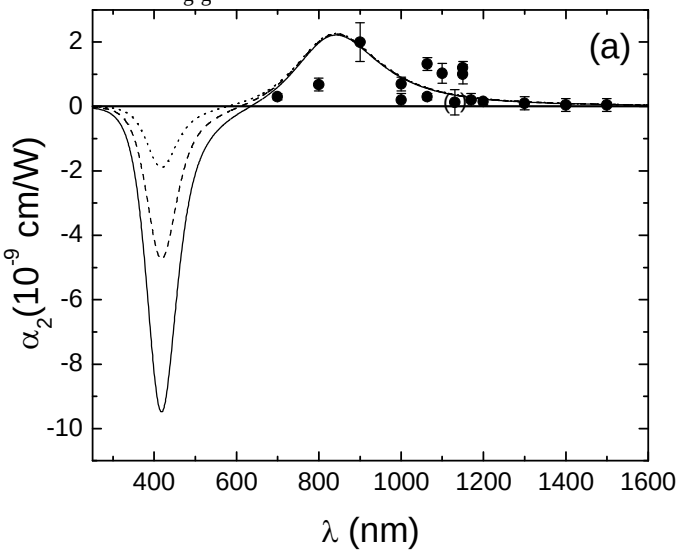

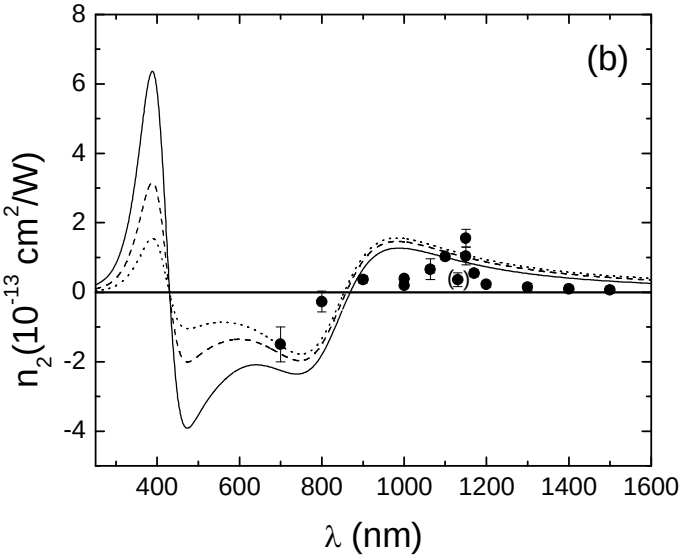

Fig. 6.5: Nonlinear spectra α_2 (a) and n_2 (b) of P3BT-ra films measured using nonlinear prism coupling (symbols) and calculated (lines) using Eq. (2.29). The parameters were $E_{g'g}$=2.92 eV, $\Gamma_{g'g}$=0.4 eV, $A_{g'g}$=1.0 and E_{ug}=2.88 eV, Γ_{ug}=0.5 eV, A_{ug}=0.5 (dotted), A_{ug}=1.0 (dashed), A_{ug}=2.0 (full).

In Fig. 6.5 lines are calculated nonlinear optical spectra, which are composed of normalized n_2 and α_2 of one-photon and two-photon process spectra in Fig. 6.4 with weighted constants $A_{g'g}$ and A_{ug}, respectively. Since we do not have experimental data in the range of the SA resonance, we present lines with different A_{ug} values. Obviously, the model successfully fits the whole TPA region of α_2 and longer wavelength region of n_2. The reasons of large discrepancies between model and experimental data points of n_2 in the range of 800 – 1000 nm might be caused by the large experimental error and also the lack of data points in SA region, which were not accessible experimentally at $\lambda < 680$ nm because the tuning range of the OPG is only between 680 nm and 2000 nm. The large discrepancies of n_2 are might be caused by limitation of the model which have been discussed in section 4.3.

6.2.3 Band-Gap Scaling Model of Semiconductors

We used also a dispersion and band-gap scaling model which was introduced by Sheik-Bahae [Sheik-Bahae'90] to see the generality of n_2 spectra around the band-gap E_g of semiconductors. The model was quite successful to predict the dispersion behaviour in the low energy regime ($h\nu < E_g$) and around the band-gap of inorganic semiconductors. However, electronic states in organic semiconductors are quite different compared to inorganic crystalline semiconductors (for example: band-gap definition in organic

semiconductors is extrapolated to polymer limit from the values of their oligomers [Bubeck'98 and Gierschner'07]).

Sheik-Bahae et. al. [Sheik-Bahae'90 and Sheik-Bahae'91] used Band-Gap scaling to derive n_2 which can be written as

$$n_2 = K\frac{\hbar c\sqrt{E_p}}{2n_0 E_g^4} G_2\left(\hbar\omega / E_g\right) \tag{6.3}$$

where E_p is a material independent constant and has the value E_p = 21 eV, K can be considered to be a single free parameter and material-dependent. The K value for inorganic semiconductor is found empirically to be $3.1x10^3$ in units such that E_p and E_g are measured in eV and n_2 is measured cm^2/W, and where G_2 is the universal function

$$G_2(x) = \frac{-2+6x-3x^2-x^3-\frac{3}{4}x^4-\frac{3}{4}x^5+2(1-2x)^{3/2}\Theta(1-2x)}{64x^6}, \tag{6.4}$$

where $\Theta(y)$ is the Heaviside step function defined such that $\Theta(y)=0$ for $y < 0$ and $\Theta(y)=1$ for $y \geq 0$.

Fig. 6.6 shows the model (line) and experimental data points of MEH-PPV [Bahtiar'04] and P3BT-ra (this work). In general, experimental points are following the same trends as Band-Gap scaling approach (line), which means the approach is coarsely valid also for organic semiconductors. Some deviations for example in height and width of resonance peaks (the maximum of n_2 around $h\nu/E_g=0.5$) could be discussed in terms of differences in physical properties inorganic and organic semiconductors.

Value of energy gap (E_g) of P3AT-ra according to Gierschner [Gierschner'07] is around 2.10 eV. We have adopted $K'=3.4\times10^{-8}$ of inorganic for organic semiconductors.

Resonance peaks of organic semiconductors have smaller absorption coefficient and narrower spectral widths compared to inorganic ones. Disagreement between them could be explained because of their natural difference where the dependence of magnitude $\chi^{(3)}$ or n_2 in inorganic semiconductors are proportional to Eg^{-4} and in organic semiconductor are larger (for P3HTs are proportional to $E_g^{-6.7}$ [Kishida'05], for PTs and PPVs are proportional to $E_g^{-10\pm1}$ [Mathy'96]).

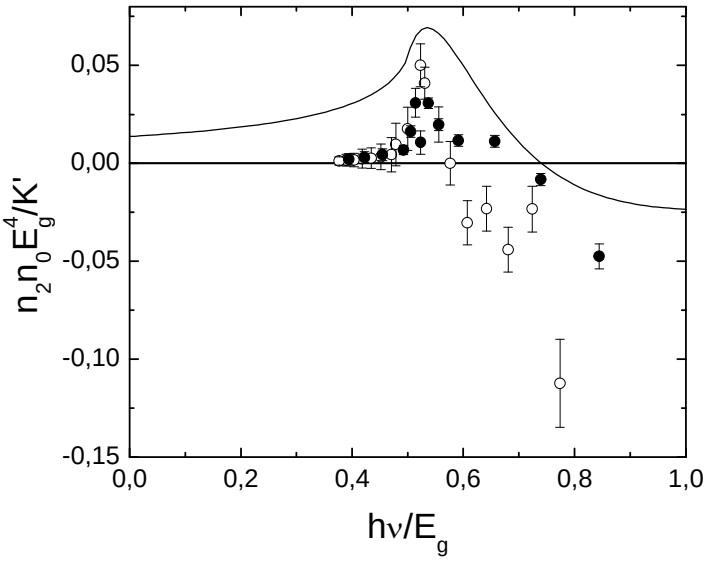

Fig. 6.6: Dispersion of scaled n_2 plotted of MEH-PPV (open circles) and P3BT-ra (filled squares). The dispersion of scaled n_2 of semiconductors (line) is redrawn after Sheik-Bahae [Sheik-Bahae'90] for comparison.

6.2.4 Figures of Merit

The measured values of α_{gw}, α_2 and n_2 from intensity dependent prism coupling were used to calculate the spectral dependences of the figures of merit (FOMs) W and T as defined in Chapter 1. We have used the total waveguide loss coefficient α_{gw} instead of α_0 and a light intensity I = 1 GW/cm^2 as in earlier estimates of W [Stegeman'93]. The dispersions of W and T are shown in Fig. 6.7.

At short wavelengths, W is close to unity due to strong absorption. At longer wavelengths, the value of W increases due to the increase of n_2. At 1100 nm, the maximum value W = 5 is observed, according to the maximum of the nonlinear refractive index. At λ > 1300 nm, W decreases monotonically with increasing wavelength. The dispersion of T is displayed in Fig. 6.7b. Strong two photon absorption dominates at shorter wavelength. Towards longer wavelengths T decreases and becomes close to 1 at 1100 nm < λ < 1200 nm, and increasing again monotonically the as value of n_2 is decreasing.

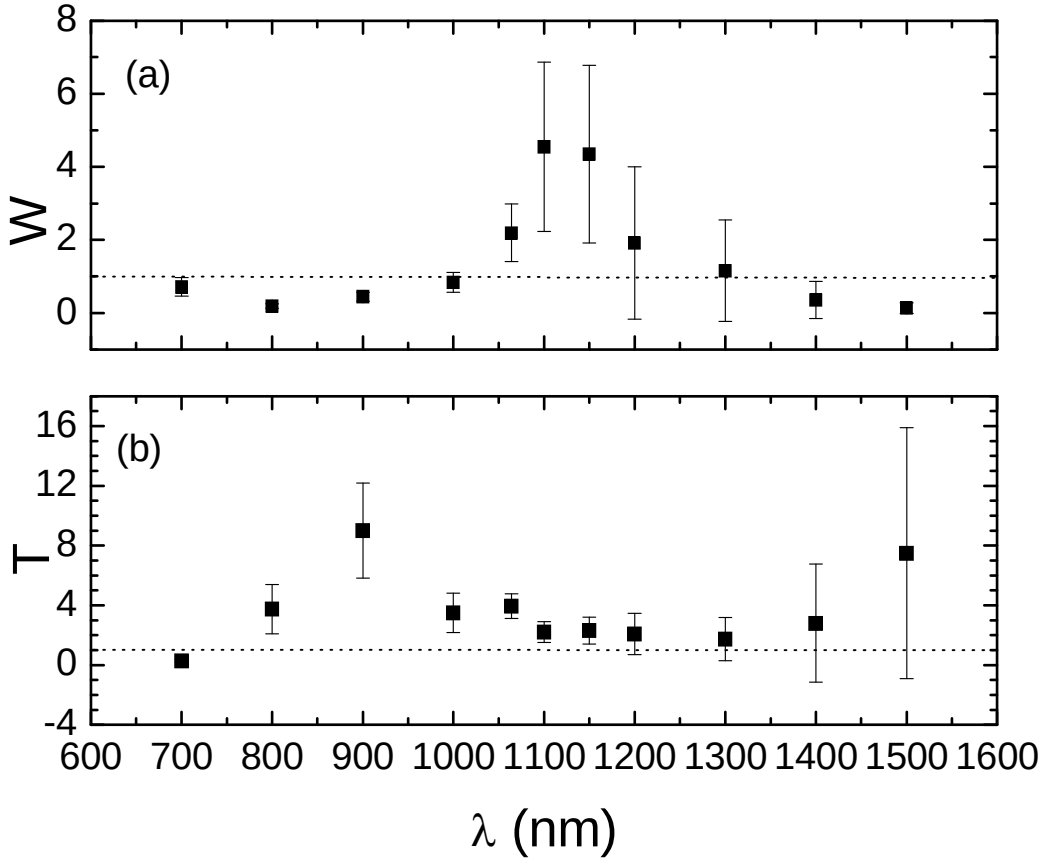

Fig. 6.7: Spectral dependences of FOMs (a) W and (b) T of P3BT-ra waveguides. Dashed lines are W=1 and T=1 respectively.

Comparison of FOMs with other materials

Recently reported FOMs of some organic semiconductors are shown in Table 6.4. Sometimes different definitions of W and T are used by other authors. We used always W and T of Stegemann [Stegemann'93] which are expressed in Chapter 1, see Eq. (1.3) and Eq. (1.4), respectively. FOMs of organic semiconductors were reported rarely because many experimental values are needed, which are not completely known. For example, nonlinear optical constants (e.g.: n_2 and α_2 or $\chi^{(3)}$) which were determined using Z-scan, THG, DFWM are reported without specifying the linear optical waveguide properties. Even sometimes waveguide optical properties values (n_2 and α_2) were extrapolated either from solution values (Z-scan) or different phenomena of $\chi^{(3)}$ (THG and DFWM). Incomplete data set of n_2, α_2 and α_{gw} leads to doubtful reports of FOM. In Table 6.4 such doubtful FOMs were not incorporated. According to Table 6.4 both MEH-PPV and P3BT-ra are promising materials for all-optical switching application around 1100 nm.

Table 6.4: Recalculated of figures of merit (FOMs) of various organic materials by means of Eqs.1.1 and 1.2. The intensity was assumed by I = 1 GW/cm^2.

MATERIAL	λ [NM]	N_2 [CM/W]	α [CM^{-1}]	α_2 [CM/GW]	W	T	REF.
PTS (crystal)	1300	3.2 x 10^{-12}	-	20	-	1.6	1
	1600	2.2 x 10^{-12}	< 0.8		> 10	< 0.1	2
Poly-4BCMU	1319	4.8 x 10^{-14}	1.8	< 0.25	0.2	~ 1.4	3
DANS	1064	7.0 x 10^{-14}	~ 3	0.8-2	0.2	2-6	4
	1319	8.0 x 10^{-14}	0.4	< 0.08	1.5	< 0.26	5
DAN2	1064	1.9 x 10^{-13}	4	1-2	~ 0.4	1-2	4
PPV	800	> 10^{-11}	-	80	-	~1.3	6
	925	5.0 x 10^{-12}	9	-	6	-	7
DPOP-PPV	880-920	~ 1.5 x 10^{-14}	< 0.35	~ 0.14	~ 0.5	~ 1.7	8
	970	1.0 x 10^{-14}	< 0.35	0.02	0.3	~ 0.3	
PPV(RCo 52)	880-920	3 - 4x10^{-14}	< 0.35	~ 0.3	> 1	> 1	8
	970	3.0 x 10^{-14}	< 0.35	0.1	0.9	~ 0.6	
MEH-PPV	1080	2.2 x 10^{-13}	0.1	1.4	20.4	1.4	9
	1130	8.0 x 10^{-14}	0.1	0.13	7.1	0.4	
	1200	2.0 x 10^{-14}	0.1	0.1	1.7	0.12	
MEH-PPV	1064	2.7 x 10^{-13}	0.1	0.1	16.9	2.5	This Work
	1100	7.3 x 10^{-14}	0.1	0.15	4.4	4.5	
P3BT-ra	1064	7.0 x 10^{-14}	0.1	1.3	2.2	4.0	
	1100	1.0 x10^{-13}	0.1	1.0	4.6	2.2	This
	1150	1.0 x 10^{-13}	0.1	1.0	4.4	2.3	Work

Reference numbers refer to: 1- Kim'94, 2- Lawrence'94, 3- Rochford'91, 4- Marques'91, 5- Kim'93, 6- Samoc'95, 7- Ueberhofen'99, 8- Gabler'98, 9- Bahtiar'04.

7 Summary

We have studied and compared the linear and nonlinear optical properties of thin films and planar waveguides of several conjugated polymers (MEH-PPV and P3AT) and polymers with π-electron rich moieties in the side chain (PVK and PS). PVK and PS have shown relatively small values of nonlinear refractive index n_2 at 532 nm of $(1.2\pm0.5)\times10^{-14}$ cm^2/W and $(2.6\pm0.5)\times10^{-14}$ cm^2/W, respectively.

We have investigated the linear optical constants of several P3ATs, in particular the influence of regioregularity and chain length of alkyl substituents. We have identified the most suitable polymer for waveguide applications, which is P3BT-ra. We have studied the optical properties of P3BT-ra thin films, which were prepared by spincoating from different solvents of different boiling temperatures. We have found that P3BT-ra film casted from toluene solutions are most suitable waveguides for intensity dependent prism-coupling experiments, because of their low waveguide propagation losses at λ=1064 nm.

We have measured the dispersions of waveguide propagation loss α_{gw}, nonlinear refractive index n_2 and nonlinear absorption coefficient α_2 of P3BT-ra waveguides in the range of 700 – 1500 nm. We have observed large values of nonlinear refractive index up to $1.5\text{x}10^{-13}$ cm^2/GW at 1150 nm. We have found that the figures of merit requirements for all-optical switching applications are satisfied in the wavelengths around 1050 – 1200 nm, which is at the lower energy tail of the two-photon absorption. These figures of merit of P3BT-ra are among the best of presently known values of conjugated polymers.

We have found that regiorandom P3BT is the most promising candidate for an integrated all-optical switching device because it shows a good combination of large third-order nonlinearity, ultimately low waveguide propagation losses and sufficient photostability.

We have performed a comparison of the measured dispersion of α_{gw} with a theoretical approach. Fitting the dispersion of α_{gw}, we have found that Rayleigh-scattering is the dominant loss mechanism in MEH-PPV and P3BT-ra waveguides. A quantum-mechanical approach of the third-order nonlinear susceptibility $\chi^{(3)}$ was used to fit the n_2 and α_2 spectra of P3BT-ra and MEH-PPV and can explain that the major effects are saturable absorption and two-photon absorption, which cause the dispersion of n_2 and α_2, respectively.

8 Zusammenfassung

Wir haben die linearen und nichtlinearen optischen Eigenschaften von dünnen Schichten und planaren Wellenleitern aus mehreren konjugierten Polymeren (MEH-PPV und P3AT) und Polymeren mit π-Elektronen Systemen in der Seitenkette (PVK und PS) untersucht und verglichen. PVK und PS haben relativ kleine Werte des nichtlinearen Brechungsindex n_2 bei 532 nm, nämlich $(1,2 \pm 0,5)\times10^{-14}$ cm^2/W und $(2,6 \pm 0,5) \times10^{-14}$ cm^2/W.

Wir haben die linearen optischen Konstanten von mehreren P3ATs untersucht, insbesondere den Einfluss der Regioregularität und Kettenlänge der Alkylsubstituenten. Wir haben das am besten geeignete Polymere für Wellenleiter Anwendungen identifiziert, welches P3BT-ra genannt ist. Wir haben die linearen optischen Eigenschaften dünner Schichten des P3BT-ra untersucht, die mit Spincoating aus verschiedenen Lösungsmitteln mit unterschiedlichen Siedetemperaturen präparieret wurden. Wir haben festgestellt, dass P3BT-ra Filme aus Toluol-Lösungen die am besten geeigneten Wellenleiter für die intensitätsabhängigen Prismen-Kopplungs Experimente sind, weil diese geringe Wellenleiterdämpfungsverluste bei λ= 1064 nm haben.

Wir haben die Dispersionen des Wellenleiterdämfungsverlustes α_{gw}, des nichtlinearen Brechungsindex n_2 und des nichtlinearen Absorptionskoeffizienten α_2 von Wellenleitern aus P3BT-ra im Bereich von 700 - 1500 nm gemessen. Wir haben große Werte des nichtlinearen Brechungsindex bis $1,5x10^{-13}$ cm^2/W bei 1150 nm beobachtet. Wir haben gefunden, dass die Gütenkriterien ("figures of merit") für rein optische Schalter im Wellenlängebereich 1050 - 1200 nm erfüllt sind. Dieser Bereich entspricht dem niederenergetischen Ausläufer der Zwei-Photonen-Absorption. Die Gütekriterien von P3BT-ra gehören zu den besten der bisher bekannten Werte von konjugierten Polymeren.

Wir haben gefunden, dass P3BT-ra ein vielversprechender Kandidat für integriert-optische Schalter ist, weil es eine gute Kombination aus großer Nichtlinearität dritter Ordnung, geringen Wellenleiterdämpfungverlusten und ausreichender Photostabilität zeigt.

Wir haben einen Vergleich der gemessenen Dispersion von α_{gw}, n_2 und α_2 mit der Theorie durchgeführt. Durch Kurvenanpassung der Dispersion von α_{gw} haben wir

gefunden, dass Rayleigh-Streuung der dominierende Dämpfungsmechanismus in MEH-PPV und P3BT-ra Wellenleitern ist. Ein quantenmechanischer Ansatz wurde zur Berechnung der nichtlinearen Suszeptibilität dritter Ordnung $\chi^{(3)}$ verwendet, um die gemessenen Spektren von n_2 und α_2 von P3BT-ra und MEH-PPV zu simulieren. Dies kann erklären, dass sättigbare Absorption und Zwei-Photonen Absorption die hauptsächlichen Effekte sind, welche die Dispersion von n_2 und α_2 verursachen.

9 References

[Abdou'91] M. S. A. Abdou, G. Diaz-Quijada, M. I. Arroyo and S. Holdcroft, "Photoimaging of electronically conducting polymer networks" Chem. Mater. **3** (1991) 1003.

[Abdou'93] M. S. A. Abdou and S. Holdcroft, "Mechanism of Photodegradation of Poly(3-alkylthiophenes) in Solution" Macromol. **26** (1993) 2954.

[Abdou'95] M. S. A. Abdou and S. Holdcroft, "Soldi-state photochemistry of π-conjugated poly(3-alkylthiophenes)" Can. J. Chem. **73** (1995) 1893.

[Adams'81]. M. J. Adams, "Introduction to Optical Waveguide", John Wiley & Sons Inc., Chichester, 1981

[Allegrini'99] M. Allegrini, A. Arena, M. Labardi, G. Martino, R. Girlanda, C. Pace, S. Patane, G. Saitta, S. Savasta, "Photoluminescence from a soluble semiconducting polymer in waveguide and microcavity configurations", Appl. Surf. Sci. **142** (1999) 603.

[Bader'02] M. A. Bader, G. Marowsky, A. Bahtiar, K. Koynov, C. Bubeck, H. Tillmann, H.-H. Hörhold and S. Pereira, "Poly(p-phenylenevinylene) derivatives: new promising materials for nonlinear all-optical switching", J. Opt. Soc. Am. B **19** (2002) 2250.

[Baehr-Jones'08] T. W. Baehr-Jones, M. J. Hochberg,"Polymer Silicon Hybrid System: A Platform for Practical Nonlinear Optics", J. Phys. Chem. C. **112** (2008) 8085.

[Bahtiar'04] A. Bahtiar, "Optical Waveguides of Conjugated Polymers for All-Optical Switching Devices", PhD Thesis, University of Mainz, 2004.

[Bahtiar'06] A. Bahtiar, K. Koynov, A. Kibrom, T. Ahn and C. Bubeck, "Multiphoton spectroscopy of polymers for all-optical switching", (Invited Paper) Proc. SPIE **6330** (2006) 63300C-1.

[Bahtiar'09] A. Bahtiar, K. Koynov, Y. Mardiyati, H-H. Hörhold and C. Bubeck, "Slab waveguides of poly(*p*-phenylenevinylene)s for all-optical switching: impact of side –chain substitution", J. Mater. Chem. **19** (2009) 7490.

[Becker'05] M. Becker, unpublished laboratory notes, Max Planck Institute for Polymer Research, Mainz, 2005.

[Bermudez'00] V. Bermudez, F. Kajzar, S. Niziol, J. Pielichowski, J. Sanetra, and Bogdal, "Linear and nonlinear optical properties of PVK and PVK substituted thin films", (Invited Paper) Proc. SPIE **4106** (2000) 165.

[Bornside'87] D.E. Bornside, C.W. Macosko, L.E. Scriven, " On the Modelling of Spin Coating", Journal of Imaging Technology **13 (4)** (1987) 122-130

[Boyd'08] R. W. Boyd, *Nonlinear Optics*, Academic Press, Orlando, 2008.

[Bruggeman'34] D. A. G. Bruggeman, "Berechnung verschiedener physikalicher Konstanten von heterogenen Substanzen" Ann. Physik (Leipzig), **24** (1935) 636.

[Bubeck'91] C. Bubeck, A. Kaltbeitzel, A. Grund and M. LeClerc, "Resonant degenerate four wave mixing and scaling laws for saturable absorption in thin films of conjugated polymers and Rhodamin 6G", *Chemical Physics*, **154** (1991) 343-348.

[Bubeck'98] C. Bubeck in Oligomer Approach (Eds. K. Müllen and G. Wegner) Wiley-VCH, Weinheim Germany, 1998

[Buthcer'90] P. N. Butcher and D. Cotter, *The Elements of Nonlinear Optics*, Cambridge University Press, Cambridge, 1990.

[Campoy'05] M. Campoy-Quiles, P. G. Etchegoin, and D. D. C. Bradley, "On the optical anisotropy of conjugated polymer thin films", Phys. Rev. B **72** (2005) 045209.

[Campoy'08] M. Campoy-Quiles, J. Nelson, P.G. Etchegoin, D.D.C. Bradley, V. Zhokhavets, G. Gobsch, H. Vaughn, A. Monkman, O. Ingänas, N. K. Persson, H. Arwin, M. Garriga, M.I. Alonso, G. Herrmann, M. Becker, W. Scholdei, M. Jahja and C. Bubeck,"On the determination of anisotropy in polymer thin films: A comparative study of optical techniques", Phys. Stat. Sol C **5** (2008) 1270.

[Chance'80] R. R. Chance, M. L. Shand, C. Hogg and R. Silbey,"3-wave mixing in conjugated polymer-solutions - 2-photon absorption in polydiacetylenes", Phys. Rev. B 22 (1980) 3540.

[Chen'93] T-A Chen, X. Wu and R.D Rieke, "Polyalkylthiophenes with smallest bandgap and the highest intrinsic conductivity", Synthetic Metals, **60** (1993) 175.

[Chen'95] T-A Chen, X. Wu and R.D Rieke, "Regiocontrolled Synthesis of Poly(3-alkylthiophenes) by Rieke Zinc: Their Characterization and Solid-State Properties", J. Am. Chem. Soc., **117** (1995) 233.

[Chen'97] D. Chen, H. Fetterman, A. Chen, W.-H. Steier, L. R. Dalton, W. Wang and Y. Shi,"Demonstration of 110 GHz electro-optics polymer

[Chichkov'96] B.N. Chichkov, C. Momma, S. Nolte, F. Von Alvensleben and A. Tunnermann,"Femtosecond, picosecond and nanosecond laser ablation of solids", Appl Phys. A **63** (1996) 109.

[Dinu'03] M. Dinu, F. Quochi and H. Garcia, "Third-order nonlinearities in silicon at telecom wavelengths", Appl . Phys. Lett, **82** (2003) 2954.
modulators", App. Phys. Lett. **70** (1997) 3335.

[de Boni'04] L. de Boni, A. A. Andrade, D. S. Corrêa, D. T. Balogh, S. C. Zilio, L. Misoguti, and C. R. Mendonça," Nonlinear absorption spectrum in MEH-PPV/Chloroform solution: A competition between two-photon and saturated absorption process", J. Phys. Chem. B **108** (2004) 5221.

[Descrovi'09] E. Descrovi,"Resonant diffraction of symmetric and antisymmetric Bloch surface waves on a corrugated periodic multilayer slab", Opt. Lett. **34** (2009) 1973.

[Edwards'85] D. F. Edwards in Handbook od Optical constants of solids (Eds. E. D. Palik) Academic Press, Weinheim Germany, 1985

[Faccinetto'08] A. Faccinetto, S. Mazzucato, D. Pedron, R. Bozio, S. Destri and W. Porzio," Non-resonant z-scan characterization of third order nonlinear optical properties of conjugated poly(thiopheneazines)", Chem. Phys. Chem. **9** (2008) 2028.

[Fitrilawati'99] F. Fitrilawati, M.O. Tjia, J. Ziegler and C. Bubeck,"fabrication of Planar Waveguides of Poly(N-vinylcarbazole)", Proc. of SPIE **3896** (1999) 697.

[Fitrilawati'02] F. Fitrilawati, M. O. Tjia, S. Pfeiffer, H. Tillmann, H. H. Hörhold, A. Deutesfeld, H. Eichner and C. Bubeck, "Planar waveguides of PPV

derivatives: attenuation loss, third-harmonic generation and photostability", Opt. Mater. **21** (2002) 511.

[Fuks'02] I. Fucks, B. Derkowska, B. Sahroui, S. Niziol, J. Sanetra, D. Bogdal and J. Pielichowski, "Third-order nonlinear optical susceptibility of polymers based on carbazole derivatives", JOSA B **19** (2002) 89.

[Gabler'98] Th. Gabler, A. Bräuer, R. Waldhäusl, U. Bartuch, H.-H. Hörhold, and F. Michelotti, *Pure and Appl. Optics* **7** (1998), 159.

[Gebler'98] D.D. Gebler, Y.Z. Wang, D.-K. Fu, T.M. Swager, A.J. Epstein,"Exciplex emission from bilayers of poly(vinylcarbazole) and pyridine based conjugated polymers", J. Chem. Phys. **108** (1998) 7842.

[Gierschner'07] J. Gierschner, J. Cornil and H.-J. Egelhaaf, "Optical Bandgaps of π-Conjugated Organic Materials at the Polymer Limit: Experiment and Theory", Adv. Mater. **19** (2007), 173.

[Greene'08] K. Greene, A Record-Breaking Optical Chip: Intel researchers have built a superfast chip for optical networking", tech. Review, June (2008).

[Holdcroft'91] S. Holdcroft,"A photochemical study of Poly(3-hexylthiophene)", Macromol. **24** (1991) 4834.

[Hu'05] X. Y. Hu, Q. H. Gong, Y. H. Liu, B. Cheng and D. Zhang," All-optical switching of defect mode in two-dimensional nonlinear organic photonic crystals", Appl. Phys. Lett. **87** (2005) 231111.

[Hu'08] X. Y. Hu, P. Jiang, C. Y. Ding, H. Yang and Q. H. Gong,"Picosecond and low-power all-optical switching based on an organic photonic bandgap microcavity", nat. photonics **2** (2008) 185.

[Hugger'04] S. Hugger, R. Thomann, T. Heinzel and T. Thurn-Albrecht, "Semicrystalline morphology in thin films of poly(3-hexylthiophene)", Colloid Poly. Sci., **282** (2004) 932.

[Hutchings'92] D. C. Hutchings, M. Sheik-Bahae, D. J. Hagan and E. W Van Stryland,"Kramers-Kronig relations in nonlinear optics", Opt. and Quantum Electron. **24** (1992) 1.

[Inagaki'77] T. Inagaki, E. T. Arakawa, R. N. Hamm and M. W. Williams, "Optical properties of polystyrene from near-infrared to x-ray region

and convergence of optical sum rules", Phy. Rev. B **15** (6) (1977) 3243.

[Jahja'10] M. Jahja and C. Bubeck, "Nonlinear optical waveguide spectroscopy of poly(3-butylthiophene)", submitted to JNOPM.

[Jonietz'10] E. Jonietz,"Faster Optical Switching Through Chemistry:Specially designed molecules could lead to all-optical data switches that could make the Internet far faster", Techology Review, 4th March 2010.

[Kadir'09] R. Kadir, A. Yimit, H. Ablat M. Mahmut and K. Itoh, "Optical Waveguide BTX Fas Sensor based on Polyacrylate Resin Thin Film", Environ. Sci. Tech. **43** (2009) 5113

[Kajzar'96] F. Kajzar and J. D. Swalen, eds., "*Organic Thin Films for Waveguiding Nonlinear Optics*", Gordon and Breach Publ. Amsterdam, (1996).

[Kim'93] D. Y. Kim, M. Sundheimer, A. Otomo, G. I. Stegeman, W. H. G. Horsthuis, G. R. Möhlmann, *Appl. Phys. Lett*. **63** (1993), 290.

[Kim'94] D. Y. Kim, B. L. Lawrence, W. E. Torruellas, G. I. Stegeman, G. Baker, J. Meth, *Appl. Phys. Lett*. **65** (1994), 1742.

[Kishida'05] H. Kishida, K. Hirota, T. Wakabayashi, H. Okamoto, H. Kokubo and T. Yamamoto, "Third-order optical nonlinearity in regio-controlled polythiophene films", Appl. Phys. Lett., **87** (2005) 121902.

[Kogelnik'79] H. Kogelnik in "*Integrated Optics: Topics in Applied Physics Vol. 7*", T. Tamir (Ed.), Springer Verlag Berlin (1079), 13.

[Koynov'02] K. Koynov, N. Goutev, F. Fitrilawati, A. Bahtiar, A. Best and C. Bubeck,"Nonlinear prism coupling of waveguides of the conjugated polymer MEH-PPV and their figures of merits for all-optical switching", J. Opt. Soc. Am. B **19** (2002) 895

[Koynov '06] K. Koynov, A. Bahtiar, T. Ahn, R. M. Cordeiro, H.-H. Hörhold and C. Bubeck, "Molecular Weight Dependence of Chain Orientation and Optical Constants of Thin Films of the Conjugated Polymer MEH-PPV", *Macromolecules* **39** (2006) 8692.

[Krüger'04] J. Krüger, W. Kautek, " Ultrashort pulse alaser interaction with dielectric and polymers", Adv. Polym. Sci 168 (2004) 247.

[Kuebler'00] S. M. Kuebler, R. G. Denning, H. L. Anderson,"Large third-order polarizability of a conjugated porphyrin polymer", Jour. of the Am. Chem. Soc. **122** (2000) 339.

[Lanzi'08] M. Lanzi and L. Pahanin, "Study of the order-disorder transitions in methoxy-functionalized polyalkylthiophenes", Eur. Polym. Journal **44** (2008) 3987.

[Lawrence'88] C.J. Lawrence, "The mechanics of spin-coating of polymer films", Physics of Fluids, 31(10) (1988) 2786-2795

[Lawrence'94] B. L. Lawrence, M. Cha, J. Kang, W. E. Torruellas, G. I. Stegeman, G. Baker, J. Meth, S. Etemad, *Electron. Lett*. **30** (1994), 447.

[Lee'86] D. L. Lee, *Electromagnetic Principles of Integrated Optics*, John Wiley Sons Inc. New York, 1986

[Lines'91] M. E. Lines, *"Physical properties of materials: Theoretical Overview,"*in Handbook of Infrared Optical Materials, P. Klocek (Ed), Marcel Dekker, New York 1991, 57.

[Liu'09] Y. Liu, F. Qin, Z.-Y. Wei, Q.-B. Meng, D.-Z. Zhang and Z-Y. Li, "10 fs ultrafast all-optical switching in polystyrene nonlinear photonic crystals" App. Phys. Lett. **95** (2009) 131116.

[Lu'07] G. Lu, L. Li and X. Yang,"Achieving Perpendicular Alignment of Rigid Backbone to the Substrate by Using Solvent-Vapor Treatment", Adv. Mater., **19** (2007) 3594.

[Lu'08] G. Lu, L. Li and X. Yang,"Morphology and Crystalline Transition of Poly(3-butylthiophene) Associated with its Polymorphic Modifications", Macromol., **41** (2008) 2062.

[Ma'02] H. Ma, A. K. –Y. Jen and L. R. Dalton, „ Polymer-based optical waveguides: Materials, Processing and devices", Adv. Mater. **14** (2002) 1341.

[Ma'07] Z. Ma, Y. Geng and D. Yan, "Extended-chain lamellar packing of poly(3-butylthiophene) in single crystals", Polymer, **48** (2007) 31.

[Mardiyati'10] Mardiyati, unpublished laboratory notes, Max Planck Institute for Polymer Research, Mainz, 2010.

[Marcuse'74] D. Marcuse, "*Theory of Dielectric Optical Waveguides*", Academic Press, New York, (1974).

[Marques'91] M. B. Marques, G. Assanto, G. I. Stegeman, G. R. Möhlmann, E. W. P. Erdhuisen, W. H. G. Horsthuis, *Appl. Phys. Lett*. **58** (1991), 2613.

[Mathy'96] A. Mathy, K. Ueberhofen, R. Schenk, H. Gregorius, R. Garay, K. Müllen, C. Bubeck, *Phys. Rev. B* **53** (1996), 4367.

[McCullough'93a] R.D. McCullough, R.D. Lowe, M. Jayaraman, D.L. Anderson, "Design, synthesis, and control of conducting polymer architectures – structurally homogenous poly(3-alkylthiophenes)", J. of Org. Chem., **58** (1993) 904.

[McCullough'93b] R.D. McCullough, S. Tristram-Nagle, S.P. Williams, R.D. Lowe and M. Jayaraman, "Self-Orienting Head-to-Tail Poly(3-alkylthiophenes): New Insights on Structure-Property Relationships in Conducting Polymers", J. Am. Chem. Soc, **115** (1993) 4910.

[Messaad'08] K. Messaad, D. Bosc, M. Thual, E. Haesaert and F. Henrio, "Investigation of the optical waveguide realization based on polymers with large third order non-linear susceptibility", Proc. of SPIE, **6999** (2008) 69991V-1.

[Moneret'00] S. Moneret, P. Huguet-Chantome and F. Flory,"m-lines technique: prism coupling measurement and discussion of homogeneous wavewguides", J. Opt. A:Pure Appl. **2** (2000) 188.

[Möller'88] K. D. Möller, "*Optics*", University Science Books, USA, 1988.

[Neher'90] D. Neher, *PhD Dissertation*, University Mainz, Germany, 1990.

[Neher'90] D. Neher,"Optical 3^{rd}-harmonic generation in substituted poly(phenylacetylenes) and poly(3-decylthiophenes)", Synth. Meth. **37** (1990) 249.

[Okawa'92] H. Okawa, T. Hattori, A. Yanase, Y. Kobayashi, A. Carter, M. Sekiya, A. Kaneko, T. Wada, A. Yamada and H. Sasabe, "Third-order optical nonlinearities of soluble polythiophenes", *Nonlinear Optics of Organic and Polymer Systems and Photonic Devices Symposium*, **3** (1992), 169

[Periasamy'92] N. Periasamy, R. Danieli, G. Ruani, R. Zamboni, and C. Taliani, "Location of the low-energy 1Ag state in a polythiophene oligomer by two-photon absortion spectroscopy:α-sexithienyl", *Phys. Rev. Lett.* **68** (1992) 919-922.

[Pfeffer'93] N. Pfeffer, P. Raimond, F. Charra and J-M, Nunzi, "Determination of the two-photon absorption spectrum of a soluble polythiophene", *Chemical Physics Letters*, **201** (1993) 357

[Prest'79] W. M. Prest Jr. and D. J. Luca, "The origin of the optical anisotropy of solvent cast polymeric films", J. Appl. Phys. **50** (1979) 6067.

[Prest'80] W. M. Prest Jr. and D. J. Luca, "The alignment of polymers during the solvent-coating process", J. Appl. Phys. **51** (1980) 5170.

[Rau'06] I. Rau, P. Armatys, P.-A. Chollet, F. Kajzar and R. Zamboni, "Conjugated Polymers Oriented Organic Thin Films for Nonlinear Optics", Mol. Cryst. Liq. Cryst., **446** (2006) 23.

[Rochford'91] K. Rochford, R. Zanoni, G. I. Stegeman, W. Krug, E. Miao, M. W. Beranek, *Appl. Phys. Lett*. **58** (1991), 13.

[Rodenberger,92] D.C. Rodenberger, J.R. Heflin and A. F. Garito, " Excited-state enhancement of optical nonlinearities in linear conjugated molecules", Nature **359** (1992) 309.

[Ryder'51] E. J. Ryder and W. Shocley,"Mobilities of electrons in high electric fields", Phys. Rev. **81** (1951) 139.

[Samoc'95] A. Samoc, M. Samoc, M. Woodruff, B. Luther-Davies, *Opt. Lett*. **20** (1995), 1241.

[Schwarz'92a] R. Schwarz, "Reflexions- und Transmissionsspektroskopie an ultradünnen Polymerschcihten und quantitative Bestimmung ihres komlexen Brechnungindex", Ph.D Thesis Universität Mainz (1992)

[Schwarz'92b] R. Schwarz, W. A. Goedel, N. Somanathan, C. Bubeck, U. Scheunemann, W. Hickel and G. Wegner, "Determination of the Optical Constants of a Polythiophene Thin film", Springer Series in Solid-State Sciences 107 (1992) 337.

[Sheik-Bahae'90] M. Sheik-Bahae, D. J. Hagan, E. W. Van Stryland, "Dispersion and band-gap scaling of the electronic Kerr effect in solids associated with two-photon absorption", *Phys. Rev. Lett.* 65 (1990) 65.

[Stegeman'93] G. I. Stegeman, *Proc. SPIE* **1852** (1993), 75.

[Stegeman'97] G. I. Stegeman, "Application of organic materials in third-order nonlinear optics", in *Nonlinear Optics of Organic Molecules and Polymers*, eds. H. S. Nalwa and S. Miyata, CRC Press Inc. (1997), pp. 799-812.

[Ta'eed'07] V. G. Ta'eed, N. J. Baker, L. Fu, K. Finsterbusch, M. R.E. Lamount, D. J. Moss, H. C. Nguyen, B. J. Eggleton, D. Y. Choi, S. Madden and B. Luther-Davies, "Ultrafast all-optical chalcogenide glass photonic circuits", Opt. Express, 15 (15) (2007) 9205.

[Tien'70] P. K. Tien, R. Ulrich,"Theory of prism-film coupler and thin-film light guides", *J. Opt. Soc. Am.* **60** (1970), 1325.

[Tien'71] P. K. Tien,"Light waves in thin films and integrated optics", *Appl. Opt.* **10** (1971), 2395.

[Tien'77] P. K. Tien,"Intergrated-Optics and new wave phenomena in optical-waveguides", *Rev. Mod. Phys.* **49** (1977), 361.

[Torruellas'90] W. E. Torruellas, D. Neher, R. Zanoni, G. I. Stegeman, F. Kajzar and M. Leclerc, "Dispersion measurements of the third-order nonlinear susceptibility of polythiophene thin films", *Chemical Physics Letters*, **175** (1990) 11.

[Ueberhofen'99] K. Ueberhofen, A. Deutesfeld, K. Koynov and C. Bubeck,"Nonlinear optical waveguide spectroscopy of a conjugated polymer: poly(p-phenylenevinylene)", *Journal of Opt. Soc. of America B*, **16** (11) (1999) 1921-1935.

[Ueberhofen'96] K. Ueberhofen, "Nichtlineare-optische Wellenleiterspektroskopie an konjugierten Polymeren", Ph.D Thesis Universität Mainz (1996)

[Ulrich'70] R. Ulrich, "Theory of the prism-film coupler by plane-wave analysis", J. Opt. Soc. Am. **60** (1970) 1337.

[Ulrich'73] R. Ulrich and R. Torge, "Measurement of thin film parameter with a prism coupler", Appl. Opt. **12** (1973) 2901.

[Yang'92] L. Yang, R. Dorsinville, Q. Z. Wang, P. X. Ye, R. R. Alfonso, R. Zamboni and C. Taliani, "Excited-state nonlinearity in polythiophene thin films investigated by the Z-scan technique", Opt. Lett. 17 (1992) 323-325.

[Yeh'05] P. Yeh, *Optical waves in layered media*, John Wiley & Sons Inc., New Jersey, 2005.

[Yoshizawa'91] M. Yoshizawa, A. Yasuda, T. Kobayashi,"Ultrafast optical-response in polydiacetylenes and polythiophenes", Appl. Phys. B **53** (1991) 296.

[Zen'06] A. Zen, M. Saphiannikova, D. Neher, J. Grenzer, S. Grigorian, U. Pietsch, U. Asawapirom, S. Janietz, U. Scherf, I. Lieberwirth and G. Wegner, " Effect of Molecular Weight on the Structure and Crystallinity of Poly(3-hexylthiophene)", Macromol., **39** (2006) 2162.

[Zhang'98] Y. D. Zhang, T. Wada and H. Sasabe,"Carbazole photorefractive materials", J. Mater. Chem. 8 (1998) 809.

[Ziegler'00] J. Ziegler, "Schichtpräparation und Characterisierung von Wellenleitern aus Polymeren", PhD Thesis Univ. Mainz (2000) 142.

Appendix A
Differential Scanning Calorimetry Curves

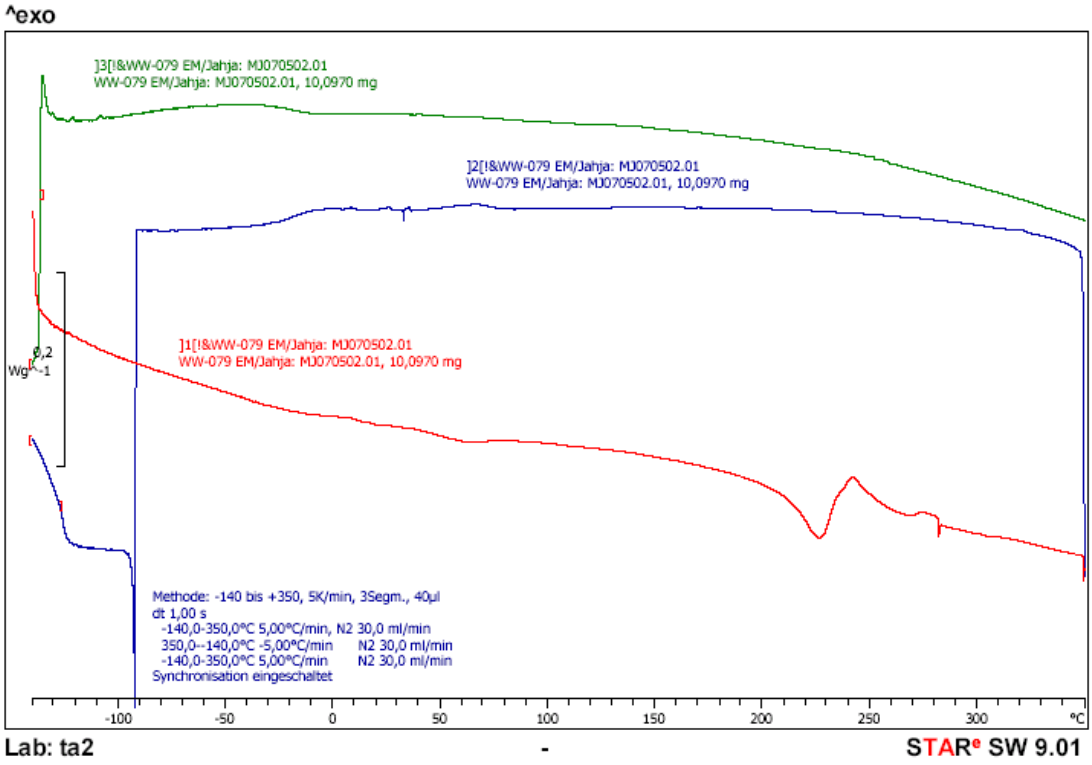

Fig. A1: Differential Scanning Calorimetry curves of regioregular Poly(3-hexylthiophene), T_m=220˚C.

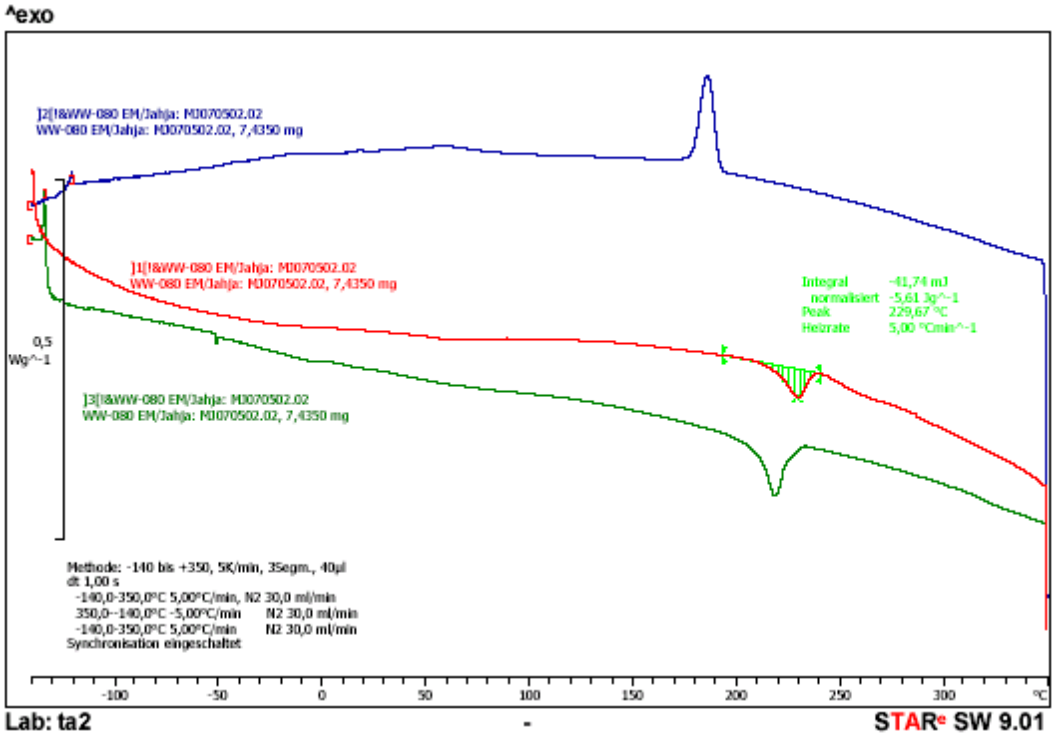

Fig. A2: Differential Scanning Calorimetry curves of regioregular Poly(3-hexylthiophene), T_m=229°C.

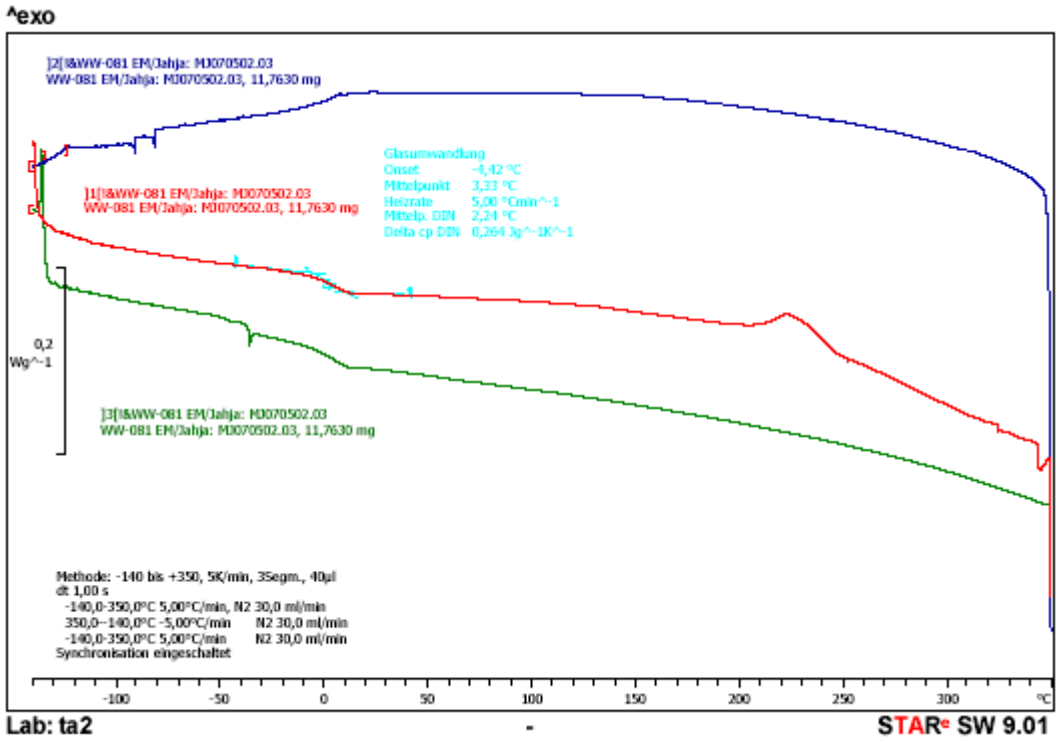

Fig. A3: Differential Scanning Calorimetry curves of regiorandom Poly(3-hexylthiophene), T_g=3°C.

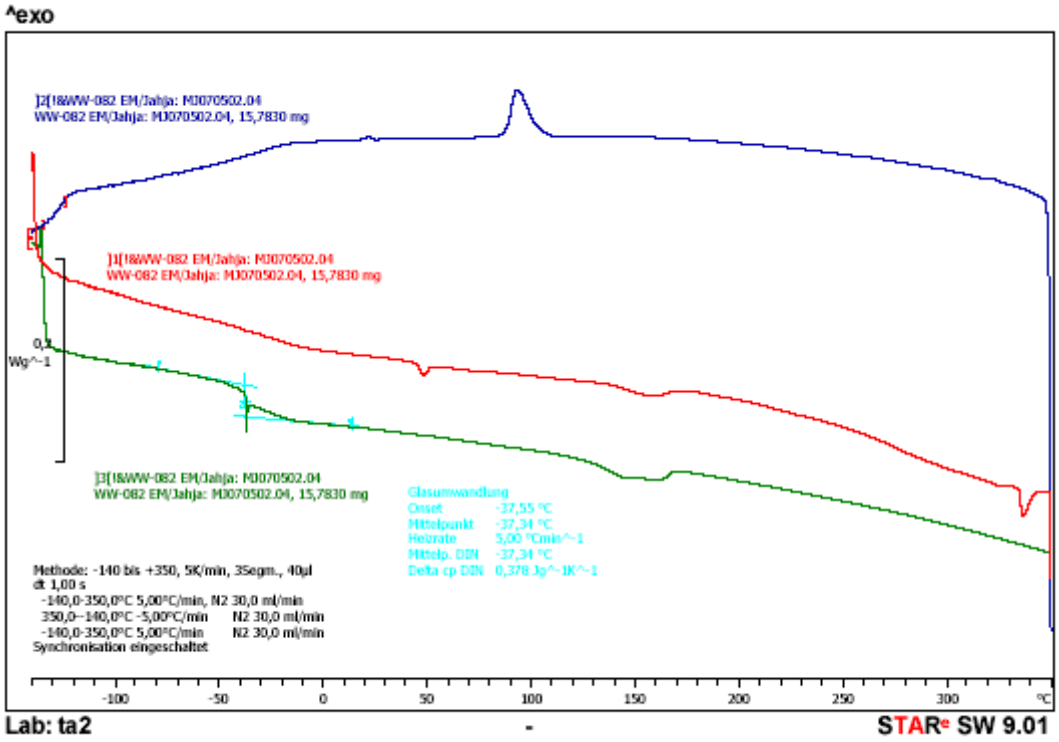

Fig. A4: Differential Scanning Calorimetry curves of Poly(3-octylthiophene), T_g=-37,34°C.

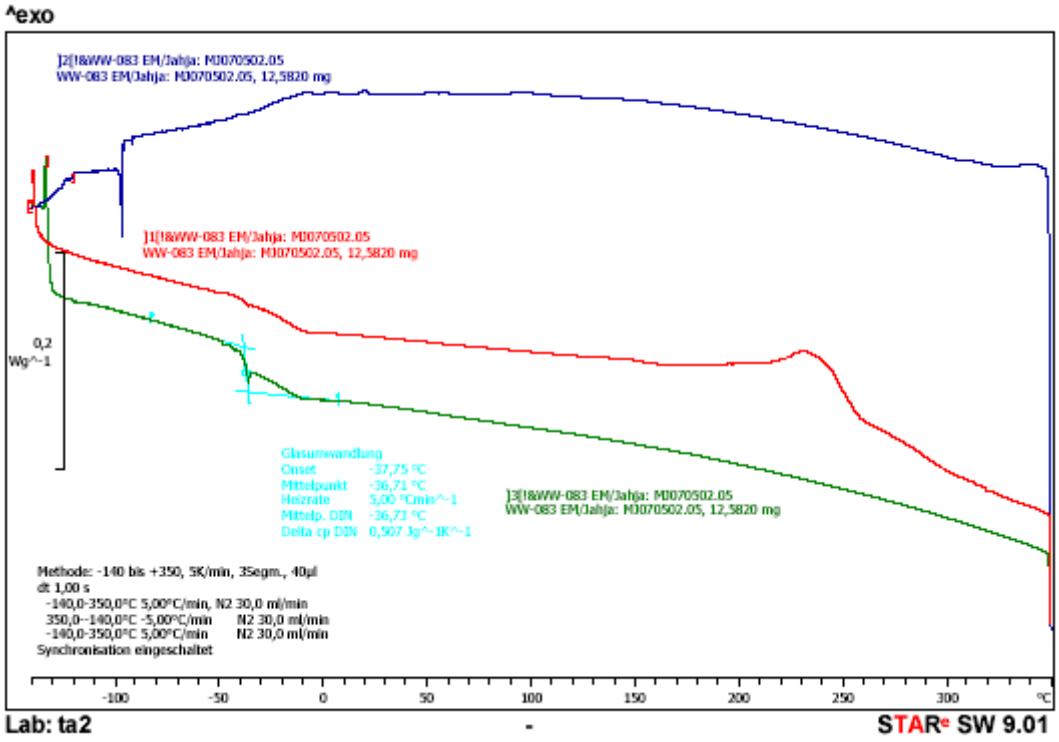

Fig. A5: Differential Scanning Calorimetry curves of regiorandom Poly(3-octylthiophene), Tg=-36,71°C.

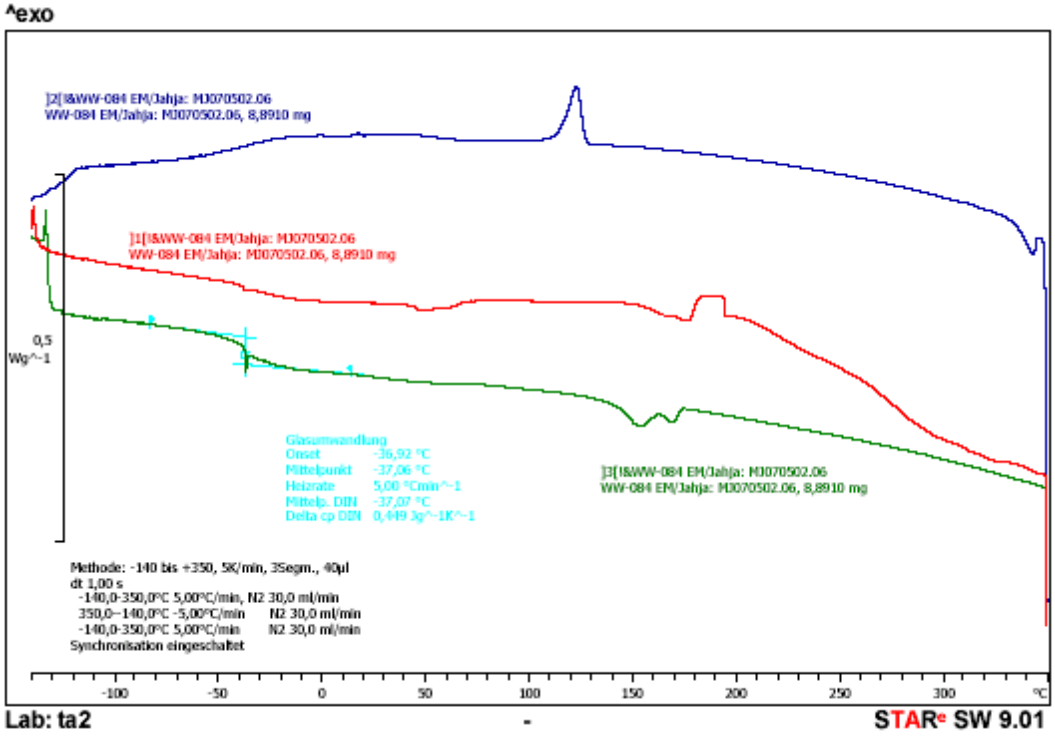

Fig. A6: Differential Scanning Calorimetry curves of regiorandom Poly(3-decylthiophene) T_g=-37,06˚C.

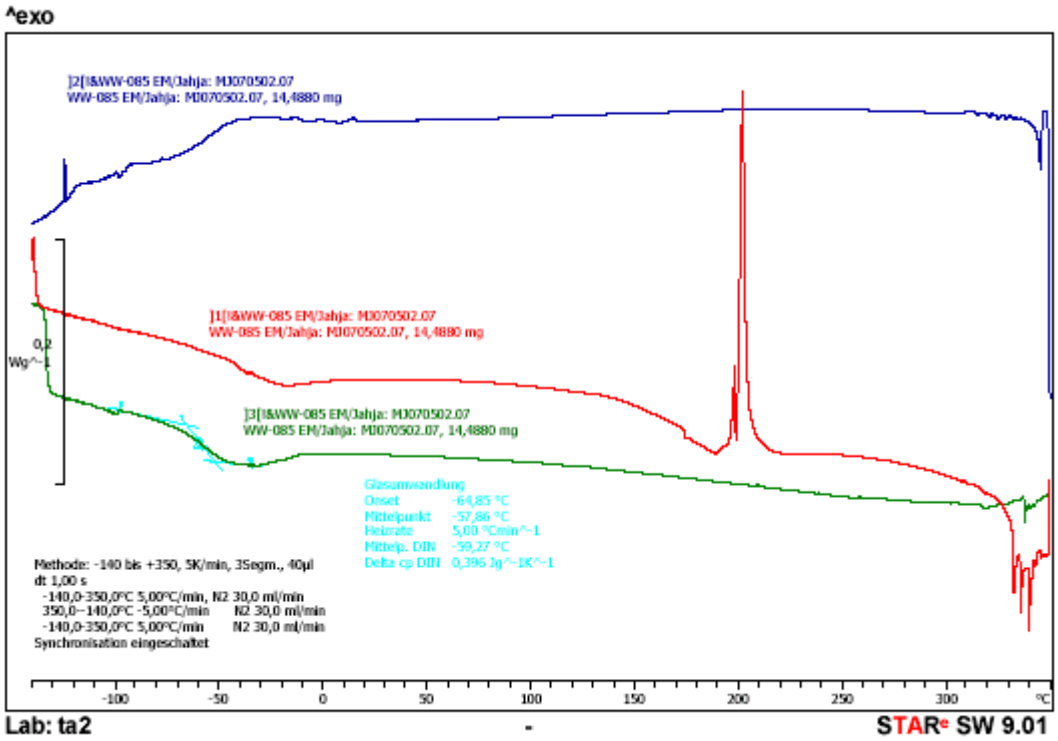

Fig. A7: Differential Scanning Calorimetry curves of regiorandom Poly(3-decylthiophene), T_g=-60˚C.

Appendix B
Molecular Weight Distribution

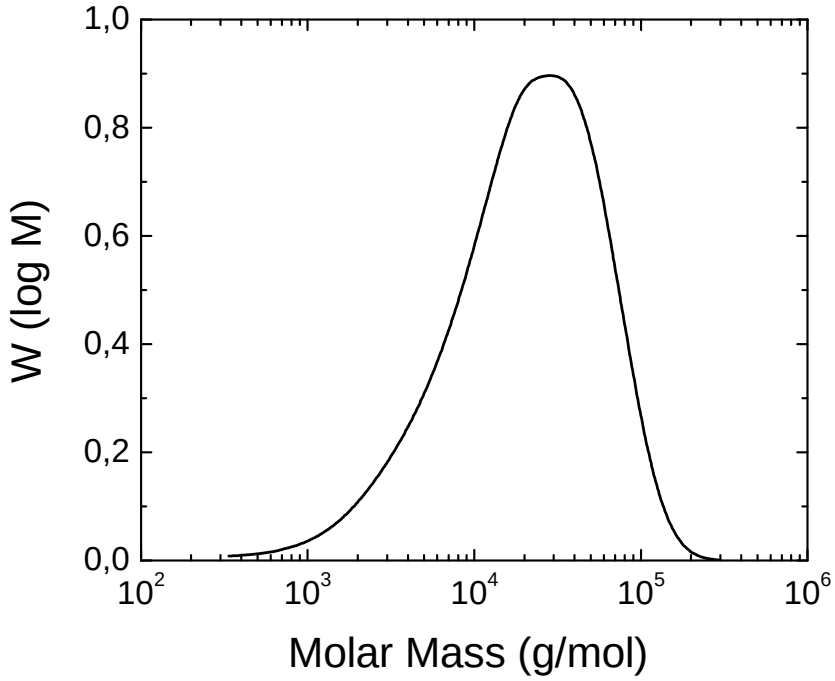

Fig. B1: Molecular Weight distribution of P3BT-ra (M_w=30,887 g/mol, M_n=10,182 g/mol, PDI=3.03). The polymer was obtained from Rieke Metals Inc, USA.

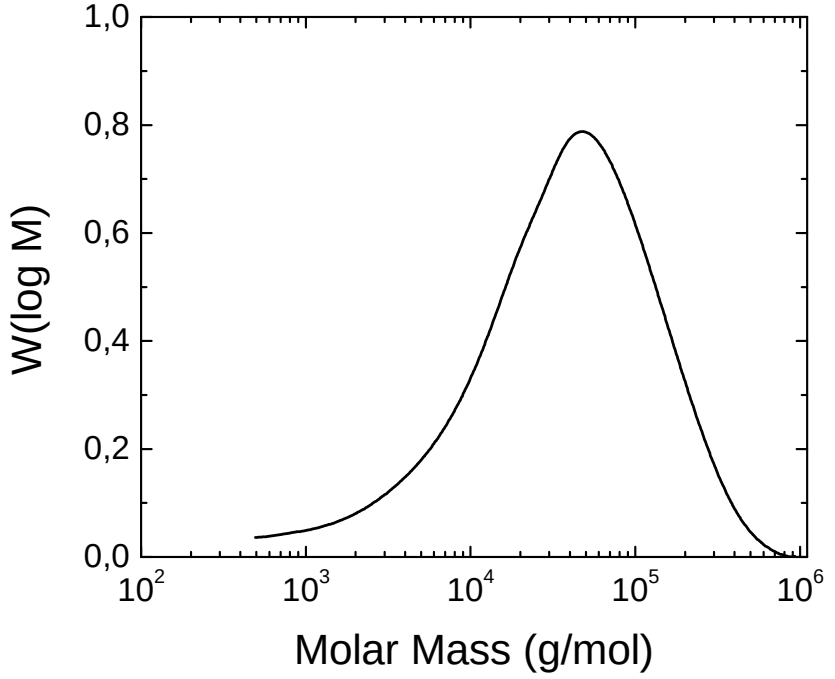

Fig. B2: Molecular Weight distribution of P3BT-ra (M_w=31,780 g/mol, M_n=11,364 g/mol, PDI=2.8). The polymer was obtained from Aldrich, USA.

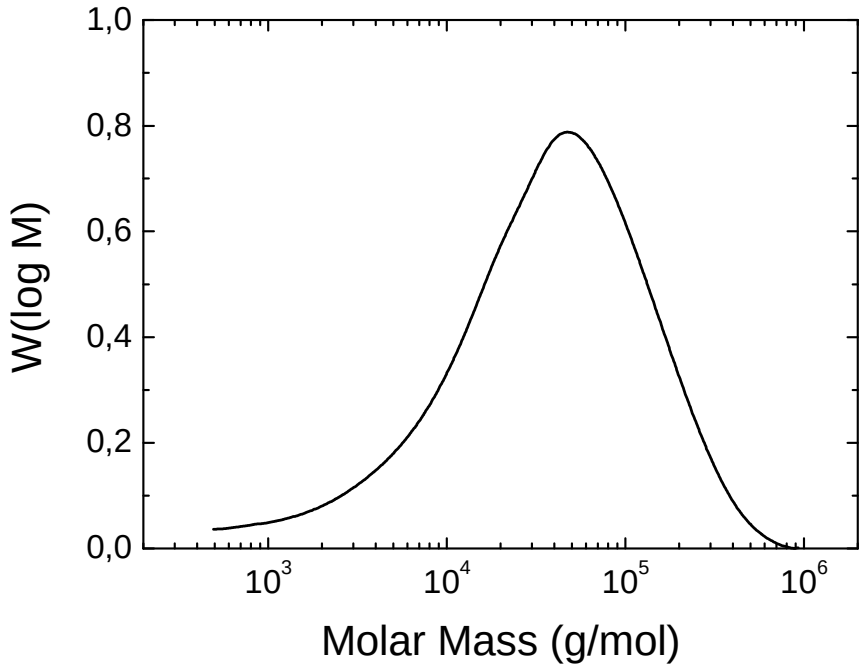

Fig. B3: Molecular Weight distribution of P3HT-ra (M_w=69,426 g/mol, M_n=15,032 g/mol, PDI=4.62). The polymer was obtained from Aldrich, USA.

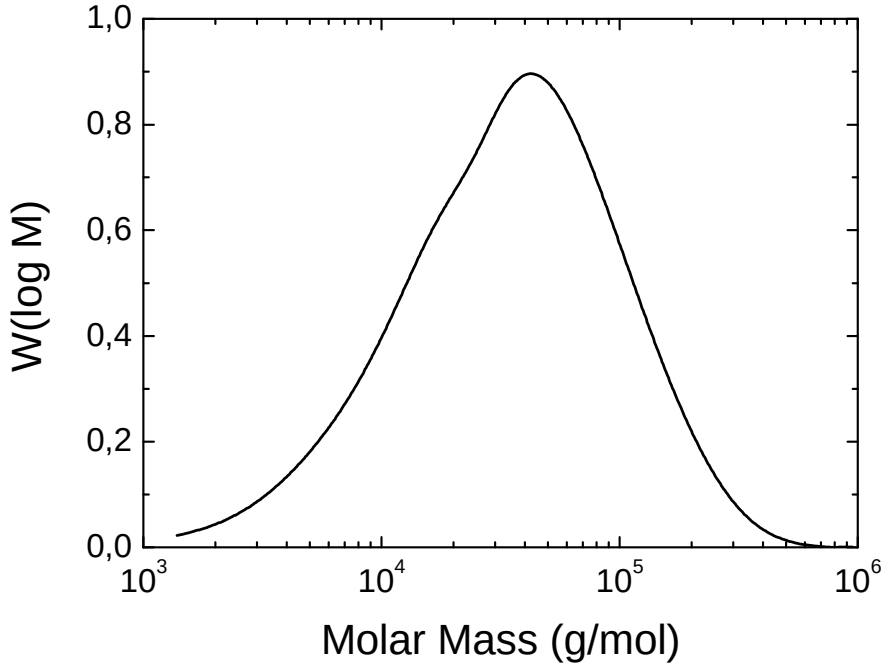

Fig. B4: Molecular Weight distribution of P3OT-ra (M_w=56,033 g/mol, M_n=17,023 g/mol, PDI=3.29). The polymer was obtained from Aldrich, USA.

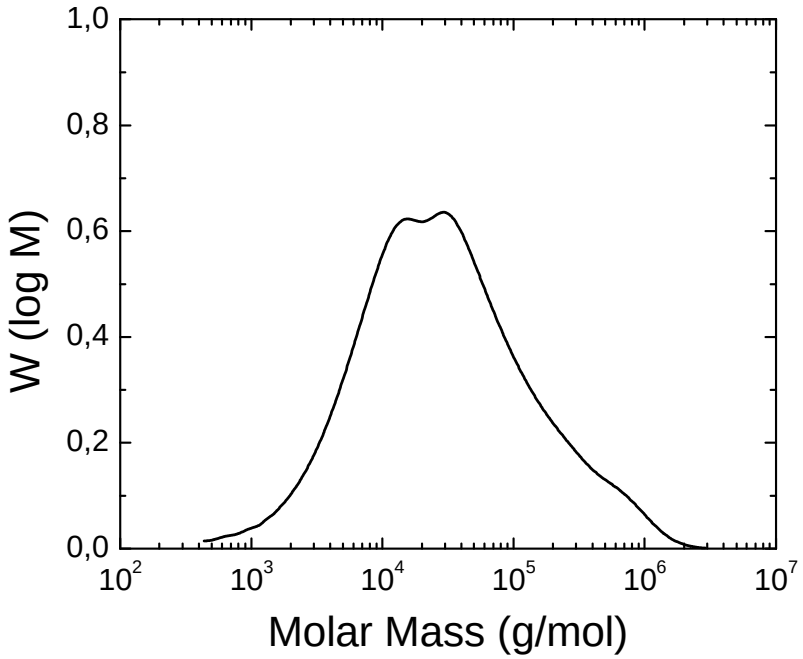

Fig. B5: Molecular Weight distribution of P3DT-ra (M_w=90,540 g/mol, M_n=10,846 g/mol, PDI=8.35). The polymer was obtained from Aldrich, USA.

Appendix C
Spin coating parameters

In this section we will elaborate how to get the so-called spin coating parameters: α, β and d_0 which are appeared in Eq. 3.1.

C1 Polystyrene (PS)

Four thin films of PS were prepared from solutions with different concentration (C_w). The films were spun cast onto the pre-clean glass substrates at different spinning speed ω. Subsequently the films were annealed in vacuum oven for more than six hours. The thickness d of the film was averaged value over 9 thickness data which were measured at 9 different positions over the surface of the films.

Table C1.1: Thickness of PS films

SAMPLE	C_W (%)	ω (10^3 RPM)	D (NM)
MJ060314.02	2	8	76 ± 4
MJ060314.04	5	8	411 ± 20
MJ060314.06	2	2	148 ± 8
MJ060314.08	5	2	823 ± 54

List of Publications

1. M. Campoy-Quiles, J. Nelson, P.G. Etchegoin, D.D.C. Bradley, V. Zhokhavets, G. Gobsch, H. Vaughn, A. Monkman, O. Ingänas, N. K. Persson, H. Arwin, M. Garriga, M.I. Alonso, G. Herrmann, M. Becker, W. Scholdei, M. Jahja and C. Bubeck,"On the determination of anisotropy in polymer thin films: A comparative study of optical techniques", Phys. Stat. Sol C **5** (2008) 1270.

2. M. Jahja and C. Bubeck, "Nonlinear optical spectra of poly(3-butylthiophene)", poster presentation at 7th International Symposium on Modern Optics and Its Applications (ISMOA 2009)", Bandung, Indonesia.

3. M. Jahja and C. Bubeck, "Nonlinear optical waveguide spectroscopy of poly(3-butylthiophene)", accepted to JNOPM.